Anthropogenic Impacts on Tropospheric Reactive Chlorine and Bromine since the Pre-industrial

Shuting Zhai

A dissertation

submitted in partial fulfillment of the

requirements for the degree of

Doctor of Philosophy

University of Washington

2023

Reading Committee:

Becky Alexander, Chair

Lyatt Jaeglé

Alex Turner

Program Authorized to Offer Degree:

Department of Atmospheric Sciences

University of Washington

Abstract

Anthropogenic Impacts on Tropospheric Halogens and Implications for Arctic Ice Core Halogen Records since the Pre-industrial

Shuting Zhai

Chair of the Supervisory Committee:
Becky Alexander
Department of Atmospheric Sciences

Tropospheric reactive halogens (chlorine, bromine, iodine) impact the oxidation capacity of the atmosphere, oxidize reduced gases such as methane and mercury, and have profound implications on air quality, climate, and eco-systems. Ice core halogens have been used as proxies for sea ice extent for the pre-satellite era, but are also shown to be heavily influenced by anthropogenic emissions. Both sea ice extent and anthropogenic emissions have changed drastically in the northern hemisphere since the pre-industrial. Using a wide range of Arctic ice core halogen records and a global chemical transport model with state-of-the-science halogen chemistry, my Ph.D. research investigates the magnitude and mechanisms of anthropogenic impacts on halogen trends observed in Arctic ice cores, and the implications for the tropospheric chlorine and bromine budgets.

In the first part of my Ph.D. project (Chapter 2), I implemented recent advances in halogen chemistry into the GEOS-Chem model, and presented new chlorine records from six Greenland ice cores covering the pre-industrial (PI) to present-day (PD) transition. The model suggests that the PI to peak-acidity (PA, 1975) increase in non-sea-salt chlorine is mainly caused by anthropogenic emissions of acidic gases, such as SO_2, NO_x, and HCl, and the decrease from PA to PD is a result of reduced HCl emission from the air pollution mitigation policies in North America and Western Europe. This highlights the importance of anthropogenic impacts on ice core chlorine trends.

In the second part of my Ph.D. project (Chapter 3), I implemented an empirically based framework for snowpack bromine production into GEOS-Chem to evaluate the post-depositional loss of bromine for various Arctic ice core sites for the first time. Results suggest that only the Akademii Nauk ice core in the Russian Arctic, shows good preservation of bromine in the snowpack, and all the Greenland ice cores suffer significant bromine loss during the sunlit season. Key factors influencing snowpack bromine preservation include time in the dark (latitude), snowfall burial rate, and potential surface melting. I point out the necessity to further understand snow bromine species and how they evolve over an annual cycle, through future field and laboratory efforts.

Based on Chapter 3 results, I explored the ice core bromine trends in Academia Nauk in the third part of my Ph.D. project (Chapter 4), using GEOS-Chem historical simulations with additional anthropogenic bromine sources from coal combustion and leaded gasoline. Model suggests that acid-catalyzed sea-salt debromination of Br_2 is the major driver for the observed increase in ice core bromine from PI to PA, consistent with the robust correlation observed between ice core bromine and acidity after 1940 ($r=0.9$). The simulation underestimates the observed decreases

from PA to PD for both bromine and acidity, suggesting uncertainties in anthropogenic emissions of acidic gas precursors in the Russian Arctic during this time period. I showed that changes in sea ice are unlikely to explain the PA to PD decrease in ice core bromine. The results highlight that anthropogenic acidity is essential for understanding ice core bromine trends, and cannot be neglected when interpreting ice core bromine.

Future work on interpretation of ice core iodine records is proposed, which rely on better understanding of iodine speciation and chemistry through field observations and model development. Large uncertainties in snowpack bromine speciation and preservation hinder the accurate model representation of snowpack bromine production, and warrants future work as well.

TABLE OF CONTENTS

List of Figures iv

List of Tables vi

Chapter 1. INTRODUCTION 1

1.1 Motivation and Scientific Goals 1

1.2 Background 3

1.3 Ice core records of chlorine and bromine 3

1.4 Snowpack bromine production 5

1.5 Summary of Work 5

1.6 Publication Plans 6

Chapter 2. Anthropogenic Impacts on Tropospheric Reactive Chlorine Since the Preindustrial ... 7

2.1 Introduction 8

2.2 Methods 9

2.2.1 Ice-Core Records 9

2.2.2 GEOS-Chem simulations 11

2.2.3 Backward Trajectory Analysis 12

2.3 Results 13

2.3.1 Ice-Core Observations 13

2.3.2 Model-Observation Comparisons 16

2.3.3 Anthropogenic Impacts on Reactive Gaseous Chlorine 19

2.4 Conclusions and Implications 21

Chapter 3. Implications of snowpack reactive bromine production for arctic ice core bromine preservation 24

3.1 Introduction 25

3.2 Methods 31

3.2.1 Arctic Ice Cores 31

3.2.2 Statistical Analysis of Ice-Core Observations 34

3.2.3 Modeling Snowpack Halogen Chemistry 34

3.3 Results 41

3.3.1 Ice-Core Bromine Trend Analysis 41

3.3.2 Modeled Snowpack Reactive Bromine Release 46

3.3.3 Model limitations 55

3.4 Conclusions and Recommendations for Future Work 58

Chapter 4. Anthropogenic influence on tropospheric reactive bromine since the preindustrial: implications for ice-core bromine trends 61

4.1 Introduction 62

4.2 Methods 64

4.2.1 GEOS-Chem model and historical simulations 64

4.2.2 Ice-core Bromine and Acidity Observations 66

4.3 Results 67

4.3.1 Ice-core bromine records at Akademii Nauk 67

4.3.2 Ice-core-model comparison 70

4.3.3 Factors controlling modeled bromine trends 72

4.4 Discussion 74

4.5 Conclusions 75

Chapter 5. Conclusions and Future Work 77

5.1 Conclusions 77

5.2 Future Work 79

Bibliography 81

Appendix A 117

Appendix B 138

Appendix C 153

..... 153

LIST OF FIGURES

Figure 1.1. A schematic diagram of the tropospheric halogen cycles. X=Cl, Br, I. 2
Figure 2.1. Annual concentrations of Na, Cl, Cl_{exc}, and acidity of the six ice cores in Greenland. 14
Figure 2.2. Relationships between annual ice-core (a and b) Na and Cl concentrations, and (c and d) snow acidity and Cl_{exc} from the six Greenland ice-core records. 15
Figure 2.3. 30°–90°N regional distributions of annual-mean surface mixing ratios of Cl_y in the three-time periods in GEOS-Chem 16
Figure 2.4. Model-observation comparison of non-SSA chlorine and model interpretation of the trends. 19
Figure 3.1. Location of the six ice cores used in this study. 31
Figure 3.2. Total bromine concentration (left), Br_{exc} (middle), and Br_{enr} (right) in the Akademii Nauk (AN), ACT_11d, Summit, Tunu, NGT_B19, and NEEM_2011_S1 ice cores.42
Figure 3.3. Ice-core records and trend analysis of (a) Br_{exc} and (b) Br_{enr} since year 1750 from the Akademii Nauk ice core. 43
Figure 3.4. Simulated Arctic spatial distribution of annual mean (a) snowpack emission fluxes of bromine (Br_2+BrCl), and (b) post-depositional loss calculated as the percentage of snowpack bromine emission fluxes (Br_2+BrCl) divided by total bromine deposition (dry + wet) from the three simulations, SURF, mToyota, and DEEP. 47
Figure 3.5. Modeled monthly mean snowpack (a) total bromine (Br_2 + BrCl) emission fluxes and (b) post-depositional loss in percentage at the six ice-core sites from the three simulations for year 2007: SURF, mToyota, and DEEP, and the DEEP simulation for year 2008.50
Figure 3.6. Comparison between the modeled hourly surface BrO concentrations at Summit during May–June in 2007 54
Figure 4.1. Total sodium, total bromine, Br_{exc}, and acidity concentrations in the Akademii Nauk ice-core. 67

Figure 4.2. Relationship between concentrations of a) total Br and acidity, and b) Br_{exc} and acidity from the AN ice core, for 1750–1850 (pre-1850), 1940–1999 (post-1940), and 1750–1999 (full record). 69
Figure 4.3. Modeled bromine burden and speciation in the three time periods and model-ice-core comparison. 70
Figure 4.4. Modeled annual mean sources and sinks of tropospheric a) Br_y b) HOBr c) $BrNO_3$ and d) BrCl in the AN TRJ for PI, PA, PD. 73

LIST OF TABLES

Table 3.1. Locations and Other Information for the Six Ice Cores Presented in This Study 32

Table 3.2. Comparison of Key Model Settings Conceived by Toyota et al. (2011) and the Three Model Simulations (mToyota, SURF, and DEEP) in This Study..... 37

Table 3.3. Annual Mean Snowpack-Air Exchange Fluxes of Total Bromine (Total Deposition, Emission, Net Upward Flux, and Post-Depositional Loss) at the Six Ice Core Locations Calculated from the SURF and DEEP Simulations..... 48

ACKNOWLEDGEMENTS

First, I would like to thank my PhD advisor Becky. Becky is the best advisor I can ask for. She encourages and inspires me to do great research and stay focused, and she trained me to be more confident and effective in presenting and communicating science. She always makes time for her students and prioritizes our needs, supporting me in every way she can, especially during the difficult times in the pandemic and the last few months before my defense. Thank you, Becky, for everything. I also greatly appreciate my committee members, Lyatt, Joel, Alex T., and my GSR TJ. Thank you for always making time for me amidst your busy schedules and consistently providing insightful feedback on my work. This work has greatly benefited from my collaborators in both the ice core and modeling communities. A special thanks to Joe McConnell and his lab at DRI for providing me with the precious ice-core halogen records to study. Xuan Wang and Thomas Sherwen's pioneering halogen modeling work have laid solid foundation for me to conduct my project. The GEOS-Chem support team and Viral Shah have helped me tremendously in learning, debugging, and developing GEOS-Chem. Koji Fujita has helped me with the back trajectory analysis.

The Alexander group has been a huge inspiration for me through my PhD journey, we encouraged, helped, and cheered for each other, and I learnt so much from each one of you. I thank my wonderful cohort 2017, I am incredibly grateful for our friendship since our 1st year, and so many fun memories we had together. I feel lucky to be able to study and work in the UW department of

Atmospheric Sciences, which is not only a great place to do science, but also a great community to make friends and get inspired.

I thank my friends here in Seattle for keeping me company and always being there for me. I thank my parents, who have always supported me to chase my dreams. I thank my husband Leo, for loving and supporting me, and for making me a home away from home. I thank our cats, Pillow and Boba, for bringing so much joy into our lives.

DEDICATION

This work is dedicated to my husband Leo, and my parents.

Chapter 1. INTRODUCTION

1.1 MOTIVATION AND SCIENTIFIC GOALS

Tropospheric reactive chlorine and bromine species play important roles in regulating tropospheric oxidation capacity through catalytic depletion of ozone and shifting HO_x (= OH + HO_2) and nitrogen oxides (NO_x = NO + NO_2) ratios (von Glasow et al., 2004; Sherwen et al., 2016). They are also important oxidants for reduced species like methane, volatile organic compounds, and mercury, and thus have profound implications for air quality (Gunthe et al., 2021), climate (Hossaini et al., 2016; Li et al., 2022; Saiz-Lopez et al., 2023), and eco-systems (Holmes et al., 2010; Brooks et al., 2011).

Ice core halogen records preserve information from the past and provide insights on the impacts of anthropogenic and natural forcing on tropospheric halogens. Figure 1.1 shows a schematic diagram of tropospheric halogen cycles. The largest source of tropospheric reactive chlorine is acid displacement on sea salt aerosol (Graedel and Keene, 1995; Finlayson-Pitts, 2003). The largest source of tropospheric reactive bromine is the acid-catalyzed debromination reaction ($HOBr + Br^- + H^+ \rightarrow Br_2 + H_2O$) from sea salt aerosol (Kerkweg et al., 2008; Yang et al., 2005). This process is influenced by anthropogenic emissions of acidic gas precursors such as sulfur dioxide (SO_2) and NO_x. Direct emissions of HCl and HBr from coal burning and waste incineration, as well as gaseous and aerosol phase bromine from leaded gasoline usage before the 1970s, can also be important sources for ice core halogens (Legrand et al., 2002; Legrand et al., 2021). Recent model developments on tropospheric halogen chemistry in global models (e.g. GEOS-Chem) made it possible to identify and quantify key drivers in ice core halogen trends, however, the relative importance of anthropogenic impacts compared to natural forcing that

influences sea salt aerosol emissions (e.g. sea ice extent) and the artifacts associated with dechlorination and debromination on Arctic ice core chlorine and bromine records since the pre-industrial has not yet been explored.

The scientific goals of my Ph.D. project are to explore the observed trends in Arctic ice core chlorine and bromine, and to evaluate the processes and importance of anthropogenic emissions in driving these trends. Using GEOS-Chem model and six Arctic ice cores, ice core chlorine records since preindustrial were statistically analyzed, and key processes driving the chlorine trends were identified (Chapter 2); An empirical representation of snowpack bromine emission is implemented in the model to evaluate the extent of post-depositional loss of ice core bromine, and I identified one ice core location that is expected to have significant bromine preservation (Chapter 3); For this one location with relatively good bromine preservation, bromine trends since pre-industrial are analyzed and attributed based on model historical simulations (Chapter 4).

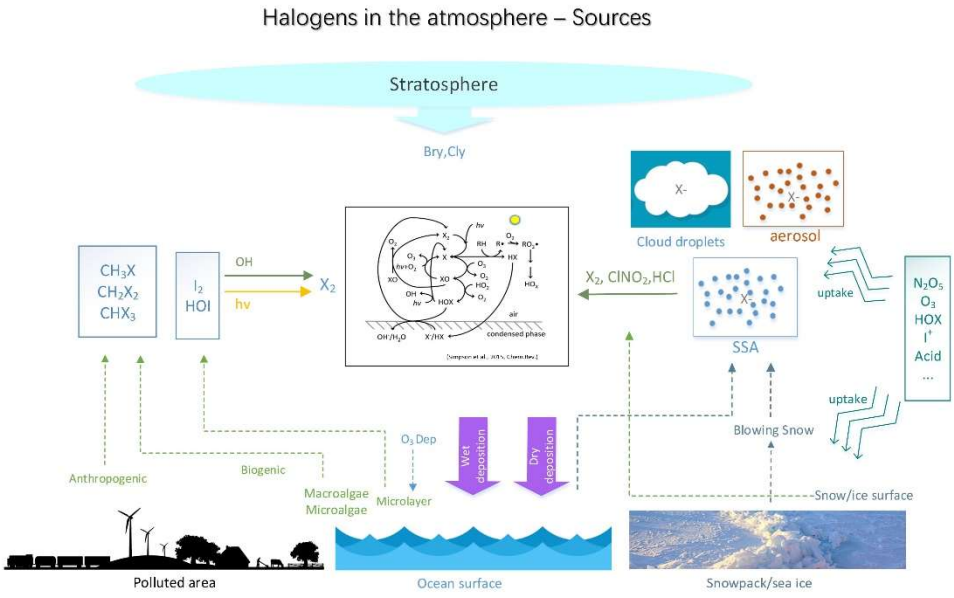

Figure 1.1. A schematic diagram of the tropospheric halogen cycles. X=Cl, Br, I.

1.2 BACKGROUND

The importance of halogen radicals was first recognized in the 1970s when scientists discovered the role of halogen catalytic cycles in destroying stratospheric ozone (Stolarski and Cicerone, 1974; Crutzen, 1974; Molina and Rowland, 1974). Not until a decade later, in the midlate 1980s, ozone depletion events (ODEs) were observed in the high Arctic lower troposphere and the anti-correlation between ozone and filterable bromine was discovered (Barrie et al., 1988), leading to the wide recognition and interest in tropospheric reactive halogen chemistry.

Halogen radicals destroy tropospheric ozone via catalytic cycles (R1–3), and ozone is the major precursor of the most important atmospheric oxidant, hydroxyl radical (OH), which regulates the lifetime of many chemical species. Halogen radicals are also oxidants themselves, influencing the formation of particles (von Glasow and Crutzen, 2004), oxidation of volatile organic compounds like methane (Allan et al., 2007) and aldehydes (Atkinson et al., 2004), dimethylsulphide (DMS) (Chen et al., 2017), and toxins like mercury (Steffen et al., 2008). Therefore, tropospheric reactive halogens have profound impacts on the oxidation capacity of the atmosphere, as well as the climate.

$$X_2 + h\vartheta \rightarrow 2X \quad \text{(R1)}$$

$$X + O_3 \rightarrow XO + O_2 \quad \text{(R2)}$$

$$2XO \rightarrow X_2 + O_2 \quad \text{(R3)}$$

1.3 ICE CORE RECORDS OF CHLORINE AND BROMINE

The majority of tropospheric reactive chlorine and bromine species (93% and 95%, respectively) are from sea salt aerosol (Wang et al., 2021), which originates from bubble bursting during wave breaking over open ocean (Blanchard,1983; Monahan et al.,1986; de Leeuw et al., 2011), as well

as sublimation of blowing snow in polar regions (Nishimura and Nemoto, 2005; Savelyev et al., 2006; Yang et al., 2008). Freshly emitted sea salt aerosol contains chlorine and bromine similar to sea water composition. As aerosol ages in the acidic atmosphere, chlorine and bromine species can be released from sea salt aerosol via acid displacement (R4–5) and debromination (R6) reactions, respectively. These processes are heavily modulated by anthropogenic emissions of acidic gas precursors.

$$Cl^- + HNO_3 \leftrightarrow HCl + NO_3^- \quad \text{(R4)}$$

$$Cl^- + H_2SO_4 \leftrightarrow HCl + HSO_4^- \quad \text{(R5)}$$

$$HOBr + Br^- + H^+ \rightarrow Br_2 + H_2O \quad \text{(R6)}$$

Ice core chlorine and bromine has been shown to be linked to both sea ice extent and anthropogenic emissions (Legrand et al., 2002; Pasteris et al., 2014; Legrand et al., 2021), with the latter including direct chlorine and bromine emissions from coal combustion and waste incineration (Lee et al., 2008; Kolesar et al., 2018; Y. Liu et al., 2018), as well as indirect influences on sea salt acid-displacement and debromination modulated by anthropogenic acidity. Sea ice has changed significantly since at least 1980, decreasing in total extent and becoming younger, saltier, and thinner in the Arctic (Confer et al., 2023). Anthropogenic emissions, especially coal combustion emitted acid precursors (SO_2, NO_x), rose with the onset of Industrial Revolution (especially after the 1940s) and declined steadily in North America and Western Europe due to the wide application of emission control technologies such as flue-gas desulphurization (FGD) and selective catalytic reactors (SCRs) (Fedkin et al., 2019; Paulot et al., 2017; etc.). As a co-benefit these technologies also effectively removed gas phase HCl and HBr (Lee et al., 2004; McCulloch et al., 1999).

1.4 SNOWPACK BROMINE PRODUCTION

Snowpack production of dihalogen species such as Br_2, BrCl has been observed in polar regions (Foster et al, 2001). Outdoor snow-chamber experiments (Pratt et al., 2013) revealed that certain conditions favor the snowpack production of Br_2, including low pH, high snow Br/Cl ratio, and the presence of ozone. These studies motivated later modeling efforts in simulating snowpack bromine emissions and its impacts on near-surface BrO and ozone depletion (Thomas et al., 2011; Toyota et al., 2011; Toyota et al., 2014; Swanson et al., 2022). Chlorine loss from the snowpack is shown to be negligible for ice core sites with snow accumulation rates greater than 40 kg m^{-2} yr^{-1} (Röthlisberger, 2003), and in the Antarctic, re-emission of bromine from snowpack is shown to be highly related to snowfall rate (McConnell et al., 2017). However, in the Arctic, no clear threshold of snowfall rate is identified to be 'safe' for snowpack bromine re-emissions before burial in the Arctic, and consideration of bromine post-depositional loss has been neglected in previous studies interpreting ice core bromine trends (Maselli et al., 2017; Spolaor et al., 2016; etc.).

1.5 SUMMARY OF WORK

This Ph.D. project investigates the impact of anthropogenic emissions on ice core chlorine and bromine trends since the pre-industrial, with halogen records from multiple Arctic ice cores and model development and historical simulations using GEOS-Chem. The first part of the project (Chapter 2) focus on the model-aided interpretation of chlorine trends in six Greenland ice cores. The second part of the project (Chapter 3) implements snowpack bromine release mechanism in GEOS-Chem, and examines the extent of bromine post-depositional loss from snowpack and its implications on ice core bromine preservation. Based on that, the third part of the project (Chapter

4) investigates bromine trends from a Russian Arctic ice core, and explores the implications of anthropogenic emissions on ice core bromine trends.

1.6 PUBLICATION PLANS

Chapter 2 has been published in Geophysical Research Letters (Zhai et al., 2021). Chapter 3 has been published in Journal of Geophysical Research: Atmospheres (Zhai et al., 2023). Chapter 4 is in preparation to be submitted for publication to Geophysical Research Letters in the near future.

Chapter 2. ANTHROPOGENIC IMPACTS ON TROPOSPHERIC REACTIVE CHLORINE SINCE THE PREINDUSTRIAL

This Chapter has been published in Geophysical Research Letters.

Zhai, S., Wang, X., McConnell, J. R., Geng, L., Cole-Dai, J., Sigl, M., Chellman, N., Sherwen, T., Pound, R., Fujita, K., Hattori, S., Moch, J. M., Zhu, L., Evans, M., Legrand, M., Liu, P., Pasteris, D., Chan, Y.-C., Murray, L. T., & Alexander, B. (2021). Anthropogenic impacts on tropospheric reactive chlorine since the preindustrial. *Geophysical Research Letters*, *48*(14). doi: 10.1029/2021gl093808

Abstract

Tropospheric reactive gaseous chlorine (Cl_y) impacts the atmosphere's oxidation capacity with implications for chemically reduced gases such as methane. Here we use Greenland ice-core records of chlorine, sodium, and acidity, and global model simulations to show how tropospheric Cl_y has been impacted by anthropogenic emissions since the 1940s. We show that anthropogenic contribution of nonsea-salt chlorine significantly influenced total chlorine and its trends after the 1940s. The modeled regional 170% Cl_y increase from preindustrial to the 1970s was driven by acid displacement from sea-salt-aerosol, direct emission of hydrochloric acid (HCl) from combustion, and chemical reactions driven by anthropogenic nitrogen oxide (NO_x) emissions. Since the 1970s, the modeled 6% Cl_y decrease was caused mainly by reduced anthropogenic HCl emissions from air pollution mitigation policies. Our findings suggest that anthropogenic

emissions of acidic gases and their emission control strategies have substantial impacts on Cl_y with implications for tropospheric oxidants, methane, and mercury.

2.1 INTRODUCTION

Chlorine (Cl) in polar ice cores can provide information about past SSA abundance since the main source of ice-core Cl is from the emission and transport of sea-salt-aerosol (SSA). Reactive gaseous chlorine

(Cl_y = BrCl + HCl + Cl + ClO + HOCl + $ClNO_3$ + $ClNO_2$ + ClOO + OClO + 2 · Cl_2 + 2 · Cl_2O_2 + ICl) from anthropogenic emissions, mainly in the form HCl, may also be a significant source of ice-core Cl (Legrand et al., 2002; Pasteris et al., 2014). The impact of anthropogenic emissions on tropospheric reactive chlorine since the preindustrial has not been quantified. Formation of HCl through acid displacement on SSA is thought to be the largest (85%) source of Cl_y in the troposphere (X. Wang et al., 2019), and is influenced by anthropogenic emissions of acid gas precursors such as sulfur dioxide (SO_2) and nitrogen oxides (NO_x = NO + NO_2). HCl is also emitted directly from combustion, mainly coal (Fu et al., 2018; Keene et al., 1999; Kolesar et al., 2018; Y. Liu et al., 2018; McCulloch, Aucott, Benkovitz et al., 1999; McCulloch, Aucott, Graedel et al., 1999). HCl contributes to acid deposition, causing damage to lakes and ecosystems, altering atmospheric acidity (Evans et al., 2011), and leads to severe haze and fog through cocondensation on aerosol (Gunthe et al., 2021). Oxidation of HCl and sea-salt chloride ($_{SSA}Cl^-$) produces more reactive forms of chlorine species, such as the chlorine radical (Cl•) (Bryukov et al., 2006), nitryl chloride ($ClNO_2$) (Finlayson-Pitts et al., 1989; Kercher et al., 2009; Raff et al., 2009), and hypochlorous acid (HOCl) (Watson, 1977). Despite the much lower abundance, these highly reactive chlorine species has potentially large local influence for ozone (Finlayson-Pitts, 2003; Knipping & Dabdub, 2003), nitrogen oxides (Haskins et al., 2019;

Thornton et al., 2010), secondary organic aerosol (Choi et al., 2020), methane (Allan et al., 2007; Platt et al., 2004), non-methane hydrocarbons (Aschmann & Atkinson, 1995; Pszenny et al., 2007), and elemental mercury (Donohoue et al., 2005; Horowitz et al., 2017). Anthropogenic emissions and acid displacement of HCl can lead to enrichment or depletion of Cl relative to sodium (Na) compared to their ratio in sea water, denoted as Cl_{exc} (Equation 2 in Methods). Legrand et al. (2002) calculated ice-core HCl after removing sea-salt and continental chloride from the measured total chloride, and attributed the increases in alpine ice cores to enhanced coal combustion and waste incineration in western Europe during 1925–1970. Observations show decreasing trends of non-SSA Cl^- deposition over the past 20–30 years in the US (Haskins et al., 2020) and UK (Evans et al., 2011), suggesting that the post-1970s air pollution mitigation policies targeting SO_2 and NO_x emissions have reduced emissions of HCl. At Summit (central Greenland), Legrand et al. (2002) found that Cl_{exc} originates mainly from acid displacement of HCl from SSA, which increased by a factor of 2–3 over the twentieth century due to enhanced aerosol acidity resulting from growing anthropogenic NO_x and SO_2 emissions. Greenland ice-core records of sulfate and nitrate, the main sinks for NO_x and SO_2, show increases beginning in the 1900s, peaking in the 1970s, followed by a rapid decline in sulfate and a more gradual decline in nitrate (Geng et al., 2014), consistent with trends of anthropogenic SO_2 and NO_x emissions from combustion (Smith et al., 2011).

2.2 METHODS

2.2.1 *Ice-Core Records*

We present ice-core chlorine, sodium, and acidity records from the six Greenland ice cores (Figure A1). Precise locations and other information are summarized in Table A1, and details on core

extraction and dating are described in previous publications (Geng et al., 2014; Iizuka et al., 2018; McConnell et al., 2019; Opel et al., 2013; Spolaor et al., 2016). Measurements of ice-core Na and Cl were using either a continuous flow analysis with an online ion chromatography system (CFA-IC) with an accuracy of 5% at annual resolution (for Summit07) (Geng et al., 2014; Iizuka et al., 2018), or Inductively Coupled Plasma Mass Spectrometry (ICP-MS) (McConnell et al., 2014; Spolaor et al., 2016) with an uncertainty of ±10% (for NEEM, NGT_B19, Tunu, ACT_11d and Summit10). For NEEM, NGT_B19, Tunu, ACT_11d and Summit10 cores, acidity (H^+) was measured directly using a flow-through bubbling chamber method described in Pasteris et al. (2012), with an error less than 5%. For Summit07 ice core, acidity was calculated based on the ion balance, according to Equation 1:

$$\left[H^+\right] = \left[Cl^-\right] + \left[NO_3^-\right] + \left[SO_4^{2-}\right] - \left[Na^+\right] - \left[NH_4^+\right] - \left[K^+\right] - \left[Mg^{2+}\right] - \left[Ca^{2+}\right] \quad (1)$$

with concentrations in units of μeq L^{-1} (Geng et al., **2014**). Note that this calculation may underestimate snow acidity because it does not consider organic-acid anions (e.g., formate and acetate), which were measured to be 0.3 ± 0.1 μM at Summit during 1767–1945 (Legrand & Mayewski, **1997**).

To separate the contribution of SSA relative to more reactive forms (e.g., HCl) of Cl, we calculated the chlorine excess (Cl_{exc}) relative to what would be expected from SSA alone, which is defined with a sea water Cl/Na mass ratio ($([Cl]/[Na])_{sea\ water}$) of 1.796 (Riley & Tongudai, 1967) (Equation 2):

$$Cl_{exc} = \left[Cl\right]_{ice\ core} - \left(\left[Cl\right]/\left[Na\right]\right)_{sea\ water} \times \left[Na\right]_{ice\ core} \quad (2)$$

ICP-MS measurements may lead to an underestimate of Cl_{exc} because it measures both the soluble Na and the insoluble Na fraction which may originate from nonsea-salt aerosol (e.g., dust), whereas IC measures the soluble Na and a small fraction of leachable Na from dust.

To analyze the relationship between measured species in the ice cores, we adopt the Passing-Bablok (PB) regression model (Passing & Bablok, **1983**). In contrast to the traditional Ordinary Least Squares regression (OLS) which only considers measurement errors on the *y*-axis variable, PB regression assumes both *x*-axis and *y*-axis variables contain measurement errors and is insensitive to outliers (e.g., due to volcanic eruptions). We use the Pearson's correlation coefficient (*r*) to show the relationships between species, and *r* is not affected by the choice of the regression model.

2.2.2 *GEOS-Chem simulations*

To estimate impacts of anthropogenic emissions on tropospheric HCl and reactive chlorine abundances, we use a global 3-D chemical transport model GEOS-Chem (version 11-02d, Text A1) described in Bey et al. (2001) with updates described in the supporting information. The model is driven by MERRA-2 assimilated meteorological observations from the Goddard Earth Observing System (GEOS) (Gelaro et al., 2017). The model simulates detailed HOx-NOx-VOC-ozone-halogen-aerosol tropospheric chemistry, which includes SSA (Jaeglé et al., 2011) and tropospheric gas-phase, liquid-phase, and heterogeneous-phase reactive chlorine chemistry (X. Wang et al., 2019), and fully coupled stratospheric chemistry (Eastham et al., 2014).

Model simulations are performed using three emission scenarios: preindustrial (PI, year 1750), peak atmospheric acidity (PA, year 1975), and present day (PD, year 2007), as summarized in Text A1 and Table A2. We run each simulation for 5 years to equilibrate stratosphere-troposphere exchange, and use only the fifth year for analysis. All simulations are conducted at 4° × 5° horizontal resolution and 72 vertical levels up to 0.01 hPa. We use MERRA-2 meteorological fields of the same year (2007) for all three simulations to isolate changes induced by anthropogenic emissions. This configuration will also keep emissions that are dependent on meteorological

parameters, such as wind-blown dust, lightning and soil NOx, biogenic VOCs, and SSA from the open ocean and sea-ice, constant. Only anthropogenic and biomass-burning emissions are allowed to vary between simulations in order to isolate their impacts on tropospheric chlorine.

2.2.3 *Backward Trajectory Analysis*

To determine the source regions of Cl_y at the six Greenland ice-core sites, we run backward trajectory analysis using the HYSPLIT model (Hybrid Single-Particle Lagrangian Integrated Trajectory) (Stein et al., 2015). We calculate the cumulative air mass probability for the 5-day backward trajectories, considering the modeled lifetime of acidic gases (e.g., SO_2 and NO_x of about 1 day), accumulation-mode aerosol (up to 6 days) (Alexander et al., 2005), and gas phase HCl (2.5 days), as well as possible seasonal variations in transport. To retrieve the source regions across the ice-core covered time periods, we conduct the backward trajectory analysis for 1959–2010, and present the averaged results. Initial altitudes of air masses are at 10, 500, 1,000 and 1,500 m above ground level (a.g.l.), and the calculation was constrained within 1,500 m a.g.l., which was assumed to be the depth of the mixing layer. Daily precipitation from the reanalysis data sets (ERA-40 and ERA-Interim (Dee et al., 2011; Uppala et al., 2005)) was used for weighting the probability of air masses. Considering the proximity of the two Summit cores, and Tunu and NGT_B19, we only conduct the analysis for four locations: NEEM, Tunu, ACT_11d, and Summit, and chose a region that covers most of the backward trajectory probabilities as the backward trajectory region (TRJ) (Figure A2).

2.3 RESULTS

2.3.1 *Ice-Core Observations*

Figure 2.1 shows annual concentrations of Na, Cl, Cl_{exc}, and acidity from six Greenland ice cores (Figure A1). Positive mean Cl_{exc} values (1.0–5.9 ng g^{-1}) over the reported time periods (1750 or 1776–end of the records) in all records are consistent with negligible loss of HCl from the snowpack after atmospheric deposition where snow accumulation rates are greater than 40 kg m^{-2} yr^{-1} (Röthlisberger, 2003) (Table A1). Cl_{exc} represents a higher fraction of total Cl in lower latitude (medians of 9%–49% over the full records) compared to higher latitude ice cores (medians of 8%–17% over the full records) (Figure A3) likely due to closer proximity to North American (NA) and Western European (WE) anthropogenic source regions, as determined by back trajectory analysis (Figure A2). For all ice cores, Cl_{exc} records show no trends before 1940, followed by a twofold to sevenfold increase until ~1975. After 1975, Cl_{exc} either declined (Summit07, ACT_11d) or leveled off (Summit10, Tunu, NEEM, and NGT_B19). ice-core acidity is similar to Cl_{exc}, with no long-term trends before the 1900s (lower latitude cores) or 1940s (higher latitude cores), an increase from 1940 to 1975, followed by a leveling off or decrease. Acidity trends are consistent with previous Greenland ice-core sulfate records (Geng et al., 2014) and trends in anthropogenic sulfur emissions in NA and WE (Smith et al., 2011).

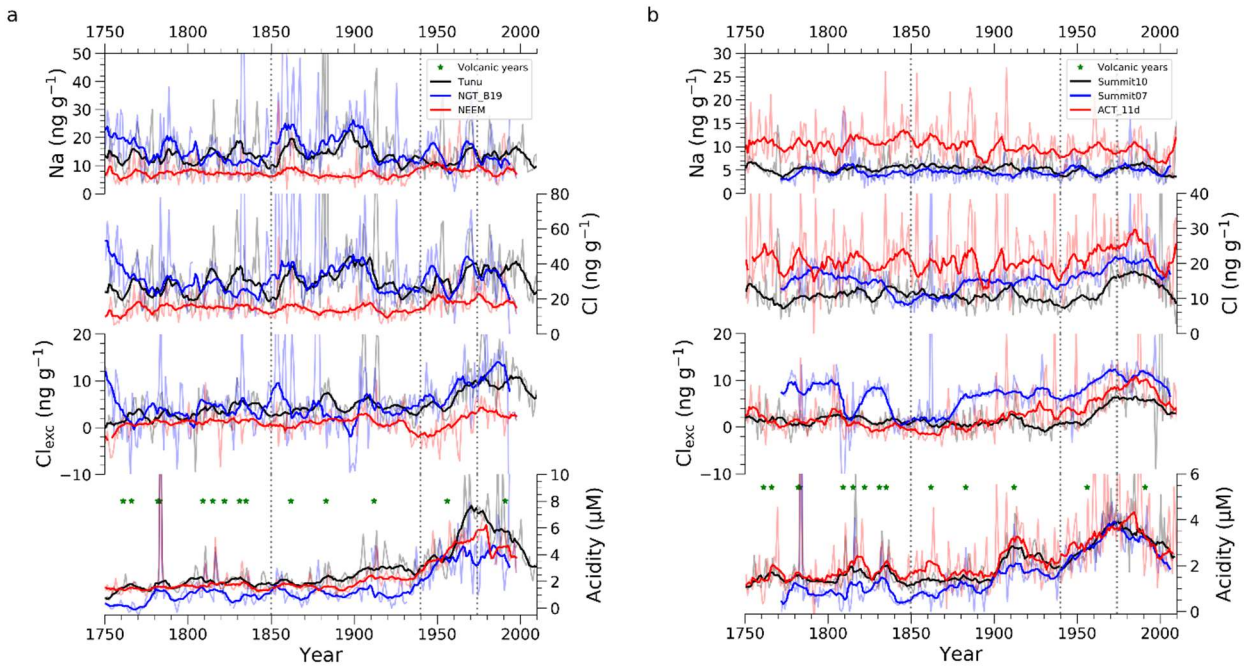

Figure 2.1. Annual concentrations of Na, Cl, Cl_{exc}, and acidity of the six ice cores in Greenland. (a) Records from higher latitude Greenland ice cores Tunu (black), NGT_B19 (blue), and NEEM (red). (b) Records from lower latitude Greenland ice cores Summit10 (black), Summit07 (blue), and ACT_11d (red). Gray, light blue, and pink lines represent the annual-mean concentrations. Black, blue and red lines represent the 9-years running average concentrations after removing the outliers that are outside of 1.5 × IQR (interquartile range). Green stars mark volcanic eruption years (Text S2). Ion concentrations are reported for Summit07, whereas elemental concentrations are reported for other ice cores. Vertical gray dotted lines mark the years 1850, 1940, and 1975.

Figure 2.2 and Table S3 show relationships between annual ice-core Na and Cl, and between ice-core acidity and Cl_{exc}. Na and Cl were strongly correlated in all ice cores, with a stronger relationship in higher latitude (r = 0.86–0.94) compared to lower latitude (r = 0.49–0.80) cores. Continued strong correlation after the 1940s (Table S3) suggests that SSA was the dominant source of chlorine throughout the records. Correlations between acidity and Cl_{exc} were stronger in post-1940s (r = 0.33–0.72), compared to pre-1940s (r = −0.02–0.43) when acidity was relatively low (Table S3). Lower latitude cores show a higher correlation (r = 0.67–0.72) post-

1940s than higher latitude cores (r = 0.33–0.38) due to their closer proximity to anthropogenic source regions.

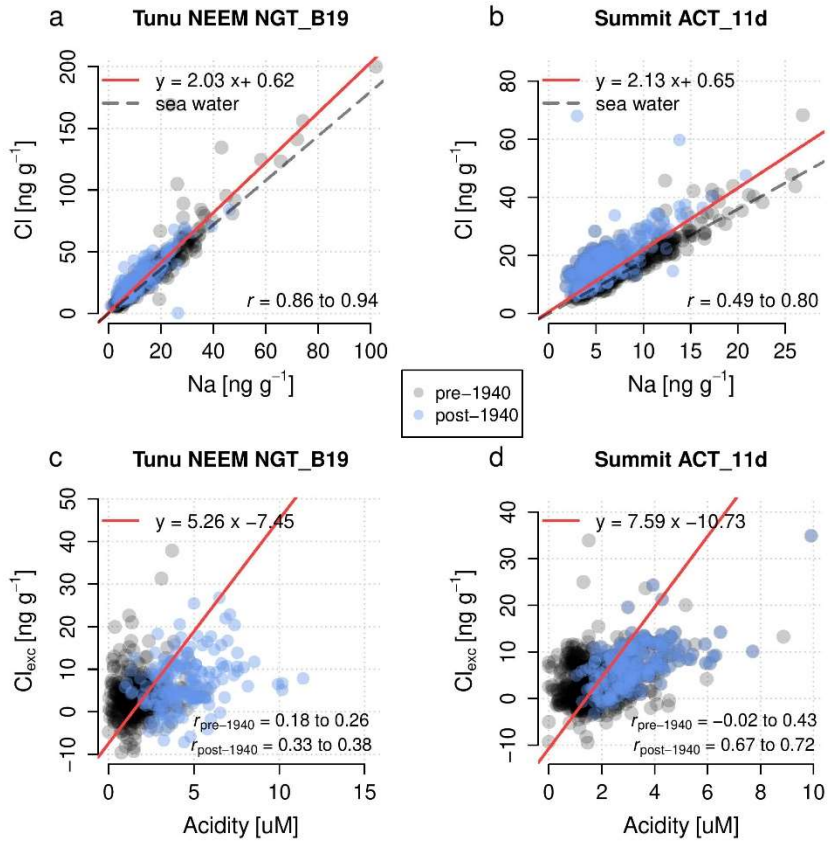

Figure 2.2. Relationships between annual ice-core (a and b) Na and Cl concentrations, and (c and d) snow acidity and Cl_{exc} from the six Greenland ice-core records. (a and c) Higher latitude cores including Tunu, NEEM, NGT_B19, (b and d) the lower latitude cores including Summit07, Summit10, and ACT_11d. Black circles are the pre-1940 record and blue circles represent post-1940 records. Red lines and the equation show the PB regression for the full record. Dashed black lines show the relationship between Na and Cl in sea water. r, $r_{pre\text{-}1940}$, and $r_{post\text{-}1940}$ represent, respectively, the Pearson's correlation coefficients for the full records, pre-1940 and post-1940 records, and the range of r values is from individual ice cores in the group. Outliers outside the 1.5 × IQR (interquartile range) are removed. All r values are significant with p values lower than 0.05.

2.3.2 *Model-Observation Comparisons*

Figure 2.3 shows the 30°–90°N regional distribution of modeled annual-mean surface Cl_y in PI, PA, and PD, where the model considers past changes in anthropogenic emissions (Methods, and Text A1). Surface Cl_y is shown because most tropospheric Cl_y is confined to lower altitudes (2 km) due to the dominance of direct surface emissions and near-surface chemistry sources (Figure A4). The highest surface Cl_y concentrations in PA and PD are distributed in continental outflow regions where anthropogenic acids encounter $_{SSA}Cl^-$, leading to acid displacement of HCl. The tropospheric burden of Cl_y in the 30°–90°N region increased 132% from PI to PA and 7% from PA to PD. While surface Cl_y increases everywhere in the region from PI to PA and PI to PD, the trend from PA to PD shows spatial variability that is, consistent with regional trends in anthropogenic emissions of SO_2 and NO_x.

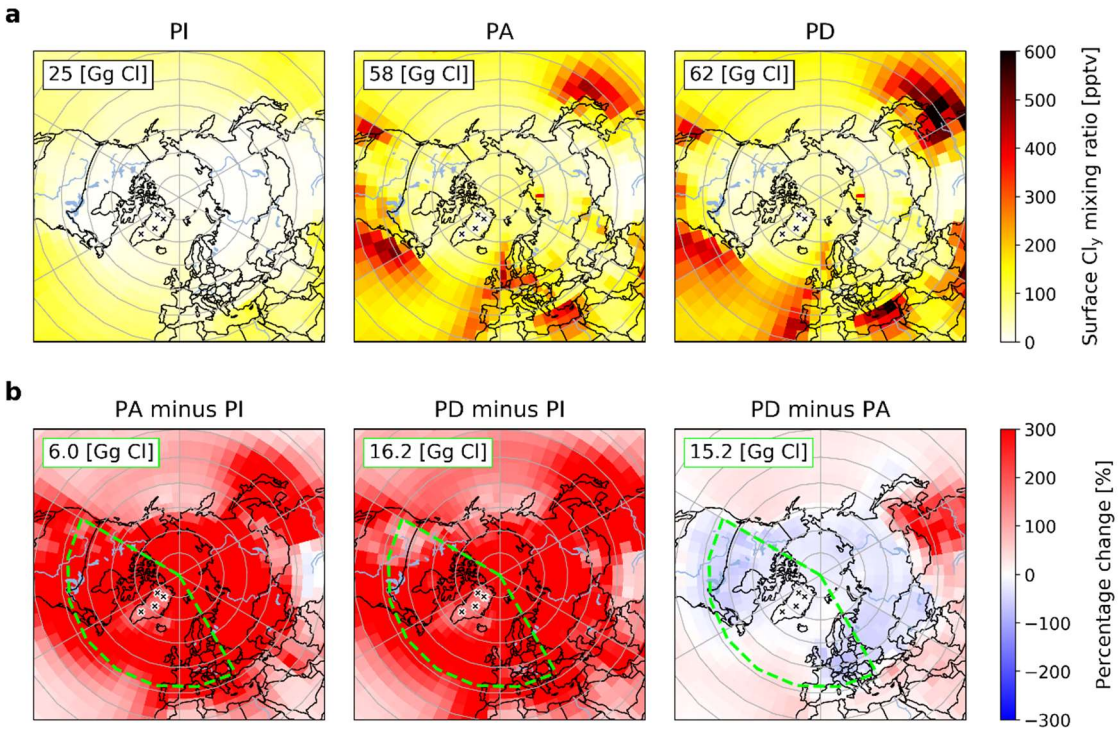

Figure 2.3. 30°–90°N regional distributions of annual-mean surface mixing ratios of Cl_y in the three-time periods in GEOS-Chem (a), and the percentage difference of Cl_y surface mixing

ratio between the three-time periods (b). Gray grid lines show 10° latitude and 60° longitude distance. Black crosses mark the ice-core sites. Dashed green lines show the back trajectory region (TRJ, 120°W–30°E, 42°–90°N) for the six Greenland ice cores based on the 5-day back trajectory analysis. The annual-mean tropospheric Cl_y burdens for 30°–90°N regions are shown on the top-left corners of subplots in (a), and the burdens for the TRJ region are shown similarly in (b).

The simulated trends in Cl_y in the calculated 5-day back trajectory region (TRJ, green dashed region in Figure 2.3) are qualitatively consistent with and within the ranges of the observed trends in Greenland ice-core Cl_{exc} (Figure 2.4a). On average, the modeled Cl_y burden in TRJ increased by 170% from PI to PA, and decreased by 6% from PA to PD. From PI to PA, ice-core Cl_{exc} showed increases ranging from 105% to 631%, with an average increase of 335%. Although modeled average trends from PI to PA lie below the 25th percentile of observations, the modeled increase in Cl_y in continental outflow regions of NA (276%) and WE (203%) lie within the interquartile range (IQR) of the observations, suggesting that trends in chlorine deposition in inland Greenland may be more influenced by these source regions. From PI to PD, the simulated average TRJ Cl_y increased 153%, similar to the median increase (163%) in the observations, and was within the IQR range of the ice-core trends. The average modeled trend (+153%) fell on the lower end of the observed range, but again the simulated trends in NA and WE continental outflow regions (223% and 185%, respectively) showed a more robust comparison with the average change in ice-core Cl_{exc} (253%). From PA to PD, most inland Greenland ice cores showed a decreasing trend in Cl_{exc}, with an average decrease of 20%, and a median decrease of 41%. The magnitude of the average modeled Cl_y trends from PA to PD in the TRJ region (−6%) was smaller than the average of ice-core observations, but the modeled changes in the NA and WE continental source regions (−13%) were more similar to the observations. The range of PA to PD changes in the model (−46% to 19%) fell within the range

of the ice-core observations (−114% to 102%). The modeled PI-to-PA (210%) and PA-to-PD (−25%) change in Cl_y at the location of the Col du Dome ice core in the French Alps also was qualitatively consistent with ice-core Cl_{exc} changes (383% from PI to PA, −71% from PA to PD) from Legrand et al. (2002). Model underestimation of the trends may be due in part to uncertainties in anthropogenic HCl emissions (Methods).

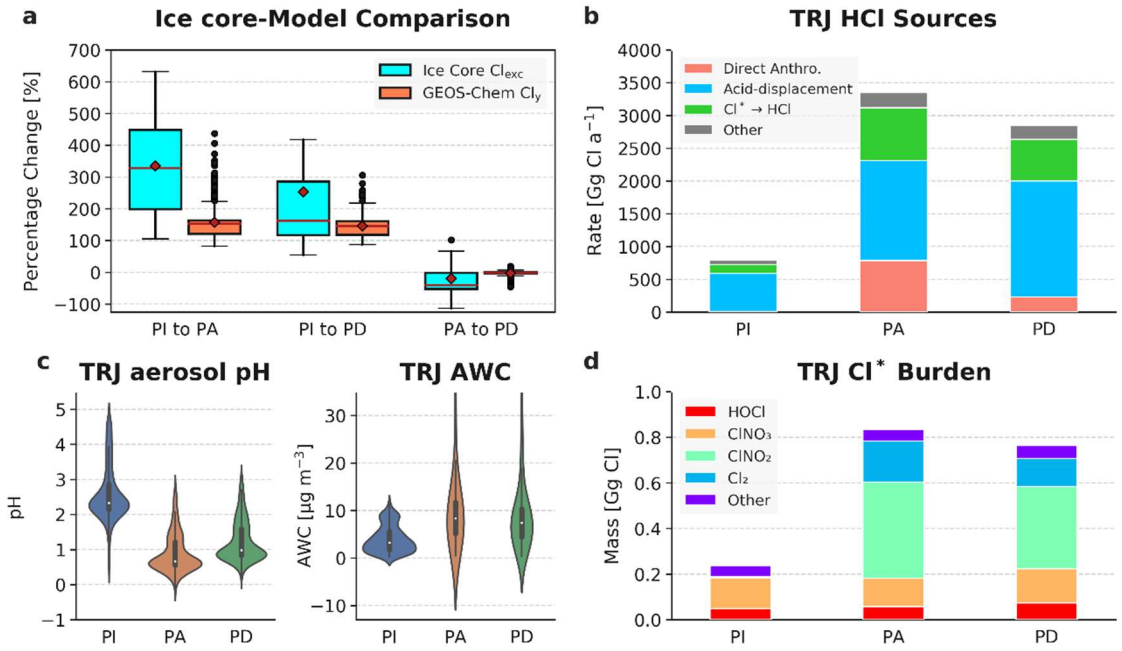

Figure 2.4. Model-observation comparison of non-SSA chlorine and model interpretation of the trends. (a) Comparison of percentage changes in the Cl_{exc} concentrations from the six Greenland ice cores (blue boxes) and modeled Cl_y burdens in TRJ (orange boxes) between PI, PA, and PD. ice-core statistics are calculated from 1750 to 1760 for PI, 1970–1980 for PA, and the last 10 years of the records for PD. Boxplots show the range of percentage changes, red diamonds mark the mean values and red lines represent the medians. Black dots are model grid boxes outside the range of 1.5 IQR. (b) Modeled HCl sources in TRJ for PI, PA, and PD. "Direct Anthro." refers to direct anthropogenic emissions of HCl. "Cl* → HCl" represents the net conversion of Cl* into HCl. "Other" sources include the stratosphere to troposphere exchange and transport from outside of TRJ (<7%), biomass burning (<2%), and HCl formed from organochlorines (<0.1%). (c) Violin plots for modeled accumulation-mode aerosol pH in TRJ (left panel) and aerosol water content (AWC) in TRJ for PI, PA, and PD. (d) Modeled annual-mean tropospheric Cl* burden (in Gg Cl) in TRJ for PI, PA, and PD. "Other" Cl* species include BrCl, Cl, ClO, ClOO, Cl_2O_2, and ICl.

2.3.3 *Anthropogenic Impacts on Reactive Gaseous Chlorine*

Simulated trends in Cl_y reflect trends in HCl, since >94% of the burden and 99% of deposition is of the form HCl (Figure A5). The dominant source of HCl in all three-time periods is acid

displacement of $_{SSA}Cl^-$, contributing 73%, 47%, and 61% to the total source in PI, PA, and PD, respectively (Figure 2.4b). Chemical reactions that convert Cl* (= Cl_y − HCl) to HCl is the second largest source (20%, 27%, and 26% in PI, PA, and PD, respectively). In PA, the Cl* source is closely followed by direct anthropogenic HCl emissions, which contributes 21% of the total source. Other sources are minor (<10%). The increase in HCl from PI to PA in the TRJ region (mean of 238%) is driven by increases in direct anthropogenic emissions of HCl (35%), acid displacement (29%), and heterogeneous reactions involving Cl* (29%). The 12% decrease in HCl from PA to PD is driven by decreases in the direct anthropogenic source of HCl (71%) and in conversion of Cl* to HCl (16%), and is partly compensated by a continued increase (15%) in acid displacement.

HCl acid displacement is controlled by thermodynamic equilibrium between gas phase (HCl) and aerosol phase ($_{SSA}Cl^-$). Lower aerosol pH and aerosol water content (AWC) both favor acid displacement of HCl (Haskins et al., 2018), but the relationship is nonlinear. At higher pH in PI, the equilibrium is more sensitive to pH than to AWC. At lower pH in PA and PD, AWC becomes more important (Haskins et al., 2018). From PI to PA, the mean aerosol pH in TRJ decreased 1.7 pH units, resulting in a large increase in HCl displacement despite the increase in AWC (223%) (Figure 2.4c). From PA to PD, continued increase in HCl displacement is driven by lower AWC in the PD relative to the PA. Although accumulation-mode aerosol pH increases slightly from PA to PD (0.3 pH units), the equilibrium is less sensitive to aerosol pH at the lower pH values during the PA and PD (Haskins et al., 2018) (Figure 2.4c).

The HCl source from Cl* chemistry originates from reactions between Cl• with hydrocarbons and the in-cloud reaction between dissolved SO_2 and HOCl (Figure A5). Trends in the Cl* source of HCl reflect trends in Cl* abundance. The Cl* burden increased by 252% from PI to

PA, and decreased by −9% from PA to PD in TRJ (Figure 2.4d). Enhanced formation of $ClNO_2$ (395-fold) from heterogeneous reaction of N_2O_5 with particulate chloride, driven by elevated NO_x emissions (Figure A6), dominates the increase in Cl* from PI to PA. The decrease in Cl* from PA to PD is caused by the decrease of $ClNO_2$ (−14%) and Cl_2 (−32%) from PA to PD due to less N_2O_5 in continental outflow regions (Figure A7) driven by a decrease in NO_x emissions (Figure A6), consistent with satellite observations (Kim et al., 2006; Konovalov et al., 2010).

Changes in $ClNO_2$ production from PI to PA and PA to PD drive changes in total Cl* abundance and in all individual Cl* species except Cl• (Figure A5). Opposite to the Cl* trends, Cl• abundance decreased 27% from PI to PA and increased 20% from PA to PD in the TRJ region. These changes are driven by their reactions with alkanes producing HCl (Figure A5 and Table A4). Enhanced emissions of alkanes from transportation and energy extraction (Hoesly et al., 2018) and increasing methane from PI to PA (Murray, 2016) increased conversion rate of Cl• to HCl, driving the Cl• decrease. From PA to PD, although methane levels continue to increase, anthropogenic emissions of alkanes in NA and WE decrease (Hoesly et al., 2018), resulting in an increase in Cl• from PA to PD. Changes in sink reactions of Cl• are driving the conversion of Cl* to HCl, which shows an increase from PI to PA and a decrease from PA to PD (Figure 2.4d).

2.4 Conclusions and Implications

This study investigates total and nonsea-salt chlorine (Cl_{exc}) trends since preindustrial time using six Greenland ice cores and examines the contribution of anthropogenic emissions to these trends using the GEOS-Chem model. Observed trends in inland Greenland ice-core Cl_{exc} are captured by historical model simulations that isolate the impact of changes in anthropogenic emissions while

holding meteorology constant. Model results indicate that from PI to PA, the increases in acid displacement of HCl from SSA, direct anthropogenic HCl emissions and enhanced Cl* production were responsible for the increasing trend in Cl_y. From PA to PD, acid displacement continued to increase, but was overcompensated by reduced direct anthropogenic HCl emissions and chemical conversion of Cl* to HCl. Although direct anthropogenic emissions of HCl represent <21% of the total HCl source, it is required to explain the decreasing trends in Cl_{exc} observed in ice cores since PA.

Cycling of Cl_y species can destroy O_3 directly through catalytic cycles, and indirectly through reducing NO_x abundance (X. Wang et al., 2019). Consequently, increases in Cl_y lead to decreases in OH due to reduction in ozone. The implications of Cl_y for ozone, OH and NO_x have been demonstrated previously (X. Wang et al., 2019). This study shows that anthropogenic emissions of HCl, SO_2 and NO_x have had significant impacts on tropospheric Cl_y abundance (up to +170%), which should be considered in the estimation of anthropogenic impacts on changes in tropospheric oxidation capacity.

In addition to the impact of Cl_y on oxidants such as OH, Cl• serves as an oxidant itself (Sherwen et al., 2016; X. Wang et al., 2019), with reactivity 1–2 orders of magnitude higher than OH in oxidizing alkanes (Atkinson et al., 2006; Finlayson-Pitts & Pitts, 1999; Ji et al., 2013; Xie et al., 2017; Young et al., 2014). Although a minor sink for methane, reaction with Cl• has a large impact on methane's isotopic composition (Strode et al., 2020), which is used to constrain the methane budget in present and past climates (Allan et al., 2001, 2007; Bock et al., 2017; Strode et al., 2020; Whiticar & Schaefer, 2007). Our model simulations suggest that anthropogenic emissions alone have changed the global Cl• abundance by up to −16% since preindustrial times,

which will influence the isotopic composition of methane and potentially the isotope-based interpretation of the methane budget.

Chapter 3. IMPLICATIONS OF SNOWPACK REACTIVE BROMINE PRODUCTION FOR ARCTIC ICE CORE BROMINE PRESERVATION

This Chapter has been published in Journal of Geophysical Research: Atmospheres.

Zhai, S., Swanson, W., McConnell, J. R., Chellman, N., Opel, T., Sigl, M., Meyer, H., Wang, X., Jaeglé, L., Stutz, J., Dibb, J. E., Fujita, K., & Alexander, B. (2023). Implications of snowpack reactive bromine production for Arctic ice core bromine preservation. Journal of Geophysical Research: Atmospheres, 128(20). doi: 10.1029/2023jd039257

Abstract

Snowpack emissions are recognized as an important source of gas-phase reactive bromine in the Arctic and are necessary to explain ozone depletion events in spring caused by the catalytic destruction of ozone by halogen radicals. Quantifying bromine emissions from snowpack is essential for interpretation of ice-core bromine. We present ice-core bromine records since the pre-industrial (1750 CE) from six Arctic locations and examine potential post-depositional loss of snowpack bromine using a global chemical transport model. Trend analysis of the ice-core records shows that only the high-latitude coastal Akademii Nauk (AN) ice core from the Russian Arctic preserves significant trends since pre-industrial times that are consistent with trends in sea ice extent and anthropogenic emissions from source regions. Model simulations suggest that recycling of reactive bromine on the snow skin layer (top 1 mm) results in 9–17% loss of deposited bromine across all six ice-core locations. Reactive bromine production from below the snow skin layer and within the snow photic zone is potentially more important, but the magnitude of this source is

uncertain. Model simulations suggest that the AN core is most likely to preserve an atmospheric signal compared to five Greenland ice cores due to its high latitude location combined with a relatively high snow accumulation rate. Understanding the sources and amount of photochemically reactive snow bromide in the snow photic zone throughout the sunlit period in the high Arctic is essential for interpreting ice-core bromine, and warrants further lab studies and field observations at inland locations.

3.1 INTRODUCTION

Tropospheric reactive bromine (Br_y = Br + $2Br_2$ + HOBr + BrO + HBr + $BrNO_2$ + $BrNO_3$ + IBr + BrCl) impacts the oxidizing capacity of the atmosphere by depleting ozone and perturbing OH to HO_2 ratios toward OH (von Glasow et al., 2004; Sherwen et al., 2016). In polar regions, Br_y is largely responsible for surface ozone depletion events (ODEs) in coastal regions in the spring (Barrie et al., 1988; Oltmans et al., 1989, 2012). Reactive iodine also plays a role in ODEs (Benavent et al., 2022), with a smaller contribution from reactive chlorine (Wang et al., 2021). Br_y is also associated with atmospheric mercury depletion events in the Arctic (Horowitz et al., 2017; Steffen et al., 2008). Major sources of tropospheric reactive bromine include sea salt aerosol (SSA) debromination (Kerkweg et al., 2008; Yang et al., 2005), emissions of organobromine species from the marine biosphere (Liang et al., 2010; Quack & Wallace, 2003), emissions from saline lakes (Hebestreit et al., 1999; Matveev et al., 2001), and volcanoes (Aiuppa et al., 2005; Bobrowski et al., 2003). Anthropogenic-related sources of Br_y include agricultural emissions (Clerbaux et al., 2007), emissions from vehicles using leaded gasoline (Habibi, 1973; Thomas et al., 1997), coal combustion (Lee et al., 2018), biomass burning (Reeves, 2003), and stratospheric transport from degradation of organobromines and halons (Liang et al., 2014). In the Arctic, debromination of

SSA originating from blowing snow (Huang et al., 2020; Yang et al., 2008) and direct emissions of reactive bromine from snowpack have been observed (Abbatt et al., 2012; Dibb et al., 2010; Foster et al., 2001; Pratt et al., 2013; Simpsonet al., 2007a, 2007b; Stutz et al., 2011) and are necessary to explain depletion of surface ozone in the spring (Lehrer et al., 2004; Michalowski et al., 2000; Piot & von Glasow, 2008; Swanson et al., 2022).

The major sink of tropospheric Br_y is uptake by aerosols, and both Br_y and aerosol bromide are removed from the atmosphere through wet and dry deposition to the surface. Bromine in snowpack originates from deposition of gaseous and aerosol phase bromine. Bromine in snow over first year sea ice has additional sources from wind-blown frost flowers and upward migration from sea ice (Domine et al., 2004). Deposition of bromine to the cryosphere is reversible due to snowpack bromine chemistry, potentially affecting the preservation of bromine in ice cores (McConnell et al., 2017; Vallelonga et al., 2021). Ice-core bromine records have been interpreted to reflect changes in sea ice extent (Maffezzoli et al., 2021; Spolaor et al., 2013a, 2013b, 2016a, 2016b), atmospheric acidity (Maselli et al., 2017), and anthropogenic bromine emissions (Legrand et al., 2021) under the assumption that bromine species are well preserved in ice cores with high snow accumulation rates typical of the Arctic and mid-latitudes. Understanding the magnitude and mechanisms of snowpack reactive bromine release is important for interpretation of ice-core bromine measurements.

Snowpack emissions of reactive bromine involve both gas-phase and heterogeneous chemistry across the atmosphere-snowpack interface. Gas-phase reactions that occur in the atmosphere (R 1–5) also occur in the snowpack interstitial air (SIA) (Pratt et al., 2013; Toyota et al., 2014).

$$O_3 + Br \rightarrow BrO + O_2 \quad \text{(R1)}$$

$$HO_2 + BrO \rightarrow HOBr + O_2 \quad \text{(R2)}$$

$$HOBr + h\vartheta \rightarrow OH + Br \quad \text{(R3)}$$

$$Net: HO_2 + O_3 \rightarrow 2O_2 + OH$$

$$BrO + NO_2 + M \rightarrow BrNO_3 + M \quad \text{(R4)}$$

$$BrNO_3 + H_2O(liq) \rightarrow HOBr + HNO_3\,(aq) \quad \text{(R5)}$$

$$2OH(aq) + 2Br^-(aq) + 2H^+(aq) \rightarrow Br_2 + 2H_2O \quad \text{(R6)}$$

$$O_3(aq) + Br^-(aq) + H^+(aq) \rightarrow HOBr(aq) + O_2(aq) \quad \text{(R7)}$$

$$BrNO_3 + H_2O(liq) \rightarrow HOBr(aq) + H^+(aq) + NO_3^-(aq) \quad \text{(R8)}$$

$$HOBr(aq) + X^-(aq) + H^+(aq) \rightarrow BrX + H_2O \quad \text{(R9)}$$

Similar to bromide (Br^-) in SSA, Br^- at the surface of snow grains can be oxidized by OH (R6) and O_3 (R7) or react with $BrNO_3$ (R8, R9) and HOBr (R9) to form BrX (where X = Br or Cl) (R6–9). Since bromide is expected to be enhanced at the snow grain surface (Ghosal et al., 2000, 2005; Gladich et al., 2011) relative to bulk snow, and Br^- reacts much faster with OH compared to Cl^- (Abbatt et al., 2010), Br_2 and BrCl are preferentially formed compared to Cl_2 (Custard et al., 2017). Preferential production of Br_2 over BrCl was shown in lab studies for snow with high Br^-/Cl^- ratios (Sjostedt & Abbatt, 2008). The resulting BrX can transfer to SIA and mix with the atmosphere above via wind pumping and gas-phase diffusion (Thomas et al., 2011; Toyota et al., 2014). These reaction pathways are largely photochemically driven. Possible dark reaction mechanisms include heterogeneous reactions of Br^- with HOBr, $BrNO_3$, and O_3 (R7–9). Another potentially important factor in heterogeneous reactions is snow acidity, since both bromine cycling within snowpack via R6, R7, and R9 and OH formation in the snowpack via nitrate photolysis are acid-catalyzed (McConnell et al., 2017; Mozurkewich, 1995).

Concentrations of Br_2 and BrCl in coastal Arctic surface air during spring have been observed to be as high as several tens of ppt (Foster et al., 2001; J. Liao et al., 2012, 2014; Spicer et al., 2002)

and are thought to originate at least partially from snow emissions. Foster et al. (2001) first reported the release of photolabile bromine compounds from the snowpack at Alert, Canada by showing that measured molecular bromine (Br_2) in SIA just below the surface of the snowpack reached 2ppt, about twice that measured in the air above. Pratt et al. (2013) conducted an outdoor snow chamber experiment in Utqiagvik, Alaska and demonstrated that snow bromine release is facilitated by ozone-mediated photochemical production of Br_2 in snow with enhanced Br^-/Cl^- ratios and high acidity. Also at Utqiagvik, Custard et al. (2017) measured molecular halogens in SIA and calculated a mean emission flux of $\sim 5 \times 10^8$ molecules cm^{-2} s^{-1} and $\sim 3 \times 10^8$ molecules cm^{-2} s^{-1} for Br_2 and Cl_2, respectively, out of snowpack into the atmosphere. The study also reported up to 500 ppt of Br_2, up to 45 ppt of BrCl, and up to 25 ppt of Cl_2 in SIA at a snow depth of 10 cm under artificial irradiation conditions.

Elevated atmospheric BrO concentrations were also observed in inland Arctic. Peterson et al. (2018) observed enhanced BrO vertical column densities (VCD) 200 km from the coast of Utqiagvik, Alaska, especially near the surface of the snowpack. Stutz et al. (2011) reported elevated BrO (1–3 ppt) at Summit, Greenland in May, June, and July, even when the air mass was not from oceanic regions. During the same field campaign at Summit, Dibb et al. (2010) found that gas phase soluble Br^- measured in the pore spaces of firn air is higher than in the air above the snowpack, and that ambient Br^- peaks around local noon. These studies indicate that photochemical production of reactive bromine from local snowpack is the primary source of the observed BrO at inland locations.

To investigate the role of snow halogen chemistry in ODEs, several box models and 1D models were developed to simulate the dynamic interaction between snowpack and the overlying atmosphere. Although these models suffer uncertainties due to limited knowledge of snow

microphysics and chemistry (Domine et al., 2013), they are useful for testing our understanding of the main sources of reactive bromine and causes of ODEs at specific locations and times. Using coupled 1D atmosphere-snow models at Summit, Greenland, Thomas et al. (2011, 2012a) and Toyota et al. (2014) found that bromine production from below the snow surface skin layer (top 1 mm, Erbland et al., 2013) dominates total snowpack emissions and is driven by photochemistry, which is highly dependent on the solar zenith angle (SZA) (Bourgeois et al., 2006; Grannas et al., 2007; Lee-Taylor & Madronich, 2002; Simpson et al., 2002; Warren, 1982). Snowpack emissions of bromine from the skin layer are driven by dry deposition of atmospheric HOBr, while deeper snowpack production (1–250 mm) is driven by both SIA Br_y chemistry (R1–5) and aqueous phase oxidation of bromide (R6–9) (Toyota et al., 2014). Piot and von Glasow (2009) used a box model to calculate the required fluxes of halogens to account for the observed effects on ozone in Alert, Canada in early spring, and estimated a Br_2 flux ranging from 5×10^7 to 1.5×10^9 molecules cm^{-2} s^{-1}. Other box and 1D modeling studies estimated maximum emissions of Br_2 of $2 – 5 \times 10^8$ molecules cm^{-2} s^{-1} at Utqiagvik, Alaska in March (Ahmed et al., 2022; Wang & Pratt, 2017), within the same order of magnitude of those from previous observation-based estimates from the same site (Custard et al., 2017).

Several global chemical transport models have incorporated snowpack bromine emissions to evaluate their role in explaining the spatiotemporal variability of ODEs across the Arctic. Toyota et al. (2011) implemented a snowpack chemistry mechanism in a 3D air quality model GEM-AQ by calculating the molar yield of BrX based on dry deposition of O_3, HOBr, and $BrNO_3$ for different snow types including first-year sea ice, multi-year sea ice, and land snow. The model was able to capture the spatial distribution of ODEs in April 2001 in the Arctic, and modestly agrees with satellite observations of BrO VCD. Although the GEM-AQ model does not explicitly include

deeper snow production, the empirically determined molar yield parameters as a function of sunlight are meant to reflect influences from photochemically driven deeper production (Toyota et al., 2011). Falk and Sinnhuber (2018) applied the same framework in a global chemistry-climate model EMAC, and showed that the model was able to reproduce many bromine enhancements and ODEs in both hemispheres over a full annual cycle. Similar frameworks have been implemented recently in WRF-Chem (Herrmann et al., 2021, 2022; Marelle et al., 2021) and GEOS-Chem (Swanson et al., 2022), and good agreements were found between models and satellite and in situ observations of BrO and O_3 in coastal Arctic spring.

Most previous snowpack bromine studies were conducted for coastal Arctic sites during springtime, with a focus on springtime ODEs. For inland snow regions such as Greenland, previous global modeling studies predict negligible bromine production from the snowpack, either because of the assumption of minimal snow bromide replenishment from dry deposited HBr (Toyota et al., 2011), or a 500 m elevation filter to restrict inland snowpack emissions (Swanson et al., 2022). In this study, we examine inland Arctic sites, where most ice cores are located, in a global model for the first time. We present bromine records from six Arctic ice cores spanning from 1750–2007 CE and investigate their trends via statistical analysis. We used a global chemical transport model, GEOS-Chem, that includes snowpack reactive bromine emissions to examine the potential magnitude and spatial distribution of snowpack emissions relative to atmospheric deposition over the course of a full annual cycle, and evaluate the implications for preservation and interpretation of bromine records for these six ice cores.

3.2 METHODS

3.2.1 *Arctic Ice Cores*

We present ice-core sodium, bromine, and acidity records from six Arctic ice cores covering the pre-industrial to present day transition (since 1750 CE), with five from the Greenland ice sheet and one from the Russian Arctic. Figure 3.1 shows the locations of the six ice-core sites. Table 3.1 summarizes the ice-core locations, age range, snow accumulation rates and references for previously published data. Here, we briefly describe the measurement techniques for the unpublished ice-core records, which include sodium, bromine, and acidity records from the Russian Arctic (Akademii Nauk), as well as bromine records from the five Greenland ice cores (ACT_11d, Summit_2010, NEEM_2011_S1, Tunu2013, NGT_B19).

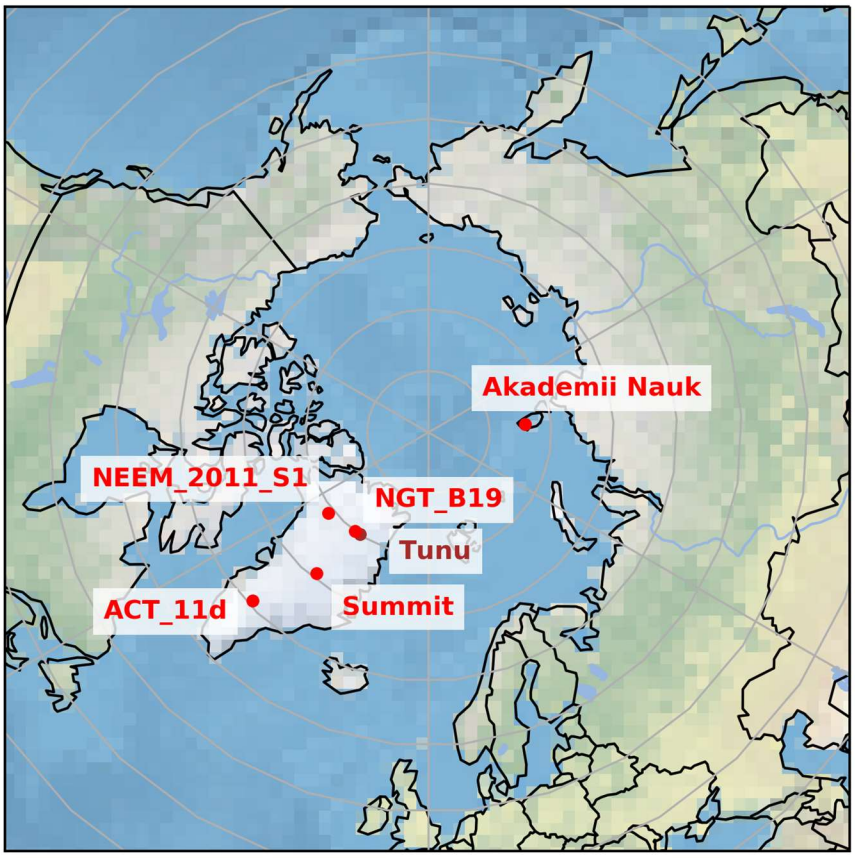

Figure 3.1. Location of the six ice cores used in this study.

Table 3.1. Locations and Other Information for the Six Ice Cores Presented in This Study

Ice core	Latitude	Longitude	Elevation (m)	Snow Accum. (kg m^{-2} yr^{-1})	Estimated age range (BCE/CE)	Elements and reference
Akademii Nauk (AN)	80.5ºN	94.8ºE	750	440	−200–1999	Br, Na (Spolaor et al., 2016a)
Tunu2013	78.0ºN	33.9ºW	2,105	108	275–2012	Acidity, Br and Na (Maselli et al., 2017)
NGT_B19	78.0ºN	36.4ºW	2,270	100	746–1993	Acidity and Na (Maselli et al., 2017)
NEEM_2011_S1	77.5ºN	51.1ºW	2,454	211	88–1999	Acidity and Na (Maselli et al., 2017)
Summit_2010	72.6ºN	38.3ºW	3,258	226	1743–2010	Acidity, Br and Na (Maselli et al., 2017)
ACT_11d	66.5ºN	46.3ºW	2,148	334	1161–2010	Acidity and Na (Maselli et al., 2017)

A 724 m-long ice core was collected from the AN ice cap at Severnaya Zemlya in the central Russian Arctic from 1999 to 2001 (Fritzsche et al., 2002; Opel et al., 2013). Due to summertime surface melting, percolation into deeper layers and refreezing, the age scale was determined using an iterative approach based on annual layer counting using multi-parameter aerosol records constrained by absolutely dated reference horizons, called the DRI_Akademii_Nauk chronology, as described in McConnell et al. (2019). Uncertainty in the age scale was estimated to be less than 5 years. Tunu2013 (hereafter Tunu), North Greenland Traverse B19 (NGT_B19), NEEM_2011_S1, Summit_2010 (hereafter Summit), and ACT_11d are located on the Greenland ice sheet. Details of ice-core extraction and dating for these five ice cores can be found in previous publications (McConnell et al., 2019; Sigl et al., 2013).

For all ice cores, chemical analysis of elemental Na and elemental Br were conducted using continuous high resolution inductively coupled plasma mass spectrometry (HR-ICP-MS), at the Desert Research Institute (Maselli et al., 2017; McConnell et al., 2019), with an uncertainty of ±10%. Acidity (H^+) was directly measured continuously as described in Pasteris et al. (2012), with an error less than 5%.

Two metrics are normally used to assess the relative contribution of Br from sea salt and atmospheric processes, bromine excess (Br_{exc}) and bromine enrichment (Br_{enr}). The non-sea-salt Br concentration (Br_{exc}) is calculated as:

$$[\mathrm{Br_{exc}}] = [Br]_{ice\ core} - [ssNa]_{ice\ core} \times \left(\frac{[Br]}{[Na]}\right)_{sea\ water} \quad (1)$$

where [X] represents mass concentrations in ng X g ice^{-1}, and ([Br]/[Na])$_{\text{sea water}}$ is the sea water Br/Na mass ratio of 0.00624 (Millero et al., 2008). [ssNa] is calculated based on ice core calcium concentrations, as described in Maselli et al. (2017). The non-dimensional factor Br_{enr} is defined as the enrichment of Br relative to sea salt Br, and is calculated as:

$$[\mathrm{Br_{enr}}] = \frac{[Br]_{ice\ core}}{[ssNa]_{ice\ core} \times ([Br]/[Na]_{sea\ water}} \quad (2)$$

A positive Br_{exc} is equivalent to $Br_{enr} > 1$, and a negative Br_{exc} is equivalent to $Br_{enr} < 1$. Br_{enr} will only be 0 if Br is under the detection limit. Br_{enr} is most often used as an ice core proxy because it is not influenced by changes in snow accumulation rates and absolute emissions of sea salt, and represents the degree of gas-aerosol re-partitioning including sea salt debromination (R8 –R9, with X = Br) (Spolaor et al., 2013a, 2013b). Trends in Br_{exc} will be more representative of trends in the concentration of Br_y in the atmosphere, facilitating comparison with atmospheric chemistry models.

3.2.2 *Statistical Analysis of Ice-Core Observations*

We use a recursive Bayesian change point algorithm based on dynamical programming (Ruggieri, 2013) to analyze the trends in ice core Br_{enr} and Br_{exc} records since pre-industrial time (1750 CE). Change points are defined as changes in the parameters of a regression model used to describe a climatic time series. Assuming a maximum of six change points in the ice core annual records since 1750 CE, a minimum separation time of 15 years between adjacent change points, and a linear fit in each identified regime, we sample 500 solutions independently from the posterior distribution, and calculate the best fit change point model (Ruggieri, 2013).

There are five parameters for the changepoint analysis, including the maximum number of change points allowed (k_{max}), the minimum distance between adjacent change points (d_{min}), and three hyperparameters for the prior distribution. We have chosen the three hyperparameters based on the recommendations from Ruggieri (2013), and conducted several sensitivity studies on choosing k_{max} and d_{min}. Tests with k_{max} ranging from 6 to 20, and d_{min} ranging from 5 to 20 show very similar results in changepoint identification, thus we show one of the results with $k_{max} = 6$ and $d_{min} = 15$.

3.2.3 *Modeling Snowpack Halogen Chemistry*

We use a 3-D global chemical transport model, GEOS-Chem (version 11-02d) (https://github.com/geoschem/geos-chem/tree/v11-02d-prelim), to examine post-depositional loss of snow bromine and its impact on ice-core bromine preservation. GEOS-Chem is driven by MERRA-2 assimilated meteorological observations from the Goddard Earth Observing System (Gelaro et al., 2017) and has detailed HO_x-NO_x-VOC-ozone-halogen-aerosol tropospheric chemistry, including comprehensive tropospheric multi-phase reactive halogen chemistry (Wang et al., 2019, 2021) and fully coupled stratospheric chemistry (Eastham et al., 2014). This model

also incorporates blowing snow-sourced SSA emissions (Huang & Jaeglé, 2017). Gas phase and heterogeneous bromine chemistry are described in previous papers (Chen et al., 2017; Sherwen et al., 2016; Wang et al., 2021). Sea-salt aerosol debromination occurs on both open ocean and blowing snow sourced SSA (Huang et al., 2020). Gases and water-soluble aerosols are wet deposited in GEOS-Chem based on scheme described in Amos et al. (2012) and Liu et al. (2001), respectively. Dry deposition is based on the resistance-in-series scheme introduced in Wesely (1989) as implemented by Wang et al. (1998). Among Br_y species, Br_2, HOBr, HBr, BrCl, IBr and aerosol bromide are both wet and dry deposited, and $BrNO_3$ is dry deposited only. We updated the O_3 dry deposition scheme onto snow and ice surface, such that the dry deposition velocity is about 0.01 cm s^{-1}, consistent with observations (Simpson et al., 2007a) and assumptions made in Toyota et al. (2011). We run all simulations at 4 × 5° horizontal resolution and 72 vertical levels up to 0.1 hPa for 1 year using 2007 meteorology, after spinning up the model for 1 year. An additional sensitivity simulation was performed using 2008 meteorology. Coal combustion and leaded gasoline emitted bromine are not included in the model, because the former suffers large uncertainty (Lee et al., 2018) and is considered a minor source, and the latter is not important in present day (Lammel et al., 2002; Thomas et al., 1997).

Bromine from snowpack is emitted into the lowest level of the model. Modeling snow chemistry emissions from the snow surface skin layer (approximately 1 mm at the top, Erbland et al., 2013) adopts the framework from Toyota et al. (2011), with several updates to represent surface snow production of BrX at inland locations as described below. In Toyota et al. (2011), reactive halogen release from the surface snowpack is driven by deposition of HOBr, $BrNO_3$, and O_3 with molar yields dependent on snow type and availability of snow halides. Toyota et al. (2011) assumed unlimited snow bromide for first-year sea ice, limited bromide sourced from dry

deposition of HBr and infinite chloride for multi-year sea ice, and no snow halides for land snow. Dry deposited HOBr and $BrNO_3$ are fully converted to BrX based on availability of snow halides. For sea ice regions, once snow bromide is depleted, dry deposited HOBr and $BrNO_3$ react with snow chloride to form BrCl, with a molar yield of 100%. Br_2 formation through reactive uptake of O_3 on surface snow is represented by converting the O_3 deposition flux on surface snow into the emission flux of Br_2, with a molar yield of 0.1% under dark conditions and 7.5% under sunlit conditions. The value 0.1% represents Br_2 formed via ozone uptake on frozen seawater in the dark (Oum et al., 1998; Wren et al., 2010), while 7.5% is the adjusted value based on the comparison between the model and hourly measurements of surface ozone at the coastal sites of Alert, Barrow, and Zeppelin in April 2001 (Toyota et al., 2011). This empirically adjusted molar yield for sunlit conditions (7.5%) is used in the GEM-AQ model (Toyota et al., 2011) to account for the deeper snow production of reactive bromine, which is highly dependent on solar radiation. This molar yield also introduces some uncertainty when applied to inland sites like Greenland, since its value is based on coastal observations.

Table 3.2 describes three model simulations performed here. All three simulations account for surface recycling of bromine from deposition of HOBr and $BrNO_3$ to form Br_2 using a molar yield of unity, and from deposition of O_3 using a molar yield of 0.1% to form Br_2. The treatment of surface recycling is similar to Toyota et al. (2011), except that we explicitly track surface snow bromide concentration for all snow types, instead of assuming unchanging bromide content based on snow types. Surface recycling of reactive bromine is limited by the availability of reactive bromide in the snow. Surface snow bromide originates from dry deposition of HBr and SSA bromide, and is lost by chemical production of Br_2 (R6, R7, and R9). In contrast, Toyota et al. (2011) assumed only dry deposition of HBr as a source of snow bromide.

Table 3.2. Comparison of Key Model Settings Conceived by Toyota et al. (2011) and the Three Model Simulations (mToyota, SURF, and DEEP) in This Study

	Model simulation			
	Toyota et al. (2011)	mToyota (Modified Toyota)	SURF (surface production only)	DEEP (surface and deep production)
Snow Bromide Concentration	Constant Br^-: infinite Br^- on FYI Br^- on MYI and LS only replenished by dry deposition of HBr	Track surface snow Br^-: Snow Br^- = initial + HBr dry deposition + sea salt Br^- dry deposition—released Br_2	Track surface snow Br^-	Track surface snow Br^-, unlimited deeper snow bromide
Surface snow production	100% molar yield of Br_2/BrCl on HOBr and $BrNO_3$ deposition; 0.1% molar yield on O_3 deposition	Same as Toyota et al. (2011)	Same as Toyota et al. (2011)	Same as Toyota et al. (2011)
Deeper snow production	Implicitly represented: 7.5% molar yield of Br_2 on O_3 deposition under sunlit conditions	Same as Toyota et al. (2011)	No deep production	$F_{Br2} = F_{1Dmax} \times \cos(SZA)$
Additional threshold	Temperature below −10, −15, or −20°C	Temperature below 0°C. Snow depth >10 cm for land snow	Temperature below 0°C. Snow depth >10 cm for land snow	Temperature below 0°C. Snow depth >10 cm for land snow albedo >0.7

We assume fresh snowfall contains no reactive bromide, effectively assuming that wet deposited bromide is trapped in the frozen snow grain and not available for surface reactions (Domine et al., 2013). Processes such as snow sublimation and re-deposition may alter the location of

bromide within the snow grain over time, likely rendering this an underestimation of snow bromide on the surface of snow grains that is available for surface chemical reactions. On the other hand, temperature gradient snow metamorphism is shown to facilitate the burial of bromide, resulting in the absence of bromide from the air–ice interface (Edebeli et al., 2020). We also do not consider the upward migration of bromide in snow from sea ice as a replenishing source for surface snow bromide, which may result in an underestimate of snow bromide concentrations over sea ice (Domine et al., 2004). However, upward migration is not a source of bromide in inland snow, where ice cores are drilled, which is the focus of this study. The model simulation that contains only surface snow recycling source is referred to as SURF.

For the other model simulations, we included two representations of deeper snow production in addition to surface recycling. In the "mToyota" simulation, we increase the molar yield of Br_2 production from ozone deposition to 7.5% under sunlit conditions to account for deeper snow production as in Toyota et al. (2011). Although deeper snow production is unlikely to be directly influenced by ozone deposition to the skin layer, this parameterization was shown to provide good agreement with BrO observations in springtime at specific coastal locations and time periods in the Arctic spring time.

In the "DEEP" simulation, we effectively assume that ozone and OH production deeper in the snow originates from the photolysis of snow nitrate and H_2O_2 (e.g., Grannas et al., 2007), and that oxidants produced in the SIA will react with bromide in the deeper snow to form HOBr (R6 and R7) (Thomas et al., 2011; Toyota et al., 2014). The production of HOBr in SIA is necessary for in-snow bromine production of Br_2 (R9). Since photolysis of snow nitrate and H_2O_2 is driven by sunlight, we scale Br_2 release from deeper snow to the SZA with a maximum flux based on

order-of-magnitude estimates from previous 1D snow photochemistry modeling studies (Toyota et al., 2014), as shown in Equation 3.

$$F_{Br_2} = F_{1Dm} \quad \times \cos(SZA) \tag{3}$$

where F_{Br2} is the Br_2 emission flux, F_{1Dmax} is the maximum Br_2 emission flux from previous 1D model simulations, and SZA is the solar zenith angle. We chose F_{1Dmax} to be 1×10^8 atom Br cm^{-2} s^{-1} (8.64×10^{12} atom Br cm^{-2} day^{-1}) based on Toyota et al. (2014), which is roughly the daily maximum upward flux of total inorganic gaseous bromine below the snow skin layer in March. This value is similar in magnitude to that of Thomas et al. (2011), which used a 1D model to simulate snowpack bromine emissions at Summit Greenland in June 2008. Note that F_{1Dmax} is 1 order of magnitude smaller than the measured emission flux reported in February at Utqiagvik, Alaska (Custard et al., 2017), and the 1D model (Toyota et al., 2014) assumes the source of snow bromide to be only from atmospheric deposition. Thus, the DEEP simulation is anticipated to underestimate coastal snow bromine emissions by at least an order of magnitude. We added a temperature and albedo threshold to reflect the impact of surface melting on snowpack bromine release. When albedo is below 0.7 (Custard et al., 2017; McConnell et al., 2017) or surface temperature are greater than 0°C (Burd et al., 2017), the deeper snow production of bromine is ceased. In comparison, Toyota et al. (2011) allows snowpack bromine emissions only when temperature is below a "critical temperature," which varies between −10°C and −20°C in their sensitivity studies. Following Swanson et al. (2022), we adopt a threshold of snow depth of 10 cm over which snowpack bromine release is allowed for land snow regions, preventing excessive bromine production in lower-latitude snow-covered regions. We assume bromine content is not a limiting factor for deeper snow production, similar to Toyota et al. (2014), because we are unable to track snow bromide in deep snow over time without an

explicit 3D snow module. Unlike surface snow, bromide in deeper snow cannot be replenished through atmospheric deposition, so this assumption may lead to a model overestimate of bromine release from deeper snow at inland locations. We do not explicitly consider the effect of wind pumping and snow acidity in this simplified scheme, both of which facilitate snow bromine release (Custard et al., 2017; McConnell et al., 2017).

Total snowpack bromine emission flux (F_{eBr}) is the sum of Br_2 and BrCl emissions from the surface skin layer, and the Br_2 emissions from deeper snow (F_{Br2}). Post-depositional loss of bromine is evaluated in the model by comparing total surface deposition fluxes to snow emissions fluxes (Equation 4):

$$R_{loss} = \frac{F_{eBr}}{F_{dBr}} \times 100 \quad (4)$$

where R_{loss} is the post-depositional loss of bromine in percentage, F_{eBr} is the total snowpack emission flux of bromine including Br_2 and BrCl emissions, and F_{dBr} is the total deposition flux including wet and dry deposition of HBr and SSA bromide.

We do not include snow chemistry for molecular chlorine (Cl_2) in this study. Cl_2 was not observed above the instrument detection limit of 2 ppt during field campaigns in Alert, Canada (Foster et al., 2001; Spicer et al., 2002), or in the snow chamber experiment in Utqiagvik, Alaska (Pratt et al., 2013), but was detected at up to 400 ppt in spring at Utqiagvik, AK (Custard et al., 2016; Liao et al., 2014). Cl_2 production is likely limited by the snow Cl^- availability, since snow temperature is likely below the eutectic point (251K) for the formation of $NaCl{\cdot}2H_2O$ (Koop et al., 2000). Studies report different ranges for molecular chlorine emission flux from snowpack, but almost all observation-based calculations show that Cl_2 fluxes and concentration are much lower than Br_2. Compared to the chlorine deposition flux in polar regions (10^{13} –

10^{14} molecules cm^{-2} s^{-1}) (Zhai et al., 2021), the snowpack emission of Cl_2 is at least four orders of magnitude smaller, thus is unlikely to represent a significant loss process for ice core chlorine.

3.3 RESULTS

3.3.1 *Ice-Core Bromine Trend Analysis*

Figure 3.2 shows bromine records from the six Arctic ice cores. The average total bromine concentrations in AN ice core are 4–10 times higher than those for the Greenland ice cores. This is likely due to the proximity of AN to open ocean and the relatively low elevation compared to inland Greenland, as indicated by the average sodium concentrations at AN that are 8–28 times higher than those for Greenland locations (Figure B1 in Appendix B1). AN also has 3–11 times higher Br_{exc} concentrations compared to the Greenland ice cores. Br_{enr} values at AN are smaller (0.2–0.8 times) compared to Greenland ice cores. This suggests that the extent of aerosol debromination at AN is not as extensive as in inland Greenland. Since AN is located closer to the open-ocean and sea-ice sea salt emission sources compared to the Greenland sites, it will experience more bromine-depleted coarse mode sea salt deposition. In contrast, only gas phase bromine and accumulation mode sea salt, which are bromine-enriched and have a longer lifetime, are transported the longer distance from sea salt source regions to the Greenland sites, resulting in higher Br_{enr} (Domine et al., 2004; Nandan et al., 2017; Hara et al. (2002)).

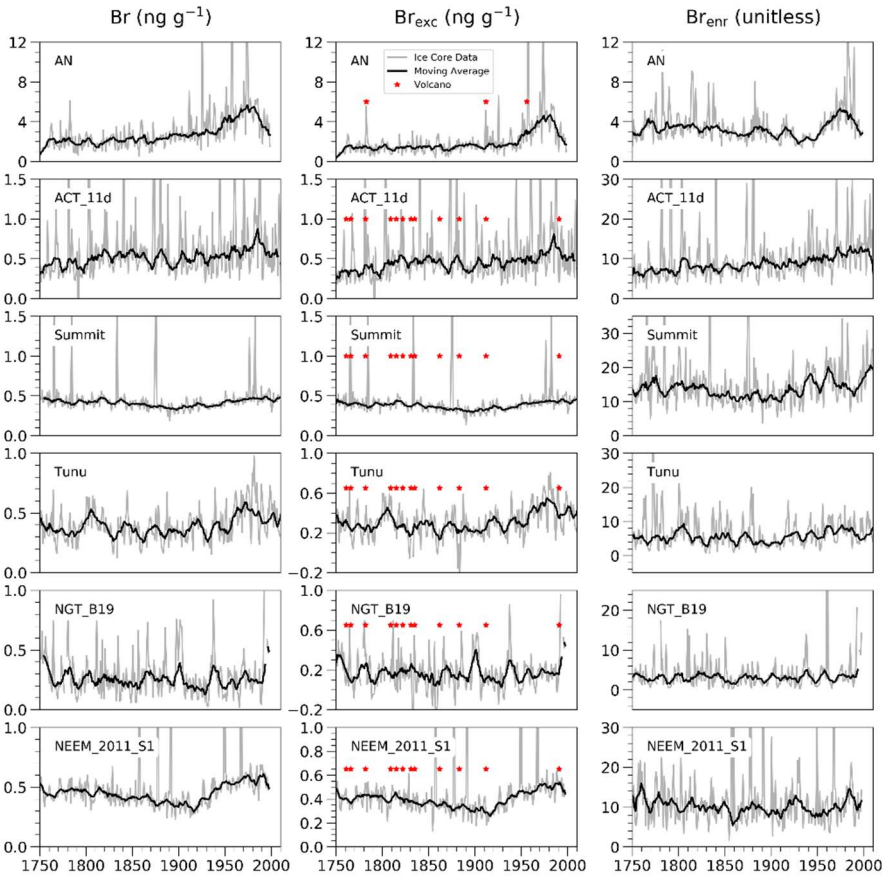

Figure 3.2. Total bromine concentration (left), Br_{exc} (middle), and Br_{enr} (right) in the Akademii Nauk (AN), ACT_11d, Summit, Tunu, NGT_B19, and NEEM_2011_S1 ice cores. Gray lines are the measured annual ice core concentrations (total bromine) or calculations (Br_{exc} and Br_{enr}), and black lines are the 9-year running average, with outliers outside of 1.5 × IQR (interquartile range) removed. Red stars mark the large and moderate volcanic years identified in previous studies (Opel et al. (2013) for AN and Cole-Dai et al. (2013) and Sigl et al. (2013) for Greenland ice cores, see also Figure B1 in Appendix B1).

Change point analysis shows that of the six ice cores, only AN has significant trends in Br_{exc} and Br_{enr} since the pre-industrial (Text S2, Figures S2, and S3 in Appendix B1). Figure 3.3 shows the results of the change point analysis for the AN core, with volcanic years removed (Opel et al., 2013). AN Br_{exc} remained at a relatively stable concentration of 1.5 ± 0.8 ng·g^{-1} from 1750 to 1940, showed a 3.7-fold increase from 1940 to 1975 (5.6 ± 3.5 ng·g^{-1}), and decreased afterward

by −57% (2.4 ± 0.9 ng·g^{-1}). AN Br_{enr} before 1850 had an average value of 3.3 ± 1.5. After 1940, AN Br_{enr} increased 1.6-fold until 1975 (5.3 ± 1.5), and decreased by −21% afterward (4.2 ± 2.7).

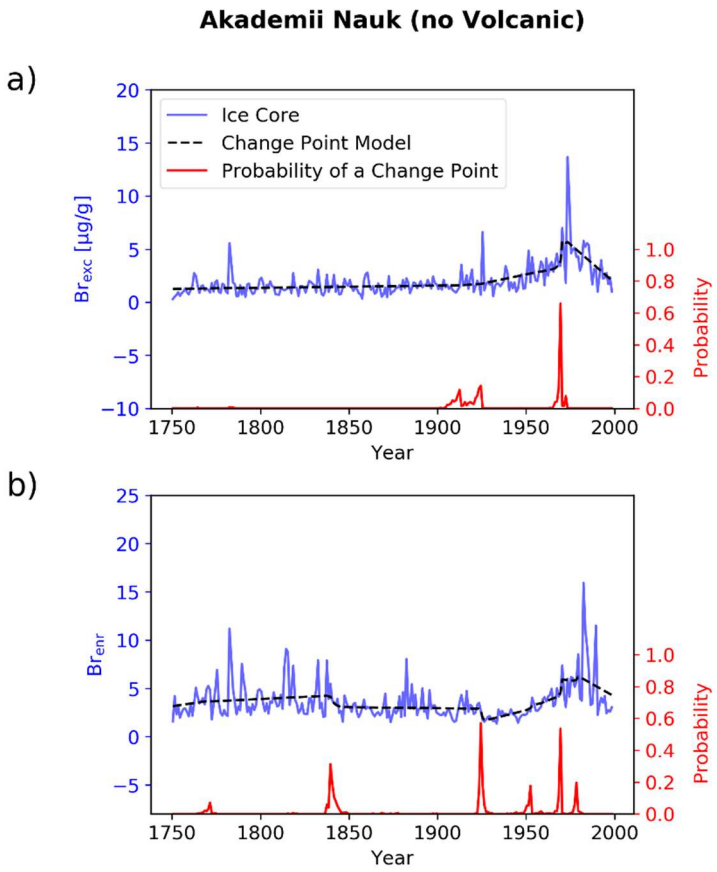

Figure 3.3. Ice-core records and trend analysis of (a) Br_{exc} and (b) Br_{enr} since year 1750 from the Akademii Nauk ice core. Blue lines are ice core Br_{exc} and Br_{enr} values calculated based on ice core measurements of sea-salt sodium and bromine, with previously identified volcanic years removed (Opel et al., 2013). Dashed black lines are the model predicted trends by the Bayesian Change Point algorithm. The heights of red spikes at the bottom of each panel indicate the probability of a potential change point. Tall, narrow spikes suggest relative certainty in the timing of a change point, whereas shorter and wider spikes suggest more uncertainty. No spikes are visible if no change points are identified by any of the 500 sampled solutions. Similar analysis for other ice core locations are in Figures S2 and S3 in Appendix B1.

The presence or absence of ice core bromine trends in and of themselves is not necessarily indicative of the degree of bromine preservation, at least in part because the source regions for

each ice core location may differ from one another. Previous studies have attributed ice core bromine trends to changes in sea ice extent (Spolaor et al., 2013a, 2013b, 2016a, 2016b; Maffezzoli et al., 2021), atmospheric acidity (Maselli et al., 2017), and anthropogenic bromine emissions from leaded gasoline (Legrand et al., 2021). Figure B4 in Appendix B1 shows the calculated 5-day back trajectory probability from the HYSPLIT model for AN, and readers are referred to Figure B2 in Zhai et al. (2021) for 5-day back trajectory plots for the Greenland ice core locations. Major sea ice source regions (>60% regional contribution) for the Greenland ice cores are the Greenland Sea, Baffin Bay and Labrador Sea, while for AN are the Laptev Sea, Kara Sea, Barents Sea, and the Arctic Ocean. Sea ice extent has been declining across the Arctic since 1980 (Brennan & Hakim, 2021), but sea ice extent in the Russian Arctic, especially in Barents Sea, has been decreasing faster than the source regions for Greenland ice cores (Comiso et al., 2017). Major source regions of potential anthropogenic emissions are eastern North America and Northwestern Europe for Greenland ice cores, and Russia and Eastern Europe for AN.

Spolaor et al. (2016a) found that ice core Br_{exc} concentration in AN was positively correlated ($r = 0.44$, p-value = 0.02) with the Laptev Sea spring sea ice extent since 1979. Although satellite observations of sea ice are not available prior to 1979, sea ice reconstructions suggest small increases in sea ice extent after about 1940 until about 1980 in the Russian Arctic, East Greenland Sea, and Baffin Bay (Brennan & Hakim, 2021; Mahoney et al., 2008), qualitatively consistent with the increasing trends in AN Br_{enr} and Br_{exc} from 1940 to the 1970s (Figures 2 and 3). If Greenland ice core bromine is influenced by sea ice extent, then we would also expect to see an increase in Br_{enr} and Br_{exc} between 1940 and the 1970s followed by a more rapid decrease since 1979, which is not observed (Figures S2 and S3 in Appendix B1).

Assuming that ice core methanesulfonic acid (MSA) is a sea ice proxy, Maselli et al. (2017) calculated sea-ice sourced bromine based on the linear regression of ice core MSA and bromine during 1750–1880 CE, and attributed trends in non-sea ice bromine in Greenland ice cores (Summit and Tunu) after the mid-20th century to changes in atmospheric acidity, which is known to facilitate aerosol debromination reactions. Measured acidity is similar in all six ice cores, with an increasing trend beginning in the 1940s followed by a decreasing trend after the 1970s (Figure B1 in Appendix B1). These trends in acidity are similar to the observed trends in Br_{exc} and Br_{enr} in the AN core. The existence of acidity trends combined with the lack of bromine trends over the same time period in the Greenland ice cores suggest either that acidity is not influencing Greenland ice core bromine trends, or that acidity-driven trends in bromine are not preserved in the Greenland ice cores.

Legrand et al. (2021) found that anthropogenic emissions from leaded gasoline, which is the largest historical anthropogenic source of bromine, is the major driver of summertime ice core bromine trends from the Col du Dome (CDD) ice core in French Alps. Trends in leaded gasoline usage are similar to the acidity trends (Figure B1 in Appendix B1), increasing from the 1940s to 1970s and decreasing since the 1970s in North America, Europe, and Russia (Thomas et al., 1997), which are the major source regions for the Greenland ice cores and AN (Figure B4 in Appendix B1). We note that sea ice extent, atmospheric acidity, and anthropogenic emissions of bromine all increased between the 1940s and the 1970s and declined after the 1970s, but only the AN core shows corresponding trends in Br_{exc} and Br_{enr} over this time period. The lack of significant trends in Greenland ice core bromine metrics may be due to poor preservation of bromine in snow and ice at these locations.

3.3.2 *Modeled Snowpack Reactive Bromine Release*

Figure 3.4a shows the model simulated annual mean snowpack bromine emission fluxes in the Arctic region. The model likely underestimates the total Br_2 emission flux at coastal sites for all three model simulations, based on comparisons of the modeled emissions fluxes and prior field measurements. For example, at Utqiagvik in February, the model calculates a monthly average bromine emission flux of 6.3–9.1 × 10^{10} atom Br cm^{-2} day^{-1} for the three simulations, about three orders of magnitude lower than those reported in Custard et al. (2017) from February 14th and 16t 2014 (0.7–12 × 10^{8} molecules cm^{-2} s^{-1}, or 1.2–21 × 10^{13} atom Br cm^{-2} day^{-1}). The modeled snowpack bromine emission fluxes in the sea ice regions from DEEP and mToyota are also about 1 order of magnitude smaller than reported in previous 3D models for Arctic conditions in April (Swanson et al., 2022; Toyota et al., 2011). The underestimation in coastal regions is due to our conservative assumption of surface snow bromide content, which lacks replenishment from upward migration from sea ice (Domine et al., 2004; Nandan et al., 2017). This suggests that upward migration of bromide through the snow layer from sea ice may be important for reactive bromine emissions and ODEs in the coastal Arctic.

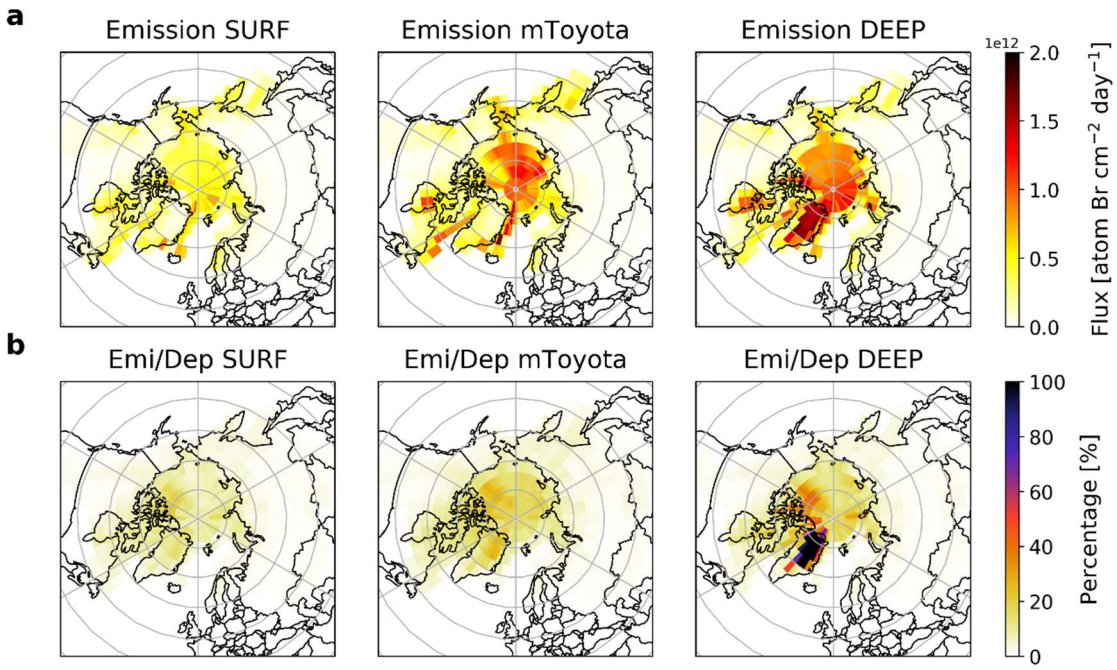

Figure 3.4. Simulated Arctic spatial distribution of annual mean (a) snowpack emission fluxes of bromine (Br_2+BrCl), and (b) post-depositional loss calculated as the percentage of snowpack bromine emission fluxes (Br_2+BrCl) divided by total bromine deposition (dry + wet) from the three simulations, SURF, mToyota, and DEEP.

Figure 3.4b shows the model simulated annual post-depositional loss of snow bromine in the Arctic region, calculated by comparing bromine surface deposition with snow emissions (Equation 4). The modeled maximum annual mean post-depositional loss across the Arctic is 26%, 50%, and >100% from SURF, mToyota, and DEEP simulations, respectively. In DEEP, post-depositional loss >100% is calculated only in inland central and northern Greenland, where most of the ice cores are drilled, suggesting that DEEP overestimates snowpack bromine emissions at these sites.

Table 3.3 shows the deposition and emission fluxes between the snowpack and atmosphere for the six ice core locations from the SURF and DEEP simulations. The calculations for mToyota are in between these two simulations and are shown in Appendix B1 (Table B1). SURF simulation

predicts similar post-depositional loss (9–17%) across all six ice-core locations, suggesting that factors such as snow accumulation rate, elevation, and distance from the coast have minimal impact on bromine loss from surface recycling. The largest snowpack bromine emission flux in the SURF simulation is 5.5×10^{11} atom Br cm^{-2} day^{-1} at AN, twice the value at ACT_11d, and 8–9 times of the values at northern Greenland ice-core sites. The relatively large emissions flux from surface recycling at AN and ACT_11d is driven by larger HBr and sea salt Br^- deposition flux at these two locations. Compared to the observed annual mean ice core bromine concentrations, SURF simulated snow bromide is about 2–8 times higher (Table B2 in Supporting Information S1), suggesting that loss from deeper snow production is needed to explain the observed snow bromine concentrations in ice cores. The mToyota simulation, which assumes a higher yield of Br_2 from O_3 deposition during sunlit periods compared to SURF, predicts higher emission fluxes and therefore slightly higher post-depositional loss of 13–25% across all six ice core locations.

Table 3.3. Annual Mean Snowpack-Air Exchange Fluxes of Total Bromine (Total Deposition, Emission, Net Upward Flux, and Post-Depositional Loss) at the Six Ice Core Locations Calculated from the SURF and DEEP Simulations

Ice core	Total deposition [$\times 10^{11}$ atom Br cm^{-2} day^{-1}]	Emission (Br_2+BrCl) [$\times 10^{11}$ atom Br cm^{-2} day^{-1}]	Post-depositional loss (Emission/deposition)
AN	33–38	5.5–12	−28 to −26
Summit_2010	4.3–8.6	0.6–15	−3.7 to +6.4
Tunu2013	4.7–11	0.6–15	−4.1 to +4.0
ACT_11d	22–26	2.0–13	−2.0 to −1.3
NEEM_2011_S1	7.2–13	0.7–15	−6.5 to +2.0

Note: The lower and higher ends of the range are values calculated from the SURF and DEEP, respectively.

The DEEP simulation predicts much higher post-depositional loss everywhere compared to the other two simulations, especially in inland Greenland (Figure 3.4). In DEEP, total annual snow emissions are larger than total annual deposition at all ice-core sites except AN and ACT_11d. Since deposition is the only source of snow bromine at inland locations, this is not physically possible, demonstrating that our assumptions of snow emissions in DEEP constrained by 1D model studies in coastal spring and summertime inland sites result in an overestimate of annual snow bromine emissions. However, even with the overestimated bromine emissions from deeper snow in the model, the DEEP simulation still predicts significant (68%) preservation of snow bromine at the AN location, consistent with the observation that only this ice core has significant trends in Br_{exc} and Br_{enr}. The four northern Greenland ice cores (Summit, Tunu, NEEM_2011_S1, and NGT_B19) have very similar emission fluxes, since deeper production in the model is determined by F_{1Dmax} scaled by the cosine of SZA. Emissions at AN and ACT_11d are slightly lower due to summertime surface melting in the modeled year (2007), which shuts down deeper production in the model. The comparison between SURF and DEEP shows that bromine loss within the snow photic zone but beneath the snow surface layer dominates total loss from the snowpack in the model in the DEEP simulation, in agreement with Toyota et al. (2014).

Figure 3.5a shows modeled seasonality in snowpack bromine emissions at the six ice-core sites for each model simulation. Monthly mean bromine emission fluxes range from 1×10^9 to 1×10^{12} atom Br cm^{-2} day^{-1} at all sites throughout the year from surface recycling only (SURF). Loss from surface recycling is largely driven by the seasonality of dry deposition of total bromine (Br_y + sea salt Br^-) and ozone (Figure B5 in Appendix B1). The mToyota simulation predicts higher emission fluxes in April at AN but similar emission fluxes with SURF in other months and locations, mainly driven by the seasonality in the deposition flux of ozone, the availability of solar

radiation, and snow Br^- concentrations. In April, the high values of dry deposition fluxes of ozone and bromine (thus snow Br^-) accelerates snow Br^- oxidation by ozone. Whereas in May, even though ozone deposition remains large, limited snow Br^- hinders further production of bromine from the snowpack.

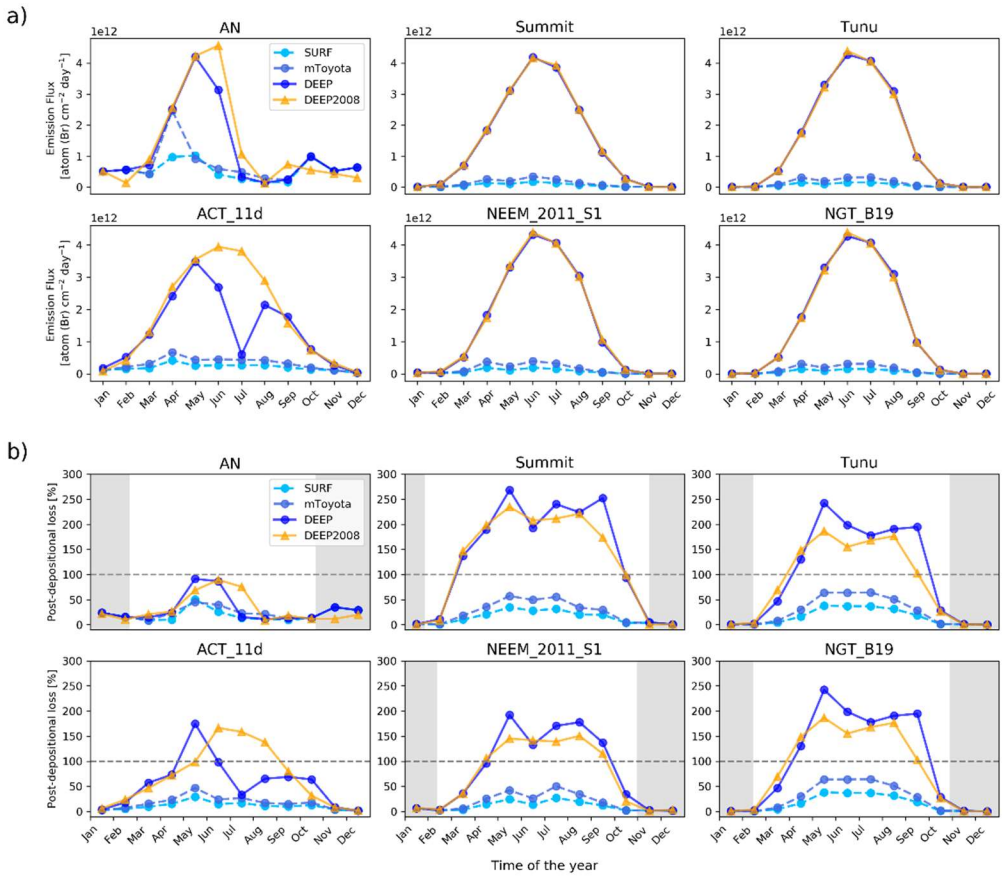

Figure 3.5. Modeled monthly mean snowpack (a) total bromine (Br_2 + BrCl) emission fluxes and (b) post-depositional loss in percentage at the six ice-core sites from the three simulations for year 2007: SURF, mToyota, and DEEP, and the DEEP simulation for year 2008. Dashed gray lines mark 100% loss, above which there is mass imbalance (i.e., total emission larger than total deposition). Gray area is the dark period in polar winter.

The DEEP simulation results in much higher maximum emission fluxes compared to SURF and mToyota, and are similar in seasonality and magnitude (with a maximum of ~4×10^{12} atom Br cm^{-2} day^{-1}) among the ice-core sites since they are limited by the value

of F_{1Dmax} (8.64×10^{12} atom Br cm^{-2} day^{-1}) scaled to the SZA. Peak monthly emissions at all sites except for AN and ACT_11d are predicted in June following the seasonality of the SZA. Surface melting at AN and ACT_11d in summer shuts down the deeper snow bromine production, resulting in late spring peak (May) in snowpack bromine release at these two sites. For AN, surface melting occurs in summer and autumn (June–October in year 2007) which explains the low bromine emission fluxes beginning in June until the next polar sunrise. At ACT_11d, surface melting and the shutdown of deep snow photochemical reactions occurs from June to early August in year 2007 (Figure B6 in Appendix B1), and similar emission fluxes to those of the other Greenland ice cores are found in other months.

Annual variations in summertime temperature and albedo have a large impact on the seasonality of snowpack bromine emissions at AN and ACT_11d. A sensitivity model simulation of the DEEP parameterization for year 2008 shows that the emission flux of bromine peaked in June at AN and ACT_11d for year 2008, instead of May for the year 2007 (Figure 3.5a). For AN, surface melting does not start until July 2008 (Figure B6 in Appendix B1). For ACT_11d, the albedo remained above 0.7 throughout summer 2008 (Figure B6 in Appendix B1), resulting in a bell-shaped seasonality in snowpack bromine release similar to other Greenland sites. Comparison between year 2007 and 2008 shows that, lower summertime temperature and later melt onset date postponed the peak emission time at AN and ACT_11d from late spring (May) to early summer (June), and increased the post-depositional loss from 32% in 2007 to 35% in 2008 for AN, and 51% in 2007 to 68% in 2008 for ACT_11d.

Figure 3.5b shows the monthly average percentage post-depositional loss at each ice-core site calculated according to Equation 4. In our deep snow bromine production mechanism, there is no limit on available snow bromide that can sustain the photochemistry to produce molecular

bromine, therefore we are essentially assuming infinite supply of snow bromide in the snow photic zone below the skin layer. As a result, most Greenland ice cores have mass imbalance (total bromine emission fluxes exceeding total bromine deposition fluxes) lasting for 5–7 months. This is not possible, since the photochemically available snow bromide will be depleted at some point, and will not sustain further bromine production from deeper snowpack due to lack of replenishment. At that point, surface recycling should be the only mechanism that is producing bromine from the snowpack.

Satellite observations show that BrO VCDs peak in coastal Artic spring (Bougoudis et al., 2020), suggesting factors other than SZA and actinic flux as drivers of deeper snow reactive bromine production. We speculate that photochemically reactive bromide deeper in the snow is depleted at some point and becomes a limiting factor for snow bromine emissions during the sunlit season. Because snow bromide concentrations are always greater than zero in Arctic ice cores (Figure 3.2), bromide that is subject to photochemical or reactive loss may represent only a fraction of total bromide in snow and ice. It is also possible that precursors to oxidant formation in the snowpack such as photolabile nitrate and H_2O_2 also become depleted and limit the production of oxidants and thus bromine loss deeper in the snowpack over the course of the sunlit season.

Our model underestimates the source of Br_y in the sea ice region, and this underestimate would mostly impact the transport and deposition of bromine to the AN core due to its closer proximity to sea ice compared to the Greenland ice cores. The model's mass imbalance in Greenland may also be partially explained by underestimated source of Br_y to the atmosphere. The model does not include anthropogenic bromine emissions from coal combustion (Lee et al., 2018). Both Greenland and AN ice cores show trends in anthropogenic emissions of acidity (Figure B1 in Appendix B1), showing that emissions from anthropogenic source regions influence Arctic ice

core records. Our model for deep snow production of Br_2 is a simplified parameterization that is solely based on SZA and independent of snowpack bromine concentrations. The lack of anthropogenic emissions of bromine species leads to an underestimate of total deposition, which in turn could cause an overestimate of post-depositional loss due to the low bias in the denominator (deposition flux).

The only available ground-based observations of near surface bromine species in an inland Arctic region were during May–June in 2007 and June–July in 2008. Stutz et al. (2011) observed a typical BrO mixing ratio of 1–3 pmol mol^{-1} and a maximum of up to 5 pmol mol^{-1} at Summit, Greenland using long-path differential optical absorption spectroscopy (LP-DOAS), which was shown to have excellent agreement with BrO measured by chemical ionization mass spectrometry (Liao et al., 2011a, 2011b). During the same campaign, Dibb et al. (2010) used Mist Chamber-Ion Chromatography to measure soluble Br^- concentrations, with soluble Br^- determined to be $[Br^-] = 0.9[Br_2] + 1.0[HOBr] + 0.4[BrO] + 0.95[HBr]$ (in mol) (Liao et al., 2012), and reported mean soluble Br^- values of 0.7 ppt for 2007 and 0.3 ppt for 2008 (Dibb et al., 2010). Comparison of LP-DOAS BrO and mist-chamber soluble bromide observations shows that the observed BrO alone can exceed soluble bromide observations, even when accounting for the factor of 0.4 contribution of BrO to the mist-chamber observations. The observed LP-DOAS BrO of 1–3 ppt suggest that BrO would contribute typically 0.4–1.2 ppt to the mist-chamber soluble bromide. This exceeds the mean of the observed mist-chamber soluble bromide (0.7 ppt).

The DEEP modeled hourly surface BrO mixing ratio shows good agreement with the observed BrO from LP-DOAS (Figure 3.6), but overestimates soluble Br^- (Figure B7 in Appendix B1). Modeled afternoon boundary layer height at Summit during the campaign seasons is 267–357 m, similar to the daytime boundary layer height estimated in Thomas et al. (2011) (20–30 m at night,

and 200–300 m during daytime). The modeled BrO concentrations in the DEEP simulation are between 0 and 4 ppt, with an average of 1.2 ppt for 2007 and 0.9 ppt for 2008, which is similar to those observed by Stutz et al. (2011). However, the modeled soluble Br^- has an average of 3.1 ppt for 2007 season and 3.7 ppt for 2008 season from the DEEP scheme, more than a factor of 3 higher than those observed by Dibb et al. (2010). As shown in Fig.S7, the major components for soluble $Br^-$are HOBr and HBr. BrO in the SURF simulation is 0.2 and 0.1 pmol mol^{-1} for 2007 and 2008 season, respectively (Figure 3.6), about 1 order of magnitude lower than Stutz et al. (2011) reported. However, SURF simulated mean soluble Br^- is 0.5 ppt for both 2007 and 2008 seasons, which are much closer to values reported in Dibb et al. (2010). The discrepancy between these observations has not been reconciled.

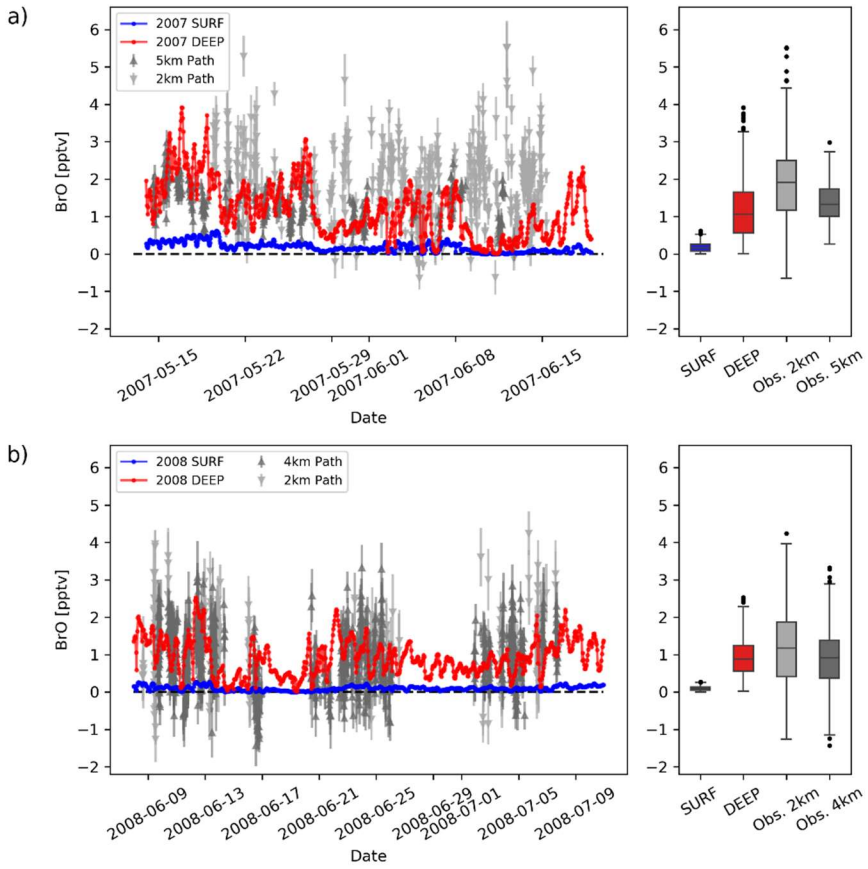

Figure 3.6. Comparison between the modeled hourly surface BrO concentrations at Summit during May–June in 2007 (a), and June–July in 2008 (b) from the SURF (blue lines and boxes)

and DEEP (red lines and boxes) simulations, and the long-path differential optical absorption spectroscopy observed BrO concentrations from Stutz et al. (2011). Each panel has the time series of BrO (left) and box and whisker plot (right). The DEEP modeled average BrO concentrations are 1.2 and 0.9 ppt for 2007 and 2008 seasons, respectively, similar to the values reported in Stutz et al. (2011).

In summary, the agreement between the DEEP simulated and the LP-DOAS observed BrO provides some validation to the large emission flux estimated in DEEP, even though LP-DOAS observed BrO is higher compared to the soluble Br^- observations. However, this large emission flux cannot be sustained by current bromine deposition flux in the model, likely due to a combination of overestimated emission and underestimated deposition. It is possible that snow bromine and/or snow oxidants are getting depleted at some point during the sunlit season, and the model lacks atmospheric bromine sources due to unaccounted anthropogenic sources or uncertainties in long-range transport (Thomas et al., 2012b). Alternatively, there may be an unknown source or mechanism (Grannas et al., 2007) that replenishes bromine in the snow photic zone in inland Greenland. Further investigations on the sources, evolution, and loss of snow bromine throughout the sunlit season are crucial for better constraining the deeper snow processes.

3.3.3 *Model limitations*

We implemented a snowpack bromine emission scheme into a global chemical transport model based on previous 1D and 3D modeling work (Swanson et al., 2022; Thomas et al., 2011; Toyota et al., 2011, 2014). Unlike previous global models, our model explicitly tracked snow bromide in surface skin layer, shut down bromine emissions when surface melting occurs (Burd et al., 2017;

Jeong et al., 2022), and separately represented the deposition-driven bromine recycling at the surface skin layer and the photochemistry-driven deeper snow reactive bromine production.

A major limitation of our global model is that it does not have an explicit representation of physical processes in the snow pack. Production of reactive bromine from deeper in the snow beneath the surface skin layer is calculated in our model using a simplified parameterization based on results from 1D snow-atmosphere models constrained by field observations (Thomas et al., 2011; Toyota et al., 2014). The 1D snow models on which the deeper snow production of reactive bromine was based were run over short time periods (3–8 days) during the spring (Toyota et al., 2014) or summer (Thomas et al., 2011), and compared well with concurrent surface observations (Liao et al., 2011; Stutz et al., 2011). Our simplified parameterization based on these 1D models resulted in an overestimate of reactive bromine emissions from beneath the snow skin layer over an annual cycle. Apart from the underestimation in atmospheric Br_y deposition, this could also suggest that the photochemical reactivity of snow bromide in snow layers below the surface skin layer decreases over time after polar sunrise, and may become the major limiting factor for photochemical reactive bromine production in snowpack later in the sunlit season. A recent laboratory study found a factor of 4–7 decrease in heterogeneous reactivity of bromine in snow after 12 days of temperature gradient dry metamorphism, likely due to the burial of bromide during the process and the subsequent absence of bromide at the air-ice interface (Edebeli et al., 2020). However, DOAS measurements at Summit during May-June, 2007 and June-July, 2008 show no drop in BrO concentrations in late summer (Stutz et al., 2011). The timing and extent of decrease in chemically reactive bromine needs further investigation.

In the model configurations employed in the previous and present studies, the photochemical reactivity of bromide captured by snow grains is pre-determined in ad-hoc manners, both in deeper layers and at the surface. For surface snow, we assume that only dry deposited bromide is photochemically reactive, effectively assuming that wet deposited bromine is encapsulated in snow grains and unavailable for surface reactions (Text S1 in Appendix B1). In their 1D snow modeling studies, Thomas et al. (2011) assumed that all bromide measured in surface melted snow is located in the liquid like layer (LLL) on snow grains and is thus photochemically reactive, while Toyota et al. (2014) calculated the reactive concentration of bromine at the surface of the snow grains by scaling the bulk bromine concentrations by the volume fraction of the LLL. Additional lab studies aimed at better understanding the details of the photochemical reactivity of snow bromine and how it evolves over time are required to inform model development efforts and improve our ability to quantify bromine preservation in the snowpack. In addition, the impact of snow acidity variations on the efficiency of bromine release is not considered in our model and is thus a source of uncertainty. Major bromine heterogeneous reactions occurring in snowpack are acid-catalyzed (R6, R7, and R9), and snow pH was shown to be important for the production of reactive bromine in snow in field experiments (Pratt et al., 2013) and lab studies (Wren et al., 2013). The ice cores presented here are acidic enough (average pH = 5.4, Figure B1 in Appendix B1) to facilitate acid-catalyzed heterogeneous reactions (Pratt et al., 2013), but the relationship between the acidity of the bulk and the LLL is unknown. Also unknown is the importance of variations in snow acidity over time, such as varying acidity over the industrial era due to anthropogenic activities or spikes in acidity due to volcanic activity (Figure B1 in Appendix B1).

3.4 Conclusions and Recommendations for Future Work

Snowpack bromine emissions are an important local source of reactive bromine over snow covered regions and are needed to explain spring Arctic ODEs (Swanson et al., 2022; Jeong et al., 2022, etc.). In contrast, loss of bromine from the snow has been considered negligible in the interpretation of long-term ice core bromine trends (Vallelonga et al., 2021). To investigate the impact of snowpack release of bromine on post-depositional loss in ice cores, we analyzed bromine trends from six Arctic ice cores dated since the pre-industrial. Among the six ice cores analyzed, the coastal Arctic ice core, AN, is the only core that shows significant trends in both Br_{exc} and Br_{enr}. The timing and direction of the observed trends in the AN core are consistent with trends in atmospheric acidity and anthropogenic emissions of bromine from leaded gasoline since 1940, and are also consistent with observed trends in sea ice extent since at least 1979.

We implemented snow bromine chemistry into a global three-dimensional model to estimate snow bromine preservation at the six ice core locations using several different assumptions. Model simulations with surface recycling show moderate snow bromine loss that is similar among the six ice core locations (9–17%). Model results with simplified photochemical bromine loss deeper in the snow beneath the skin layer suggest that photochemistry occurring in deeper snow within the snow photic zone may dominate snowpack emissions of bromine, consistent with previous modeling studies at coastal locations (Toyota et al., 2014). However, model estimates of deeper snow production over the course of a full year are unrealistically high relative to surface deposition fluxes. Model simulations that include surface recycling only, with no deeper production, agree with observations of atmospheric soluble bromine in May, June, and July at Summit, Greenland (Dibb et al., 2010), but deeper snow production is needed to explain the observed BrO (Stutz et al., 2011). Quantifying the sources of snow bromine and the extent of bromine loss within the

snow photic zone beneath the skin layer is key to understanding the extent of post-depositional loss of bromine in ice cores.

We hypothesize that snow bromine loss peaks in early spring after polar sunrise because snow Br^- concentrations are highest then. As the sunlit portion of the year progresses, the amount of photochemically reactive snow Br^- is depleted and becomes a limiting factor for deeper snow production of reactive bromine. We suggest that some portion of snow bromine is not photochemically reactive and is preserved in the snowpack, and hypothesize that this may be related to the fraction of bromine that is wet deposited to the snowpack (Text S1 in Appendix B1). If this is true, ice-core sites with higher amounts of wet deposition will be more likely to preserve atmospheric bromine trends. The availability and reactivity of wet deposited bromine species remain largely unknown and requires detailed observational and lab investigations (Bartels-Rausch et al., 2014).

The potentially significant snow bromine loss calculated in our model suggests that photochemical loss of snow bromine must be considered when interpreting ice core bromine records. Current modeling efforts lack knowledge on the photochemical reactivity of snow bromine in the snow photic zone and how it evolves throughout the sunlit season, especially in inland Arctic sites. Improving our understanding of ice-core bromine preservation requires lab studies investigating the microphysics of snow grain structure, the reactivity of snow bromine as a function of location in the snow grain, and how this might evolve over time through processes such as snow sublimation, metamorphism, melting and refreezing. It is also essential to determine how emissions of reactive bromine from the snow evolve throughout the sunlit portion of the year, particularly for inland locations where ice cores are drilled. This could be accomplished through

field studies comparing fluxes and concentrations of atmospheric and snow bromine at different times during the spring and summer.

Despite the model overestimate of loss of bromine from the deeper snow layers, the AN ice core still shows significant preservation of bromine in the model for all sensitivity simulations, consistent with the observation that it is the only ice core that demonstrates significant trends since the pre-industrial. In contrast, the large bromine loss modeled in Greenland supports the lack of trends in Greenland ice core bromine records. The AN core is also the only ice core that has snow layers that are relatively isolated from sunlight due to the high snow accumulation rate and relatively long polar night (Text S1 in Appendix B1). The observed trends in AN total bromine are qualitatively consistent with observed trends in a mid-latitude ice core, CDD (Legrand et al., 2021). The trends in the CDD ice core were mainly attributed to trends in emissions of bromine from leaded gasoline, which was phased out in Europe in 1970s (Lammel et al., 2002). This study does not quantify the role of anthropogenic emissions (including acidity and gasoline usage) or sea ice extent in regulating trends observed in the AN core. We will examine this in a follow-up study.

Chapter 4. ANTHROPOGENIC INFLUENCE ON TROPOSPHERIC REACTIVE BROMINE SINCE THE PREINDUSTRIAL: IMPLICATIONS FOR ICE-CORE BROMINE TRENDS

This work is in preparation for submission for publication. Coauthors will include Becky Alexander, Joseph R. McConnell, Nathan Chellman, Thomas Opel, Hanno Meyer, Lyatt Jaeglé, and Koji Fujita.

Abstract

Tropospheric reactive bromine (Br_y) influences the oxidation capacity of the atmosphere by acting as a sink for ozone and nitrogen oxides. Aerosol acidity plays a crucial role in Br_y abundances through acid-catalyzed debromination from sea-salt-aerosol, the largest global source. Bromine concentrations in a Russian Arctic ice-core show a 3.5-fold increase from pre-industrial (PI) to the 1970s (peak acidity, PA), followed by a −53% decrease to 1999 (present day, PD). Ice-core acidity mirrors this trend, showing robust correlation with bromine, especially after 1940 (r=0.9). Model simulations considering anthropogenic emission changes alone show that acidity is the main driver of Br_y changes, consistent with the observed relationship between acidity and bromine. The model underestimates the observed PI-to-PA increase and especially the PA-to-PD decline in bromine and acidity, indicating uncertainties in Russian Arctic anthropogenic emissions. Future effort in the interpretation of ice core bromine trends must consider changes in atmospheric acidity.

4.1 INTRODUCTION

Tropospheric reactive bromine influences tropospheric oxidation capacity, destroying ozone via catalytic cycles and perturbs OH to HO_2 ratios towards OH (von Glasow et al., 2004). In coastal polar regions, reactive bromine is responsible for springtime boundary layer ozone depletion events (ODEs) (Barrie et al., 1988; McConnell et al., 1992; Simpson, von Glasow, et al., 2007) and gaseous elemental mercury deposition (Steffen et al., 2008; S. Wang et al., 2019), thus also impacting the transfer of toxic mercury from atmosphere into the ecosystem.

Natural sources of tropospheric gaseous reactive bromine (Br_y = Br + HBr + $BrNO_2$ + $BrNO_3$ + BrO + HOBr + $2Br_2$ + IBr + BrCl) include sea-salt debromination (Kerkweg et al., 2008; Yang et al., 2005), organobromines emitted from the marine biosphere (Liang et al., 2010; Quack & Wallace, 2003), saline lakes (Hebestreit et al., 1999; Matveev et al., 2001), and volcanoes (Aiuppa et al., 2005; Bobrowski et al., 2003). Anthropogenic-related sources of Br_y includes methyl bromide (CH_3Br) emissions from agricultural pesticide (Clerbaux et al., 2007), coal burning (Lee et al., 2018), biomass burning, and stratospheric transport from halons degradation. Gaseous CH_3Br and aerosol PbBrCl exhaust emissions from leaded gasoline vehicles have been important since the 1920s, diminishing with leaded gasoline abatement in North America and Europe from the 1960s (Habibi, 1973; Lammel et al., 2002; Thomas et al., 1997). The observed 2-fold increase in summertime ice-core bromine after 1950 from the alpine ice-core Col du Dome, is largely attributed to leaded gasoline emissions (Legrand et al., 2021b). Global model simulations showed an increase in Br_y from PI to PD driven by enhanced oceanic iodine production from ozone deposition, increased anthropogenic bromocarbons, and increased bromine flux from stratosphere (Sherwen et al., 2017). However, the model did not consider leaded gasoline or sea-salt debromination, the latter being the largest global source (95%) of Br_y (X. Wang et al., 2021).

The polar regions have additional sources of Br_y from saline blowing snow sourced sea-salt-aerosol (J. Huang et al., 2020; Savelyev et al., 2006; Yang et al., 2008) and direct snowpack emissions (Abbatt et al., 2012; Foster et al., 2001; Pratt et al., 2013; Simpson, Carlson, et al., 2007; Simpson, von Glasow, et al., 2007; Stutz et al., 2011). Both sources are most efficient from snow on first-year-sea-ice (FYI), which is thinner, more saline (Confer et al., 2023; Frey et al., 2020; Yang et al., 2008), and contains more snow bromine from upward migration of brine from the sea ice surface (Nandan et al., 2017; Peterson et al., 2019) than snow over multi-year-sea-ice (MYI). The sea-ice source of Br_y has led to the use of Arctic ice-core bromine as a proxy for historical sea ice extent (Spolaor et al., 2014, 2016; Sturges & Barrie, 1988; Vallelonga et al., 2021). For example, Spolaor et al., 2016 found a positive correlation (r=0.44) between bromine excess (Br_{exc}) records from a Russian Arctic ice-core, Akademii Nauk, and spring sea ice area of the Laptev Sea during 1950–1998, with both showing a steadily decreasing trend.

Although total sea ice extent has been decreasing since at least 1979 (Cavalieri & Parkinson, 2012), FYI has been increasing with the decline of MYI (Bougoudis et al., 2020; Confer et al., 2023). Sea-salt concentrations are observed to increase by 9–12% decade^{-1} during spring and winters in 1980–2017 at Alert (Confer et al., 2023). This is consistent with modeling results from Confer et al. (2023), which show a pan-Arctic increase in surface sea-salt-aerosol concentrations since 1980, partially due to enhanced blowing snow emissions driven by increased FYI. With increased FYI in the Arctic since at least 1980, snowpack emitted bromine may also become a more efficient source (Swanson et al., 2022). Indeed, satellite observations show increasing trends in tropospheric BrO columns over Arctic sea ice (+15% decade^{-1}) during polar spring from 1996–2017 (Bougoudis et al. 2020).

Although sea-salt release of Br_y is a natural process, the debromination reaction is catalyzed by aerosol acidity (R1–2) (Eigen & Kustin, 1962; Fan & Jacob, 1992), which is influenced by anthropogenic emissions of acidic gases such as SO_2 and NO_x (= NO + NO_2).

$$BrNO_3/HOBr(aq) + Br^-(aq) + H^+(aq) \rightarrow Br_2 + H_2O/HNO_3(aq) \quad (R1)$$

$$ClNO_3/HOCl(aq) + Br^-(aq) + H^+(aq) \rightarrow BrCl + H_2O/HNO_3(aq) \quad (R2)$$

In the Arctic, snow acidity measured in ice-cores began increasing in the 1940s, peaked in the 1970s and decreased to the present day (e.g., Geng et al., 2014). Therefore, the quality of ice-core bromine as a sea ice proxy may be compromised by these anthropogenic influences (Maselli et al., 2017). The relative impacts of sea ice extent and atmospheric acidity on bromine trends since the pre-industrial remain unclear.

We use a global model to quantify the impact of anthropogenic emissions on tropospheric reactive bromine abundances since the pre-industrial. We compare the model to bromine observations in an Arctic ice-core and discuss implications of anthropogenic emissions for tropospheric Br_y abundance and the interpretation of ice-core bromine records.

4.2 METHODS

4.2.1 *GEOS-Chem model and historical simulations*

We use a global 3D chemical transport model GEOS-Chem (version 11-02d, https://github.com/geoschem/geos-chem/tree/v11-02d-prelim) for historical simulations. The model is driven by MERRA-2 assimilated meteorological fields from the Goddard Earth Observing System (GEOS) (Gelaro et al., 2017), and contains detailed HOx-NOx-VOC-ozone-halogen-aerosol tropospheric chemistry (X. Wang et al., 2021) and fully coupled stratospheric chemistry (Eastham et al., 2014). Detailed modeled bromine chemistry is shown in Figure C1–C3.

Sea-salt-aerosol debromination occurs in both open ocean (Jaeglé et al., 2011) and blowing snow (J. Huang & Jaeglé, 2017) sourced sea-salt-aerosol. Following Zhai et al. (2023), ozone dry deposition velocity onto snow and ice is updated to 0.01 cm s^{-1}, consistent with observations (Simpson, Carlson, et al., 2007). Snowpack bromine emissions (Swanson et al., 2022; Zhai et al., 2023) are not included in the model.

Model simulations are performed under three anthropogenic emission scenarios: pre-industrial (PI, year 1750), peak atmospheric acidity (PA, year 1975), and present day (PD, year 1999). Anthropogenic and biomass-burning emissions vary between simulations to reflect their impacts on tropospheric bromine. Detailed emission setup can be found in Zhai et al. (2021). After a 1-year spin-up, each simulation is run for 1 year using 2007 meteorology. By using the same meteorology, we aim to isolate changes induced by anthropogenic emissions. All simulations are conducted at 4° × 5° horizontal resolution and 72 vertical levels up to 0.01 hPa.

We added two additional anthropogenic sources of bromine to the model from coal and leaded gasoline production. Bromine emissions from coal fired power plants in the chemical form HBr is expected to be correlated with SO_2 emissions, assuming similar Br:S ratios in coal and the fact that SO_2 control strategies such as wet flue gas desulfurization also effectively removes bromine from exhaust (Lee et al., 2018; McTigue et al., 2014). To calculate coal burning emitted HBr, we scale coal burning emitted SO_2 with a scale factor of Br_x:SO_2 (where $Br_x = BrCl + BrNO_2 + 2\times Br_2$) = 1.5×10^{-4} ppb:ppb, which is the median of observed Br_x:SO_2 ratios from Lee et al. (2018). This is likely an underestimate since the major form of reactive bromine emitted from coal burning is expected to be HBr, which was not measured.

We also added historical emissions of particle-phase PbBrCl and gas-phase CH_3Br from leaded gasoline for PA. Brominated compounds were added to leaded gasoline as additives since 1923 to

prevent lead deposition in engines (Thomas et al., 1997). Leaded gasoline phase-out efforts, starting in the 1960s in North America and the 1970s in Europe, effectively eliminated global Pb emissions from this source (Hagner, 2002; S. Huang et al., 1996; Nriagu, 1990). Annual global bromine usage in gasoline peaked in the early 1970s at 170 ±20 kT, decreasing to 100±11 kT in 1980 (Thomas and Bedford, 1997). Assuming complete Br emission into the atmosphere, we estimated global bromine emissions from leaded gasoline in 1975 (average of early 1970s and 1980, 135±15 kT) using the transportation-emitted CO and global mean transportation-CO:Br ratio from a global anthropogenic emission inventory (Community Emissions Data System, CEDS) (McDuffie et al., 2020). Leaded gasoline sourced bromine is emitted as 85% PbBrCl and 15% CH_3Br based on exhaust measurements (Habibi, 1973; Harsch & Rasmussen, 1977). PbBrCl is modeled as accumulation-mode aerosol, considering the majority of lead particles emitted are under 5μm in wet diameter (Habibi 1973).

4.2.2 *Ice-core Bromine and Acidity Observations*

A 724m-long ice-core was collected from the Akademii Nauk (AN) ice cap (80.5 ºN, 94.8 ºE, 750m a.s.l.) at Severnaya Zemlya in the Russian Arctic (Fritzsche et al., 2002; Opel et al., 2013). The snow accumulation rate is about 440 kg m^{-2} yr^{-1}. The ice-core covers an estimated time range of year 200 BCE –1999 CE, but we only present records since CE 1750. This ice-core was chosen because it is expected to preserve an atmospheric signal of bromine due to its high snow accumulation rate and high-latitude location, both of which limit photochemical loss of bromine in the snowpack (Zhai et al., 2023).

Total sodium, total bromine, and acidity records from the AN core have been published before (Zhai et al., 2023) and are briefly described here. Elemental sodium (Na) and bromine (Br) were measured using the continuous high resolution inductively coupled plasma mass spectrometry

(HR-ICP-MS) at the Desert Research Institute (Maselli et al., 2017), with an uncertainty of ±10%. Acidity (H^+) was directly measured continuously (Pasteris et al., 2012), with an uncertainty below 5%. Bromine excess (Br_{exc}) is calculated as shown in Eq.1.

$$[Br_{exc}] = [Br]_{ice\text{-}core} - [ssNa]_{ice\text{-}core} \times ([Br]/[Na])_{sea\ water} \quad \text{(Eq. 1)}$$

Where [X] is the mass concentrations in ng X g ice^{-1}, and $([Br]/[Na])_{sea\ water}$ is the sea water Br/Na mass ratio of 0.00624 (Millero et al., 2008). [ssNa] is calculated based on ice-core calcium concentrations, as described in Maselli et al. (2017).

4.3 RESULTS

4.3.1 *Ice-core bromine records at Akademii Nauk*

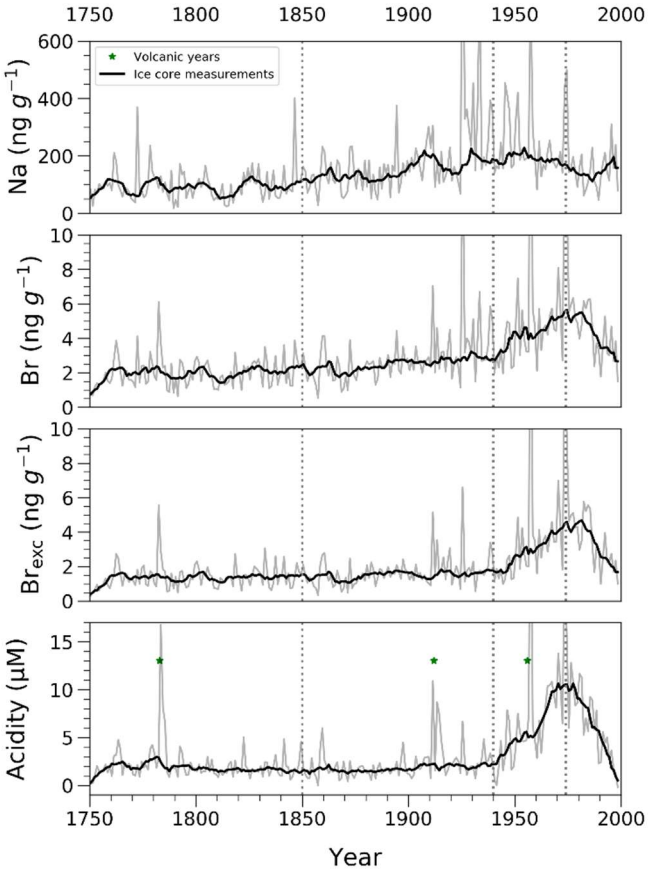

Figure 4.1. Total sodium, total bromine, Br_{exc}, and acidity concentrations in the Akademii Nauk ice-core. Gray lines are the measured annual ice-core concentrations (total sodium, total

bromine, and acidity) or calculations (Br_{exc}), and black lines are the 9-year running average, with outliers outside of 1.5×IQR (interquartile range) removed. Green stars mark the large and moderate volcanic years identified in previous studies (Opel et al. 2013). Dashed vertical gray lines mark the years 1850, 1940, and 1975.

Figure 4.1 shows the total Na, total Br, Br_{exc}, and acidity concentrations in the Akademii Nauk ice-core. Change point analysis (Ruggieri, 2013; Zhai et al., 2023) does not identify any change point in the Na record, and there is a slight increasing trend of 0.67±0.00 ng g^{-1} yr^{-1} in Na throughout the record, resulting in a 77% increase from the pre-1850 average Na concentration to that of post-1970. Total Br, Br_{exc}, and acidity show no trends during 1850–1940, and their large increases start in the 1940s. Total Br has an average concentration of 2.02±0.88 ng g^{-1} before 1850, increased by 3.5-fold from pre-1850 to the 1970s, and decreased by −53% after the 1970s to the end of the record (year 1999). Similar trends are shown in Br_{exc}, with a 4-fold increase from the pre-1850 level to the 1970s, followed by a −59% decrease afterwards (Table C1). Br_{exc}/Br ratio ranges from 26–94%, and is higher (80%±6%) in the 1970s compared to PI (1750–1850, 69%±11%) and PD (post-1989, 70%±11%). Acidity shows a similar trend as Br, with a background concentration of 2.16±1.93 μM before 1850, and an increase of 5.5-fold from pre-1850 to 1975, and decreased by −72% back to pre-industrial level by the end of the record (year 1999).

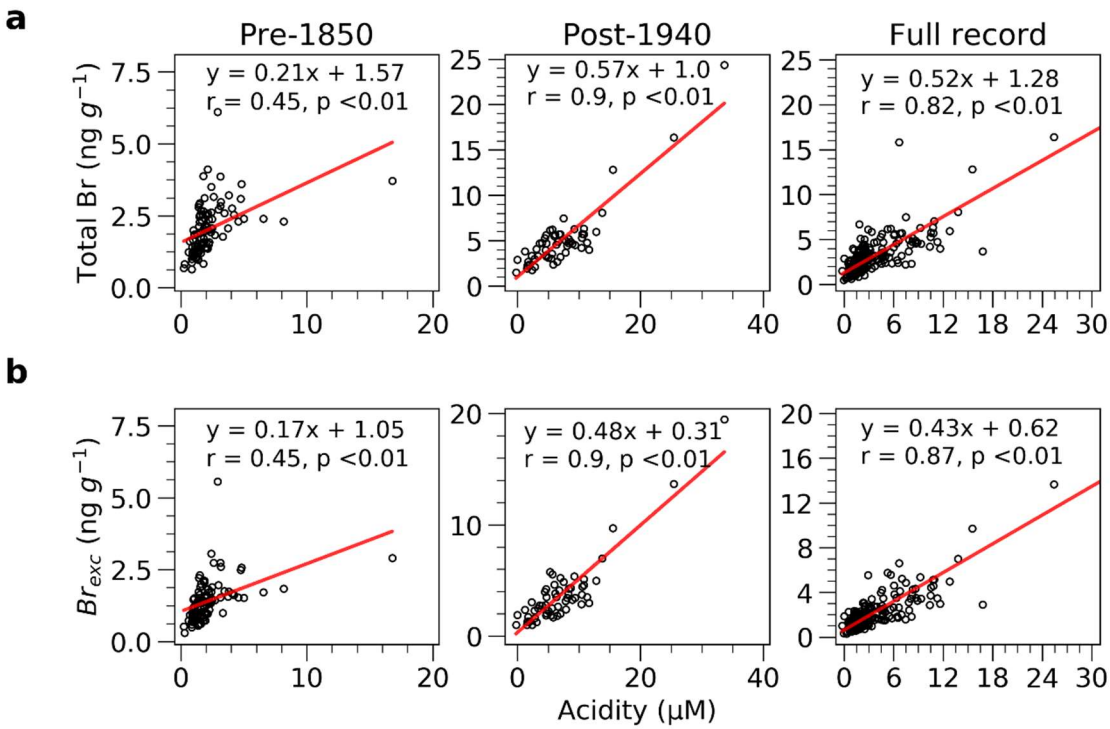

Figure 4.2. Relationship between concentrations of a) total Br and acidity, and b) Br_{exc} and acidity from the AN ice core, for 1750–1850 (pre-1850), 1940–1999 (post-1940), and 1750–1999 (full record). Black circles show the measured Br, Br_{exc}, and acidity concentrations, and red lines represent the linear least-squares fitting lines, with functions shown in each panel.

Figure 4.2 shows the relationship between ice core bromine (Br and Br_{exc}) and measured snow acidity. Significant positive correlation (p<0.01) is shown for pre-1850, post-1940, and the full record, with post-1940 showing the highest correlation coefficient (r=0.9). The relationship between ice core bromine and snow acidity throughout the record is much stronger than that of bromine and spring sea ice extent for 1980–1999 reported in Spolaor et al. (2016), suggesting that it is possible that factors other than sea ice, such as acidity, may play a role in driving ice core bromine trends.

4.3.2 *Ice-core-model comparison*

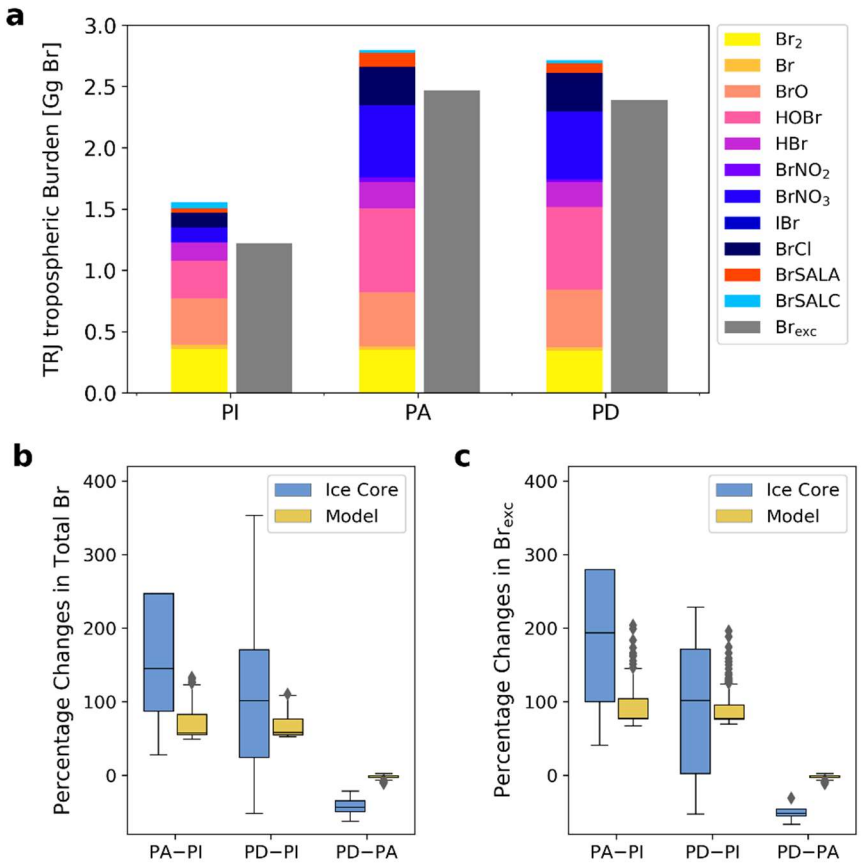

Figure 4.3. Modeled bromine burden and speciation in the three time periods and model-ice-core comparison. a) Modeled annual mean tropospheric burdens of bromine species (colored bars) and the calculated Br_{exc} burden (gray bars) in the TRJ of the AN site for PI, PA and PD. Comparison of percentage changes in annual mean tropospheric b) total Br and c) Br_{exc} burdens between PI, PA, and PD from ice-core records and model simulations.

Figure 4.3a and Table C2 show the modeled annual mean tropospheric total bromine burden and its speciation in the TRJ in PI, PA and PD. Total Br and Br_{exc} are calculated based on Eq. 2 and Eq. 3, respectively,

$$Toal\ Br = Br_y + Br_a^- + Br_c^- \quad \text{(Eq. 2)}$$

$$Br_{exc} = Total\ Br - ssNa \times \left(\frac{[Br]}{[Na]}\right)_{sea\ water} \quad \text{(Eq. 3)}$$

where Br_a^- and Br_c^- in Eq.2 are bromide in accumulation-mode and coarse-mode aerosol, respectively, and ssNa is sodium in sea-salt-aerosol (both modes).

Br_y contributes about 95% of total Br in the three time periods, while aerosol bromine is minor (5%); therefore, total Br shows similar distribution and trends with Br_y. The most abundant Br_y species in PI are Br_2 and BrO, contributing 48% of total Br. Br_2 and BrO burdens remain similar from PI to PA, while HOBr, $BrNO_3$ and BrCl increase by 125%, 392%, and 158%, contributing 24%, 21%, and 11% to total Br in PA, respectively. Increased fraction of $BrNO_3$, HOBr, and BrCl in total Bry are driven by enhanced NO_x and HO_2 concentrations and more active coupled chlorine-bromine chemistry from PI to PA. Modeled total Br burden and speciation in PD are quite similar to those of PA. HOBr, $BrNO_2$, and Br_a^-decreased slightly from PA to PD while other species increased.

Br_a^- increased 2.8-fold from PI to PA and decreased −30% from PA to PD (Figure C2–C4). In contrast, Br_c^- decreased by −40% from PI to PA and remained low in PD (−0.2% from PA to PD). The opposite trends in Br_a^- and Br_c^- from PI to PA suggests that debromination liberated bromide from coarse-mode aerosol to the gas-phase and partially re-partitioned into the accumulation-mode aerosol. Br_{exc}/total Br ratios are 78%, 82%, and 88% for PI, PA, PD, respectively, consistent with values observed in the AN ice-core (Table C1).

Figure 4.3b and c compare the percent changes in modeled total bromine and Br_{exc} burdens, respectively, with ice-core total bromine and Br_{exc} concentrations between the 3 time periods. The model predicts a 2-fold increase in total Br and Br_{exc} from PI to PA and only a small decrease (−3%) from PA to PD. In comparison, ice-core Br and Br_{exc} show a more symmetrical change centered in 1975 with a 3-fold increase from PI to PA, and −50% decrease from PA to PD. The modeled increase (75% and 96% for total Br and Br_{exc}, respectively) from PI to PD is quantitatively

consistent with ice-core observations (64% and 67% for total Br and Br_{exc}, respectively), suggesting that the model may underestimate Br burden in PA (Figure 4.3b).

4.3.3 *Factors controlling modeled bromine trends*

Figure 4.4 shows the budget analysis for Br_y, HOBr, $BrNO_3$, and BrCl in the AN TRJ. Sea-salt debromination dominants (>99%) Br_y production in PI, PA, and PD. Organobromines and anthropogenic bromine, including coal combustion and leaded gasoline emissions, contribute less than 1% to the total Br_y sources. Uptake onto sea-salt-aerosol removes >80% of Br_y, while the rest either deposits or is transported out of the TRJ region. Budget analysis (Figure C1–C3) shows that HBr uptake on fine-mode-aerosol is the dominant source of Br_a^-, at least 1 order of magnitude larger than natural emissions.

Total Br_y production rate increased by +236% from PI to PA. The increase is predominately driven by enhanced sea-salt-aerosol debromination due to a decrease in aerosol pH from 2.5 to 0.9 in the AN TRJ (Figure C6). This is consistent with the observed strong correlation (r=0.9, p<0.01) between ice core Br and acidity after 1940 (Fig.2). From PI to PA, the largest increases in Br_y burden were driven by increases in HOBr, $BrNO_3$ and BrCl. The only source of $BrNO_3$ is the reaction of BrO and NO_2, which increased by 3.5-fold caused by enhanced NO_2 (Figure C7) and BrO abundance. BrCl production rate increased by 1.6-fold, and this is mainly driven by more active halogen recycling on accumulation-mode aerosol ($HOBr + Cl^- + H^+ \rightarrow BrCl + H_2O$), caused both by elevated HOBr burden (Figure C1 and C2) and more acidic aerosol (Figure C6). HOBr production rate increased by 1.2-fold, caused mainly by increased oxidation of BrO by HO_2, which is driven by enhanced BrO abundance (+17%) and higher HO_2 mixing ratios (+33%) from PI to PA.

From PA to PD, Br_y production rate decreased by −21%, due to reduced aerosol acidity (Figure C6) and less debromination. Interestingly, modeled Br_y tropospheric burden shows minor changes (Fig. 3), because the decreases in Br_y production rate are counterbalanced by decreases in HBr uptake onto sea-salt-aerosol from PA to PD. This decreasing trend in HBr uptake is driven by lower tropospheric abundance of HBr (−6%) caused by less formation from the reaction between Br radical and acetaldehyde ($Br + CH_3CHO \rightarrow HBr + CH_3CO$), which is the main source of HBr. In other words, the reduction in tropospheric acetaldehyde burden from PA to PD (−29%) causes a decrease in Br_y sinks.

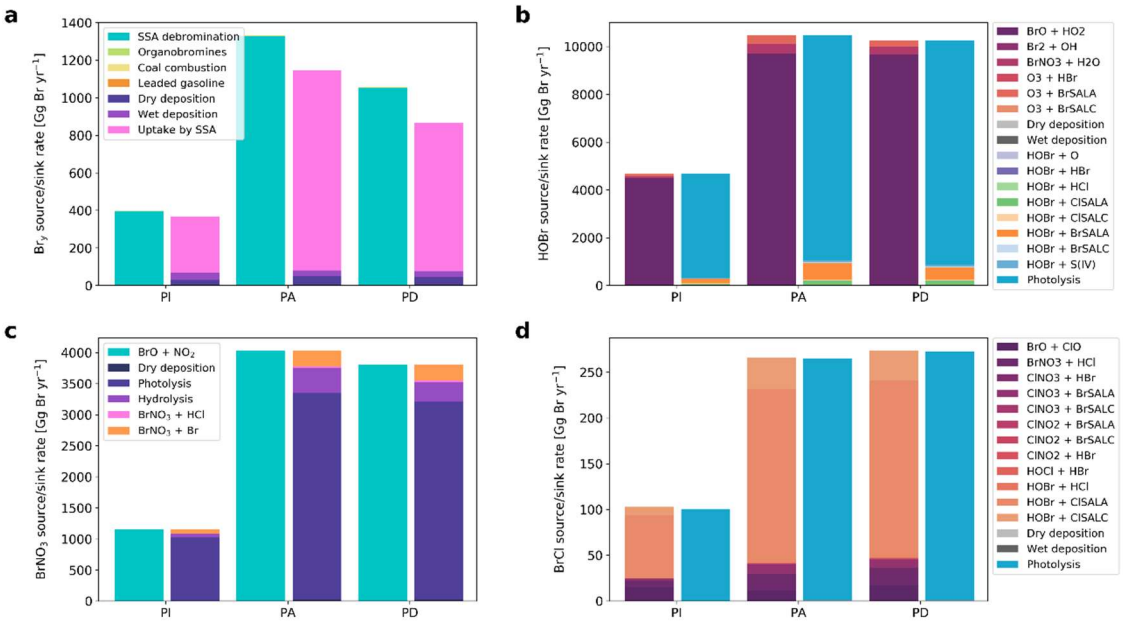

Figure 4.4. Modeled annual mean sources and sinks of tropospheric a) Br_y b) HOBr c) $BrNO_3$ and d) BrCl in the AN TRJ for PI, PA, PD. For each time period, left bar shows the sources and right bar shows the sinks. Differences between total sources and total sinks of Br_y can be explained by Br_y that transported outside of the AN TRJ. XSALA, XSALC (X=Cl, Br) are chloride and bromide in accumulation- and coarse-mode sea-salt-aerosol, respectively. S(IV) represents SO_3^{2-} and HSO_3^- in cloud droplets.

4.4 DISCUSSION

The historical simulations with changes in anthropogenic emissions alone can quantitatively capture the ice-core bromine changes from PI to PD, but they underestimate the increase in bromine from PI to PA and do not reproduce the observed −53% decrease in ice-core bromine from PA to PD. No sea ice changes are simulated, but a model sensitivity study with 1980 meteorology (lower FYI and higher MYI, Fig.S8) shows a lower (−6%) tropospheric Br burden due to decreases in blowing snow sourced sea-salt-aerosol (Fig.S9), consistent with Confer et al. (2023). The positive relationship between modeled Br_y and FYI is consistent with Bougoudis et al. (2020), and suggests that recent changes in sea ice cannot explain the decline in ice-core Br since 1975.

Bromine measured in the French Alps Col du Dome (CDD) ice-core showed a 2-fold increase in summertime ice-core bromine from the late-1940s to the mid-1970s, followed by a −22% decrease until 2000 (Legrand et al., 2021a). Our simulations quantitatively capture these bromine trends (Figure C10), and modeled cloud acidity (Fig.S11) also quantitatively captures snow acidity trends reported in Legrand et al. (2003), suggesting that anthropogenic emissions alone can explain the observed changes in the CDD ice-core. The modeled trends are caused mainly by acid-catalyzed sea-salt debromination, instead of direct emissions from leaded gasoline as suggested in Legrand et al. (2021a).

Acid-catalyzed debromination is the dominant source of Br_y and changes in acidity drive trends in Br_y in the model. The measured snow acidity at AN increased 5.5-fold from PI to PA, and decreased back to pre-industrial level in 1999 (Figure 4.1). However, neither modeled aerosol nor cloud acidity returns to pre-industrial levels in PD (Figure C6). Anthropogenic emissions of acid precursors NO_x and SO_2 in emission inventories decline by −20% and −44%, respectively, since

1975 in AN TRJ (Figure C12), but do not drop back to pre-industrial levels as observed at AN. The drastic decline in ice-core acidity was not seen in Greenland (Zhai et al, 2023) or Alpine ice-cores (Legrand et al., 2003; Preunkert & Legrand, 2001). The model underestimate in bromine decline from PA to PD may be due to the underestimated decrease in acidity. The relatively stable modeled Br concentrations from PA to PD is also due to a decline in Br_y loss rate caused by decreased atmospheric acetaldehyde.

The model's limitations include uncertainties in halogen chemistry, particularly in the HBr/sea-salt Br^- partitioning treated as a kinetic reaction with large uncertainties in GEOS-Chem (Ammann et al., 2013; X. Wang et al., 2021). This results in a model prediction of bromine depletion for accumulation-mode aerosol in the marine boundary layer, contrasting observed bromine enrichment (Sander et al., 2003). However, our previous work on ice-core chlorine indicates minimal changes in HCl partitioning from PA to PD (Zhai et al., 2021), suggesting similar stable thermodynamic HBr/sea-salt Br^- partitioning between these periods.

4.5 CONCLUSIONS

Tropospheric reactive bromine destroys surface ozone via catalytic cycles and has profound impacts on the tropospheric oxidation capacity (Barrie et al., 1988; von Glasow et al., 2004). Both acid-catalyzed debromination (X. Wang et al., 2021; Zhu et al., 2019) and sea ice variations (Spolaor et al., 2016; Vallelonga et al., 2021) can influence ice core bromine trends. However, the relative importance of these factors on Arctic ice-core bromine trends since the pre-industrial remain unclear. We present bromine records from a Russian Arctic ice-core, Akademii Nauk (AN) since the pre-industrial, and use GEOS-Chem model simulations to understand the trends and influencing factors. The AN ice-core shows a 3.5-fold increase in total Br from pre-1850 to the 1970s, followed by a decrease of −53% from the 1970s to year 1999. Measured ice-core acidity

increased by a factor of 5.5, followed by a −72% decrease after the 1970s, dropping back to pre-industrial level by the end of the record.

Sea-salt debromination is the dominant (>99%) source of Br_y in all the emission scenarios, and direct emissions of anthropogenic bromine contributes less than 1% to the total Br_y sources even in PA. Modeled changes in anthropogenic acidity alone can explain the +236% increase in Br and Br_{exc} observed in the AN ice-core between PI and PD. The modeled 2-fold increase in Br_y is smaller than the observed increase in ice-core Br_{exc} (3-fold) from pre-1850 to 1975, and the modeled increase is driven by increases in anthropogenic emissions of acid gas precursors. The modeled relationship between atmospheric Br_y and acidity is consistent with observed relationships between ice-core bromine and acidity from high-latitude Arctic (Fig.2) and mid-latitude alpine ice-cores.

The model does not capture the observed decrease in both Br_y (−53%) and acidity (−72%) after 1975, likely due to uncertainties in anthropogenic emissions of acidic gas-phase precursors in Russia. Since variability in atmospheric Br_y is driven by atmospheric acidity, the modeled underestimate of the decline in acidity since 1975 contributes to the modeled underestimate of the decline in Br_{exc}. Our historical simulations with varying anthropogenic emissions alone are able to quantitatively capture both bromine and acidity trends in a mid-latitude Alpine ice-core CDD since the 1920s (Figure C10). Our results show that anthropogenic acidity has had a profound influence on the production and abundance of tropospheric reactive bromine (Br_y), with implications for the oxidation capacity of the atmosphere. The use of ice-core bromine as a proxy for past changes in sea ice extent must consider changes in atmospheric acidity in the interpretation of observed trends.

Chapter 5. CONCLUSIONS AND FUTURE WORK

5.1 CONCLUSIONS

Tropospheric reactive chlorine and bromine play a critical role in regulating the oxidation capacity of the troposphere, but their historical trends since the pre-industrial, and how they are influenced by anthropogenic emissions remain unclear. This dissertation presents chlorine and bromine ice core records from multiple Arctic ice cores, and investigates the impact of anthropogenic emissions on their trends using historical simulations conducted in a global chemical transport model. Our results demonstrate that anthropogenic impacts, including direct emissions of halogen species and indirect modulation of natural production mechanisms, are key drivers of ice core chlorine and bromine variations since the pre-industrial.

In Chapter 2, chlorine records from six Greenland ice cores are presented and historical simulations using the GEOS-Chem model with changes in anthropogenic emissions alone are used to interpret the ice core trends. While total chlorine in Greenland ice cores mostly originates from sea salt aerosol, anthropogenic impacts on non-sea-salt chlorine significantly influenced total chlorine and its trends after the 1940s. Cl_{exc} records show no trends before the 1940s, increased by 2–7-fold during the 1940s–1970s, and decreased or leveled off afterward. Model shows that the increases are mainly driven by enhanced acid-displacement, direct HCl emissions from coal combustion, and reactions induced by anthropogenic NO_x emissions, and the decrease after the 1970s was a result of reduced HCl emissions from air pollution mitigation policies. Our study highlights the profound impacts of anthropogenic acid precursor emissions (HCl, SO_2 and NO_x) on tropospheric reactive chlorine abundance, and these impacts need to be considered in estimating anthropogenic impacts on tropospheric oxidation capacity.

In Chapter 3, an empirical parameterization of snowpack emissions is implemented in the GEOS-Chem model, and the extent of bromine post-depositional loss is quantified for six Arctic ice core locations for the first time. Trend analysis shows that a Russian Arctic ice core, Akademii Nauk, is the only ice core that preserves significant bromine trends that aligns with the influencing factors. Model results show a 9–17% loss of bromine from the snow skin layer (top 1mm) for all locations, and the more important loss is from snow photic zone below this layer. Even though the magnitude of this deeper loss suffers large uncertainties and is overestimated in the model, model results show that Akademii Nauk is most likely to preserve atmospheric bromine signals compared to the Greenland ice cores, because of its high latitude location, high snow accumulation rate, and summer melting events. Our results present the significance of bromine post-depositional loss and its influencing factors, which needs to be considered in future ice core bromine interpretation.

In Chapter 4, ice core bromine records since 1750 in Akademii Nauk are presented, and anthropogenic influences on bromine trends are examined using GEOS-Chem historical simulations, with additions of coal combustion and leaded gasoline emissions. Bromine at Akademii Nauk shows a 3.5-fold surge from pre-industrial times to the 1970s (peak acidity), followed by a halving in 1999 (present day). The acidity of the ice core mirrors this pattern, showing a strong correlation with bromine, particularly after 1940 (r=0.9). Simulations based on anthropogenic emission changes alone indicate that acidity is the primary factor influencing bromine trends, consistent with the observed relationship between acidity and bromine in the ice core. The model underestimates the observed pre-industrial to peak acidity increase and the peak acidity to present day decline in both bromine and acidity, suggesting uncertainties in anthropogenic emissions in the Russian Arctic. Future analysis of ice core bromine trends should take into account changes in atmospheric acidity.

5.2 FUTURE WORK

Tropospheric iodine regulates the pan-Arctic oxidization capacity via efficient ozone depletion, likely more important than bromine (Benavent et al., 2022), and forms ultrafine aerosol particles which may serve as cloud condensation nuclei (He et al., 2021; Huang et al., 2022), thus have implications for climate. Knowledge on both the speciation and chemistry of tropospheric iodine, especially in the aerosol phase, remains highly uncertain. Ice core iodine has been used as a sea ice proxy because of its association with bioproductivity from open ocean and fresh sea ice surfaces (Spolaor et al., 2016; Maffezzoli et al., 2021; Vallelonga et al., 2021). On the other hand, enhanced ozone concentrations since the pre-industrial caused by human activities is shown to increase the HOI and I_2 production from the ocean surface, globally the largest source of tropospheric reactive iodine (Sherwen et al., 2017). Investigating ice core iodine trends and how it is impacted by anthropogenic emissions using state-of-science global models represents a compelling avenue for future research endeavors.

As suggested in Chapter 3, understanding of the abundance and speciation of snow bromine and how they vary throughout an annual cycle is essential to quantify snowpack bromine loss. Recent development in instrumentation allows the detection of trace level bromine species in the snow. Frassati et al. (2023) shows that bromate (BrO_3^-) remains constant in deep snow that is buried in the dark, while higher concentrations of bromate were detected in the sunlit snow layers. It is possible that reactive bromine species are oxidized in the snowpack after deposition, and convert into a relatively inactive reservoir bromine species. Future field and laboratory studies need to understand the mechanism of the oxidation, and how it affects snowpack bromine preservation.

Chapter 2 and 4 present the historical trends in ice-core chlorine and bromine records, highlighting the anthropogenic influences in regulating these trends. The impacts of changing tropospheric halogens on greenhouse gases such as methane and ozone, remain highly uncertain. Sherwen et al. (2007) investigated the impact of halogen chemistry on radiative forcing of tropospheric ozone since the pre-industrial. However, the model used in this study lacks sea-salt debromination reaction, thus it cannot fully quantify halogens' impact and needs to be revisited using the latest version of GEOS-Chem. In addition, a recent study (van Herpen et al., 2023) proposes a photocatalytic chlorine atom production mechanism on mineral dust–sea spray aerosols, which generates 3.8 Tg (Cl) y^{-1} of chlorine species over the North Atlantic region, and increases global

chlorine production by 41% in a global model. This new mechanism needs to be implemented into GEOS-Chem, and its impact on Arctic ice-core chlorine trends and the global methane budget can be investigated.

BIBLIOGRAPHY

Abbatt, J. P. D., Oldridge, N., Symington, A., Chukalovskiy, V., McWhinney, R. D., Sjostedt, S., & Cox, R. A. (2010). Release of gas-phase halogens by photolytic generation of OH in frozen halide-nitrate solutions: an active halogen formation mechanism? *The Journal of Physical Chemistry. A*, *114*(23), 6527–6533. https://doi.org/10.1021/jp102072t

Abbatt, J. P. D., Thomas, J. L., Abrahamsson, K., Boxe, C., Granfors, A., Jones, A. E., et al. (2012). Halogen activation via interactions with environmental ice and snow in the polar lower troposphere and other regions. *Atmospheric Chemistry and Physics*, *12*(14), 6237–6271. https://doi.org/10.5194/acp-12-6237-2012

Ahmed, S., Thomas, J. L., Tuite, K., Stutz, J., Flocke, F., Orlando, J. J., et al. (2022). The role of snow in controlling halogen chemistry and boundary layer oxidation during arctic spring: A 1D modeling case study. *Journal of Geophysical Research*, *127*(5). https://doi.org/10.1029/2021jd036140

Aiuppa, A., Federico, C., Franco, A., Giudice, G., Gurrieri, S., Inguaggiato, S., et al. (2005). Emission of bromine and iodine from Mount Etna volcano. *Geochemistry, Geophysics, Geosystems*, *6*(8). https://doi.org/10.1029/2005gc000965

Akers, P. D., Savarino, J., Caillon, N., Magand, O., & Le Meur, E. (2022, August 24). *Photolytic modification of seasonal nitrate isotope cycles in East Antarctica*. *EGUsphere*. https://doi.org/10.5194/egusphere-2022-812

Alexander, B., Park, R. J., Jacob, D. J., Li, Q. B., Yantosca, R. M., Savarino, J., et al. (2005). Sulfate formation in sea-salt aerosols: Constraints from oxygen isotopes. *Journal of Geophysical Research*, *110*(D10). https://doi.org/10.1029/2004jd005659

Allan, W., Lowe, D. C., & Cainey, J. M. (2001). Active chlorine in the remote marine boundary layer: Modeling anomalous measurements of δ13C in methane. *Geophysical Research Letters*, *28*(17), 3239–3242. https://doi.org/10.1029/2001gl013064

Allan, W., Struthers, H., & Lowe, D. C. (2007). Methane carbon isotope effects caused by atomic chlorine in the marine boundary layer: Global model results compared with Southern Hemisphere measurements. *Journal of Geophysical Research*, *112*(D4), 467. https://doi.org/10.1029/2006JD007369

Ammann, M., Cox, R. A., Crowley, J. N., Jenkin, M. E., Mellouki, A., Rossi, M. J., et al. (2013). Evaluated kinetic and photochemical data for atmospheric chemistry: Volume VI – heterogeneous reactions with liquid substrates. *Atmospheric Chemistry and Physics*, *13*(16), 8045–8228. https://doi.org/10.5194/acp-13-8045-2013

Amos, H. M., Jacob, D. J., Holmes, C. D., Fisher, J. A., Wang, Q., Yantosca, R. M., et al. (2012). Gas-particle partitioning of atmospheric Hg(II) and its effect on global mercury deposition. *Atmospheric Chemistry and Physics*, *12*(1), 591–603. https://doi.org/10.5194/acp-12-591-2012

Aschmann, S. M., & Atkinson, R. (1995). Rate constants for the gas-phase reactions of alkanes with Cl atoms at 296 ± 2 K. *International Journal of Chemical Kinetics*, *27*(6), 613–622. https://doi.org/10.1002/kin.550270611

Atkinson, R., Baulch, D. L., Cox, R. A., Crowley, J. N., Hampson, R. F., Hynes, R. G., et al. (2006). Evaluated kinetic and photochemical data for atmospheric chemistry: Volume II--gas phase reactions of organic species. *Atmospheric Chemistry and Physics*, *6*(11), 3625–4055. Retrieved from https://acp.copernicus.org/articles/6/3625/2006/

Barrie, L. A., Bottenheim, J. W., Schnell, R. C., Crutzen, P. J., & Rasmussen, R. A. (1988). Ozone destruction and photochemical reactions at polar sunrise in the lower Arctic atmosphere. *Nature*, *334*(6178), 138–141. https://doi.org/10.1038/334138a0

Bartels-Rausch, T., Jacobi, H.-W., Kahan, T. F., Thomas, J. L., Thomson, E. S., Abbatt, J. P. D., et al. (2014). A review of air–ice chemical and physical interactions (AICI): liquids, quasi-liquids, and solids in snow. *Atmospheric Chemistry and Physics*, *14*(3), 1587–1633. https://doi.org/10.5194/acp-14-1587-2014

Beine, H., Anastasio, C., Esposito, G., Patten, K., Wilkening, E., Domine, F., et al. (2011). Soluble, light-absorbing species in snow at Barrow, Alaska. *Journal of Geophysical Research*, *116*(D00R05). https://doi.org/10.1029/2011jd016181

Benavent, N., Mahajan, A. S., Li, Q., Cuevas, C. A., Schmale, J., Angot, H., et al. (2022). Substantial contribution of iodine to Arctic ozone destruction. *Nature Geoscience*, *15*(10), 770–773. https://doi.org/10.1038/s41561-022-01018-w

Bey, I., Jacob, D. J., Yantosca, R. M., Logan, J. A., Field, B. D., Fiore, A. M., et al. (2001). Global modeling of tropospheric chemistry with assimilated meteorology: Model description and evaluation. *Journal of Geophysical Research*, *106*(D19), 23073–23095. https://doi.org/10.1029/2001jd000807

Bobrowski, N., Hönninger, G., Galle, B., & Platt, U. (2003). Detection of bromine monoxide in a volcanic plume. *Nature*, *423*(6937), 273–276. https://doi.org/10.1038/nature01625

Bock, M., Schmitt, J., Beck, J., Seth, B., Chappellaz, J., & Fischer, H. (2017). Glacial/interglacial wetland, biomass burning, and geologic methane emissions constrained by dual stable isotopic CH4 ice core records. *Proceedings of the National*

Academy of Sciences of the United States of America, *114*(29), E5778–E5786. https://doi.org/10.1073/pnas.1613883114

Bougoudis, I., Blechschmidt, A.-M., Richter, A., Seo, S., Burrows, J. P., Theys, N., & Rinke, A. (2020). Long-term time series of Arctic tropospheric BrO derived from UV–VIS satellite remote sensing and its relation to first-year sea ice. *Atmospheric Chemistry and Physics*, *20*(20), 11869–11892. https://doi.org/10.5194/acp-20-11869-2020

Bourgeois, C. S., Calanca, P., & Ohmura, A. (2006). A field study of the hemispherical directional reflectance factor and spectral albedo of dry snow. *Journal of Geophysical Research*, *111*(D20). https://doi.org/10.1029/2006jd007296

Brennan, K. M., & Hakim, G. J. (2021). Reconstructing Arctic Sea Ice Over the Common Era Using Data Assimilation. *Journal of Climate*, *1*(aop), 1–55. https://doi.org/10.1175/JCLI-D-21-0099.1

Bryukov, M. G., Dellinger, B., & Knyazev, V. D. (2006). Kinetics of the gas-phase reaction of OH with HCl. *The Journal of Physical Chemistry. A*, *110*(3), 936–943. https://doi.org/10.1021/jp053615x

Burd, J. A., Peterson, P. K., Nghiem, S. V., Perovich, D. K., & Simpson, W. R. (2017). Snowmelt onset hinders bromine monoxide heterogeneous recycling in the Arctic. *Journal of Geophysical Research, D: Atmospheres*, *122*(15), 8297–8309. https://doi.org/10.1002/2017JD026906

Cavalieri, D. J., & Parkinson, C. L. (2012). Arctic sea ice variability and trends, 1979–2010. *The Cryosphere*, *6*(4), 881–889. https://doi.org/10.5194/tc-6-881-2012

Chen, Q., Schmidt, J. A., Shah, V., Jaeglé, L., Sherwen, T., & Alexander, B. (2017). Sulfate production by reactive bromine: Implications for the global sulfur and reactive bromine

budgets: Sulfur-Halogen Interactions. *Geophysical Research Letters*, *44*(13), 7069–7078. https://doi.org/10.1002/2017GL073812

Choi, M. S., Qiu, X., Zhang, J., Wang, S., Li, X., Sun, Y., et al. (2020). Study of Secondary Organic Aerosol Formation from Chlorine Radical-Initiated Oxidation of Volatile Organic Compounds in a Polluted Atmosphere Using a 3D Chemical Transport Model. *Environmental Science & Technology*, *54*(21), 13409–13418. https://doi.org/10.1021/acs.est.0c02958

Clerbaux, C., Cunnold, D. M., Anderson, J., Engel, A., Fraser, P. J., Mahieu, E., et al. (2007). Scientific assessment of ozone depletion: 2006. *Global Ozone Research and Monitoring Project - Report No. 50*. Retrieved from https://agris.fao.org/agris-search/search.do?recordID=BE2014102317

Cole-Dai, J., Ferris, D. G., Lanciki, A. L., Savarino, J., Thiemens, M. H., & McConnell, J. R. (2013). Two likely stratospheric volcanic eruptions in the 1450s C.E. found in a bipolar, subannually dated 800 year ice core record: TWO VOLCANIC ERUPTIONS IN THE 1450s. *Journal of Geophysical Research, D: Atmospheres*, *118*(14), 7459–7466. https://doi.org/10.1002/jgrd.50587

Colosio, P., Tedesco, M., Ranzi, R., & Fettweis, X. (2021). Surface melting over the Greenland ice sheet derived from enhanced resolution passive microwave brightness temperatures (1979–2019). *The Cryosphere*, *15*(6), 2623–2646. https://doi.org/10.5194/tc-15-2623-2021

Comiso, J. C., Meier, W. N., & Gersten, R. (2017). Variability and trends in the A rctic S ea ice cover: Results from different techniques. *Journal of Geophysical Research, C: Oceans*, *122*(8), 6883–6900. https://doi.org/10.1002/2017jc012768

Confer, K. L., Jaeglé, L., Liston, G. E., Sharma, S., Nandan, V., Yackel, J., et al. (2023). Impact of changing arctic sea ice extent, sea ice age, and snow depth on sea salt aerosol from blowing snow and the open ocean for 1980–2017. *Journal of Geophysical Research*, *128*(3). https://doi.org/10.1029/2022jd037667

Custard, K. D., Pratt, K. A., Wang, S., & Shepson, P. B. (2016). Constraints on Arctic Atmospheric Chlorine Production through Measurements and Simulations of Cl2 and ClO. *Environmental Science & Technology*, *50*(22), 12394–12400. https://doi.org/10.1021/acs.est.6b03909

Custard, K. D., Raso, A. R. W., Shepson, P. B., Staebler, R. M., & Pratt, K. A. (2017). Production and Release of Molecular Bromine and Chlorine from the Arctic Coastal Snowpack. *ACS Earth and Space Chemistry*, *1*(3), 142–151. https://doi.org/10.1021/acsearthspacechem.7b00014

Dee, D. P., Uppala, S. M., Simmons, A. J., Berrisford, P., Poli, P., Kobayashi, S., et al. (2011). The ERA-Interim reanalysis: configuration and performance of the data assimilation system. *Quarterly Journal of the Royal Meteorological Society*, *137*(656), 553–597. https://doi.org/10.1002/qj.828

Dibb, J. E., Ziemba, L. D., Luxford, J., & Beckman, P. (2010). Bromide and other ions in the snow, firn air, and atmospheric boundary layer at Summit during GSHOX. *Atmospheric Chemistry and Physics*, *10*(20), 9931–9942. https://doi.org/10.5194/acp-10-9931-2010

Dlugokencky, E. J. (2016). Atmospheric Methane Dry Air Mole Fractions (1983-2015) and Atmospheric Carbon Dioxide Dry Air Mole Fractions (1968-2015) from the NOAA ESRL Carbon Cycle Cooperative Global Air Sampling Network, original data files. Retrieved from https://epic.awi.de/id/eprint/44810/

Domine, F., Sparapani, R., Ianniello, A., & Beine, H. J. (2004). The origin of sea salt in snow on Arctic sea ice and in coastal regions. *Atmospheric Chemistry and Physics*, *4*(9/10), 2259–2271. https://doi.org/10.5194/acp-4-2259-2004

Domine, F., Bock, J., Voisin, D., & Donaldson, D. J. (2013). Can we model snow photochemistry? Problems with the current approaches. *The Journal of Physical Chemistry. A*, *117*(23), 4733–4749. https://doi.org/10.1021/jp3123314

van Donkelaar, A., Martin, R. V., Leaitch, W. R., Macdonald, A. M., Walker, T. W., Streets, D. G., et al. (2008). Analysis of aircraft and satellite measurements from the Intercontinental Chemical Transport Experiment (INTEX-B) to quantify long-range transport of East Asian sulfur to Canada. *Atmospheric Chemistry and Physics*, *8*, 2999–3014. Retrieved from https://acp.copernicus.org/articles/8/2999/2008/acp-8-2999-2008.pdf

Donohoue, D. L., Bauer, D., & Hynes, A. J. (2005). Temperature and pressure dependent rate coefficients for the reaction of Hg with Cl and the reaction of Cl with Cl: a pulsed laser photolysis-pulsed laser induced fluorescence study. *The Journal of Physical Chemistry. A*, *109*(34), 7732–7741. https://doi.org/10.1021/jp051354l

Eastham, S. D., Weisenstein, D. K., & Barrett, S. R. H. (2014). Development and evaluation of the unified tropospheric–stratospheric chemistry extension (UCX) for the global chemistry-transport model GEOS-Chem. *Atmospheric Environment*, *89*, 52–63. https://doi.org/10.1016/j.atmosenv.2014.02.001

Edebeli, J., Trachsel, J. C., Avak, S. E., Ammann, M., Schneebeli, M., Eichler, A., & Bartels-Rausch, T. (2020). Snow heterogeneous reactivity of bromide with ozone lost during snow metamorphism. *Atmospheric Chemistry and Physics*, *20*(21), 13443–13454. https://doi.org/10.5194/acp-20-13443-2020

Eigen, M., & Kustin, K. (1962). The Kinetics of Halogen Hydrolysis. *Journal of the American Chemical Society*, *84*(8), 1355–1361. https://doi.org/10.1021/ja00867a005

Erbland, J., Vicars, W. C., Savarino, J., Morin, S., Frey, M. M., Frosini, D., et al. (2013). Air–snow transfer of nitrate on the East Antarctic Plateau – Part 1: Isotopic evidence for a photolytically driven dynamic equilibrium in summer. *Atmospheric Chemistry and Physics*, *13*(13), 6403–6419. https://doi.org/10.5194/acp-13-6403-2013

Evans, C. D., Monteith, D. T., Fowler, D., Cape, J. N., & Brayshaw, S. (2011). Hydrochloric acid: an overlooked driver of environmental change. *Environmental Science & Technology*, *45*(5), 1887–1894. https://doi.org/10.1021/es103574u

Falk, S., & Sinnhuber, B.-M. (2018). Polar boundary layer bromine explosion and ozone depletion events in the chemistry–climate model EMAC v2.52: implementation and evaluation of AirSnow algorithm [Data set]. https://doi.org/10.5194/gmd-11-1115-2018

Fan, S.-M., & Jacob, D. J. (1992). Surface ozone depletion in Arctic spring sustained by bromine reactions on aerosols. *Nature*, *359*(6395), 522–524. https://doi.org/10.1038/359522a0

Finlayson-Pitts, B. J. (2003). The tropospheric chemistry of sea salt: a molecular-level view of the chemistry of NaCl and NaBr. *Chemical Reviews*, *103*(12), 4801–4822. https://doi.org/10.1021/cr020653t

Finlayson-Pitts, B. J., Ezell, M. J., & Pitts, J. N. (1989). Formation of chemically active chlorine compounds by reactions of atmospheric NaCl particles with gaseous N2O5 and ClONO2. *Nature*. https://doi.org/10.1038/337241a0

Finlayson-Pitts, Barbara J., & Pitts, J. N., Jr. (1999). *Chemistry of the Upper and Lower Atmosphere: Theory, Experiments, and Applications*. Elsevier. Retrieved from https://play.google.com/store/books/details?id=mRoJUB5fxRwC

Fisher, J. A., Jacob, D. J., Wang, Q., Bahreini, R., Carouge, C. C., Cubison, M. J., et al. (2011). Sources, distribution, and acidity of sulfate–ammonium aerosol in the Arctic in winter–spring. *Atmospheric Environment*, *45*(39), 7301–7318. https://doi.org/10.1016/j.atmosenv.2011.08.030

Foster, K. L., Plastridge, R. A., Bottenheim, J. W., Shepson, P. B., Finlayson-Pitts, B. J., & Spicer, C. W. (2001). The role of Br2 and BrCl in surface ozone destruction at polar sunrise. *Science*, *291*(5503), 471–474. https://doi.org/10.1126/science.291.5503.471

Fountoukis, C., & Nenes, A. (2007). ISORROPIA II: a computationally efficient thermodynamic equilibrium model for K–Ca–Mg–NH–Na–SO–NO–Cl–HO aerosols. *Atmospheric Chemistry and Physics*, *7*, 4639–4659. Retrieved from https://www.atmos-chem-phys.net/7/4639/2007/acp-7-4639-2007.pdf

Frey, M. M., Norris, S. J., Brooks, I. M., Anderson, P. S., Nishimura, K., Yang, X., et al. (2020). First direct observation of sea salt aerosol production from blowing snow above sea ice. *Atmospheric Chemistry and Physics*, *20*(4), 2549–2578. https://doi.org/10.5194/acp-20-2549-2020

Fritzsche, D., Wilhelms, F., Savatyugin, L. M., Pinglot, J. F., Meyer, H., Hubberten, H.-W., & Miller, H. (2002). A new deep ice core from Akademii Nauk ice cap, Severnaya Zemlya, Eurasian Arctic: first results. *Annals of Glaciology*, *35*, 25–28. https://doi.org/10.3189/172756402781816645

Fu, X., Wang, T., Wang, S., Zhang, L., Cai, S., Xing, J., & Hao, J. (2018). Anthropogenic Emissions of Hydrogen Chloride and Fine Particulate Chloride in China. *Environmental Science & Technology*, *52*(3), 1644–1654. https://doi.org/10.1021/acs.est.7b05030

Galbavy, E. S., Anastasio, C., Lefer, B., & Hall, S. (2007). Light penetration in the snowpack at Summit, Greenland: Part 2 Nitrate photolysis. *Atmospheric Environment*, *41*(24), 5091–5100. https://doi.org/10.1016/j.atmosenv.2006.01.066

Gaudel, A., Cooper, O. R., Ancellet, G., Barret, B., Boynard, A., Burrows, J. P., et al. (2018). Tropospheric Ozone Assessment Report: Present-day distribution and trends of tropospheric ozone relevant to climate and global atmospheric chemistry model evaluation [Data set]. https://doi.org/10.1525/elementa.291

Gelaro, R., McCarty, W., Suárez, M. J., Todling, R., Molod, A., Takacs, L., et al. (2017). The Modern-Era Retrospective Analysis for Research and Applications, Version 2 (MERRA-2). *Journal of Climate*, *30*(Iss 13), 5419–5454. https://doi.org/10.1175/JCLI-D-16-0758.1

Geng, L., Alexander, B., Cole-Dai, J., Steig, E. J., Savarino, J., Sofen, E. D., & Schauer, A. J. (2014). Nitrogen isotopes in ice core nitrate linked to anthropogenic atmospheric acidity change. *Proceedings of the National Academy of Sciences of the United States of America*, *111*(16), 5808–5812. https://doi.org/10.1073/pnas.1319441111

Ghosal, S., Shbeeb, A., & Hemminger, J. C. (2000). Surface segregation of bromine in bromide doped NaCl: Implications for the seasonal variations in Arctic ozone. *Geophysical Research Letters*, *27*(13), 1879–1882. https://doi.org/10.1029/2000gl011381

Ghosal, S., Hemminger, J. C., Bluhm, H., Mun, B. S., Hebenstreit, E. L. D., Ketteler, G., et al. (2005). Electron spectroscopy of aqueous solution interfaces reveals surface enhancement of halides. *Science*, *307*(5709), 563–566. https://doi.org/10.1126/science.1106525

Gladich, I., Shepson, P. B., Carignano, M. A., & Szleifer, I. (2011). Halide affinity for the water-air interface in aqueous solutions of mixtures of sodium salts. *The Journal of Physical Chemistry. A*, *115*(23), 5895–5899. https://doi.org/10.1021/jp110208a

von Glasow, R., von Kuhlmann, R., Lawrence, M. G., Platt, U., & Crutzen, P. J. (2004). Impact of reactive bromine chemistry in the troposphere. *Atmospheric Chemistry and Physics*, *4*(11/12), 2481–2497. https://doi.org/10.5194/acp-4-2481-2004

Grannas, A. M., Jones, A. E., Dibb, J., Ammann, M., Anastasio, C., Beine, H. J., et al. (2007). An overview of snow photochemistry: evidence, mechanisms and impacts. *Atmospheric Chemistry and Physics*, *7*(16), 4329–4373. https://doi.org/10.5194/acp-7-4329-2007

Gunthe, S. S., Liu, P., Panda, U., Raj, S. S., Sharma, A., Darbyshire, E., et al. (2021). Enhanced aerosol particle growth sustained by high continental chlorine emission in India. *Nature Geoscience*, 1–8. https://doi.org/10.1038/s41561-020-00677-x

Habibi, K. (1973). Characterization of particulate matter in vehicle exhaust. *Environmental Science & Technology*, *7*(3), 223–234. https://doi.org/10.1021/es60075a001

Hagner, C. (2002). Regional and long-term patterns of lead concentrations in riverine, marine and terrestrial systems and humans in Northwest Europe. *Water, Air, and Soil Pollution*, *134*(1/4), 1–40. https://doi.org/10.1023/a:1014191519871

Halfacre, J. W., Shepson, P. B., & Pratt, K. A. (2019). pH-dependent production of molecular chlorine, bromine, and iodine from frozen saline surfaces. *Atmospheric Chemistry and Physics*, *19*(7), 4917–4931. https://doi.org/10.5194/acp-19-4917-2019

Hara, K., Osada, K., Matsunaga, K., Iwasaka, Y., Shibata, T., & Furuya, K. (2002). Atmospheric inorganic chlorine and bromine species in Arctic boundary layer of the winter/spring. *Journal of Geophysical Research*, *107*, 4361. https://doi.org/10.1029/2001JD001008

Harsch, D. E., & Rasmussen, R. A. (1977). Identification of Methyl Bromide in Urban Air. *Analytical Letters*, *10*(13), 1041–1047. https://doi.org/10.1080/00032717708067841

Haskins, J. D., Jaeglé, L., Shah, V., & Lee, B. H. (2018). Wintertime Gas‐Particle Partitioning and Speciation of Inorganic Chlorine in the Lower Troposphere Over the Northeast United States and Coastal Ocean. *Journal Of*. Retrieved from https://agupubs.onlinelibrary.wiley.com/doi/abs/10.1029/2018JD028786

Haskins, J. D., Lee, B. H., Lopez‐Hilifiker, F. D., Peng, Q., Jaeglé, L., Reeves, J. M., et al. (2019). Observational Constraints on the Formation of Cl 2 From the Reactive Uptake of ClNO 2 on Aerosols in the Polluted Marine Boundary Layer. *Journal of Geophysical Research, D: Atmospheres*. https://doi.org/10.1029/2019JD030627

Haskins, J. D., Jaeglé, L., & Thornton, J. A. (2020). Significant decrease in wet deposition of anthropogenic chloride across the Eastern United States, 1998–2018. *Geophysical Research Letters*, *47*(22). https://doi.org/10.1029/2020gl090195

Hebestreit, K., Stutz, J., Rosen, D., Matveiv, V., Peleg, M., Luria, M., & Platt, U. (1999). DOAS Measurements of Tropospheric Bromine Oxide in Mid-Latitudes. *Science*, *283*(5398), 55–57. https://doi.org/10.1126/science.283.5398.55

Helmig, D., Oltmans, S. J., Carlson, D., Lamarque, J.-F., Jones, A., Labuschagne, C., et al. (2007). A review of surface ozone in the polar regions. *Atmospheric Environment*, *41*(24), 5138–5161. https://doi.org/10.1016/j.atmosenv.2006.09.053

Herrmann, M., Sihler, H., Frieß, U., Wagner, T., Platt, U., & Gutheil, E. (2021). Time-dependent 3D simulations of tropospheric ozone depletion events in the Arctic spring using the Weather Research and Forecasting model coupled with Chemistry (WRF-Chem). *Atmospheric Chemistry and Physics*, *21*(10), 7611–7638. Retrieved from https://acp.copernicus.org/articles/21/7611/2021/

Herrmann, M., Schöne, M., Borger, C., Warnach, S., Wagner, T., Platt, U., & Gutheil, E. (2022). Ozone depletion events in the Arctic spring of 2019: a new modeling approach to bromine emissions. *Atmospheric Chemistry and Physics*, *22*(20), 13495–13526. Retrieved from https://acp.copernicus.org/preprints/acp-2022-334/

Hoesly, R. M., Smith, S. J., Feng, L., Klimont, Z., Janssens-Maenhout, G., Pitkanen, T., et al. (2018). Historical (1750–2014) anthropogenic emissions of reactive gases and aerosols from the Community Emissions Data System (CEDS). *Geoscientific Model Development*, *11*(1), 369–408. https://doi.org/10.5194/gmd-11-369-2018

Holmes, C. D., Bertram, T. H., Confer, K. L., Graham, K. A., Ronan, A. C., Wirks, C. K., & Shah, V. (2019). The Role of Clouds in the Tropospheric NO x Cycle: A New Modeling Approach for Cloud Chemistry and Its Global Implications. *Geophysical Research Letters*, *46*(9), 4980–4990. https://doi.org/10.1029/2019GL081990

Horowitz, H. M., Jacob, D. J., Zhang, Y., Dibble, T. S., Slemr, F., Amos, H. M., et al. (2017). A new mechanism for atmospheric mercury redox chemistry: implications for the global mercury budget. *Atmospheric Chemistry and Physics*, *17*(10), 6353–6371. https://doi.org/10.5194/acp-17-6353-2017

Huang, J., & Jaeglé, L. (2017). Wintertime enhancements of sea salt aerosol in polar regions consistent with a sea ice source from blowing snow. *Atmospheric Chemistry and Physics*, *17*(5), 3699–3712. https://doi.org/10.5194/acp-17-3699-2017

Huang, J., Jaeglé, L., Chen, Q., Alexander, B., Sherwen, T., Evans, M. J., et al. (2020). Evaluating the impact of blowing-snow sea salt aerosol on springtime BrO and O 3 in the Arctic. *Atmospheric Chemistry and Physics*, *20*(12), 7335–7358. Retrieved from https://acp.copernicus.org/articles/20/7335/2020/

Huang, S., Arimoto, R., & Rahn, K. A. (1996). Changes in atmospheric lead and other pollution elements at Bermuda. *Journal of Geophysical Research*, *101*(D15), 21033–21040. https://doi.org/10.1029/96jd02001

Iizuka, Y., Uemura, R., Fujita, K., Hattori, S., Seki, O., Miyamoto, C., et al. (2018). A 60 Year Record of Atmospheric Aerosol Depositions Preserved in a High-Accumulation Dome Ice Core, Southeast Greenland. *Journal of Geophysical Research, D: Atmospheres*, *123*(1), 574–589. https://doi.org/10.1002/2017JD026733

Jacob, D. J., Waldman, J. M., Munger, J. W., & Hoffmann, M. R. (1985). Chemical composition of fogwater collected along the California coast. *Environmental Science & Technology*, *19*(8), 730–736. https://doi.org/10.1021/es00138a013

Jaeglé, L., Quinn, P. K., Bates, T. S., Alexander, B., & Lin, J.-T. (2011). Global distribution of sea salt aerosols: new constraints from in situ and remote sensing observations. *Atmospheric Chemistry and Physics*, *11*(7), 3137–3157. https://doi.org/10.5194/acp-11-3137-2011

Jeong, D., McNamara, S. M., Barget, A. J., Raso, A. R. W., Upchurch, L. M., Thanekar, S., et al. (2022). Multiphase Reactive Bromine Chemistry during Late Spring in the Arctic: Measurements of Gases, Particles, and Snow. *ACS Earth and Space Chemistry*, *6*(12), 2877–2887. https://doi.org/10.1021/acsearthspacechem.2c00189

Ji, Y. M., Wang, H. H., Gao, Y. P., Li, G. Y., & An, T. C. (2013). A theoretical model on the formation mechanism and kinetics of highly toxic air pollutants from halogenated formaldehydes reacted with halogen atoms. *Atmospheric Chemistry and Physics Discussions: ACPD*, *13*(7), 18205–18231. https://doi.org/10.5194/acpd-13-18205-2013

Keegan, K. M., Albert, M. R., McConnell, J. R., & Baker, I. (2014). Climate change and forest fires synergistically drive widespread melt events of the Greenland Ice Sheet. *Proceedings of the National Academy of Sciences of the United States of America*, *111*(22), 7964–7967. https://doi.org/10.1073/pnas.1405397111

Keene, W. C., Khalil, M. A. K., Erickson, D. J., III, McCulloch, A., Graedel, T. E., Lobert, J. M., et al. (1999). Composite global emissions of reactive chlorine from anthropogenic and natural sources: Reactive Chlorine Emissions Inventory. *Journal of Geophysical Research*, *104*(D7), 8429–8440. https://doi.org/10.1029/1998jd100084

Kercher, J. P., Riedel, T. P., & Thornton, J. A. (2009). Chlorine activation by NO: simultaneous, in situ detection of ClNO and NO by chemical ionization mass spectrometry. Retrieved January 14, 2021, from https://core.ac.uk/download/pdf/194272417.pdf

Kerkweg, A., Jöckel, P., Pozzer, A., Tost, H., Sander, R., Schulz, M., et al. (2008). Consistent simulation of bromine chemistry from the marine boundary layer to the stratosphere – Part 1: Model description, sea salt aerosols and pH. *Atmospheric Chemistry and Physics*, *8*(19), 5899–5917. https://doi.org/10.5194/acp-8-5899-2008

Kim, S.-W., Heckel, A., McKeen, S. A., Frost, G. J., Hsie, E.-Y., Trainer, M. K., et al. (2006). Satellite-observed U.S. power plant NO x emission reductions and their impact on air quality. *Geophysical Research Letters*, *33*(22), 127. https://doi.org/10.1029/2006GL027749

Kim, Y., Kimball, J. S., Du, J., Schaaf, C. L. B., & Kirchner, P. B. (2018). Quantifying the effects of freeze-thaw transitions and snowpack melt on land surface albedo and energy exchange over Alaska and Western Canada. *Environmental Research Letters: ERL [Web Site]*, *13*(7), 075009. https://doi.org/10.1088/1748-9326/aacf72

Knipping, E. M., & Dabdub, D. (2003). Impact of chlorine emissions from sea-salt aerosol on coastal urban ozone. *Environmental Science & Technology*, *37*(2), 275–284. https://doi.org/10.1021/es025793z

Kolesar, K. R., Mattson, C. N., Peterson, P. K., May, N. W., Prendergast, R. K., & Pratt, K. A. (2018). Increases in wintertime PM2.5 sodium and chloride linked to snowfall and road salt application. *Atmospheric Environment*, *177*, 195–202. https://doi.org/10.1016/j.atmosenv.2018.01.008

Konovalov, I. B., Beekmann, M., Richter, A., Burrows, J. P., & Hilboll, A. (2010). Multi-annual changes of NOx emissions in megacity regions: nonlinear trend analysis of satellite measurement based estimates. *Atmospheric Chemistry and Physics*, *10*(17), 8481. Retrieved from http://search.proquest.com/openview/17df78241e59ef4f030b4ae7dc9fc011/1?pq-origsite=gscholar&cbl=105744&casa_token=LbjF86FaKZ0AAAAA:Z7mxXO_XwpQDgERA8H4khqhY7NRYy7kcJ2ICn4oCbxvD-RL0ZgwgIkWaDpE6AV6qdD7y_cR0YA

Koop, T., Kapilashrami, A., Molina, L. T., & Molina, M. J. (2000). Phase transitions of sea-salt/water mixtures at low temperatures: Implications for ozone chemistry in the polar marine boundary layer. *Journal of Geophysical Research*, *105*(D21), 26393–26402. https://doi.org/10.1029/2000jd900413

Lammel, G., Röhrl, A., & Schreiber, H. (2002). Atmospheric lead and bromine in Germany. *Environmental Science and Pollution Research*, *9*(6), 397–404. https://doi.org/10.1007/BF02987589

Lee, B. H., Lopez-Hilfiker, F. D., Schroder, J. C., Campuzano-Jost, P., Jimenez, J. L., McDuffie, E. E., et al. (2018). Airborne Observations of Reactive Inorganic Chlorine and Bromine

Species in the Exhaust of Coal-Fired Power Plants. *Journal of Geophysical Research, D: Atmospheres*, *123*(19), 11225–11237. https://doi.org/10.1029/2018JD029284

Lee-Taylor, J., & Madronich, S. (2002). Calculation of actinic fluxes with a coupled atmosphere–snow radiative transfer model. *Journal of Geophysical Research*, *107*(D24). https://doi.org/10.1029/2002jd002084

Legrand, M., Preunkert, S., Wagenbach, D., Cachier, H., & Puxbaum, H. (2003). A historical record of formate and acetate from a high-elevation Alpine glacier: Implications for their natural versus anthropogenic budgets at the European scale. *Journal of Geophysical Research*, *108*(D24). https://doi.org/10.1029/2003jd003594

Legrand, M., McConnell, J. R., Preunkert, S., Chellman, N. J., & Arienzo, M. (2021a). Causes of enhanced bromine levels in Alpine ice cores during the 20 th century: Implications for bromine in the free European troposphere. *Journal of Geophysical Research*. https://doi.org/10.1029/2020jd034246

Legrand, M., McConnell, J. R., Preunkert, S., Chellman, N. J., & Arienzo, M. M. (2021b). Causes of enhanced bromine levels in alpine ice cores during the 20th century: Implications for bromine in the free European troposphere. *Journal of Geophysical Research*, *126*(8). https://doi.org/10.1029/2020jd034246

Legrand, Michel, & Mayewski, P. (1997). Glaciochemistry of polar ice cores: A review. *Reviews of Geophysics* , *35*(3), 219–243. https://doi.org/10.1029/96RG03527

Legrand, Michel, Preunkert, S., Wagenbach, D., & Fischer, H. (2002). Seasonally resolved Alpine and Greenland ice core records of anthropogenic HCl emissions over the 20th century. *Journal of Geophysical Research*, *107*(D12). https://doi.org/10.1029/2001jd001165

Lehrer, E., Hönninger, G., & Platt, U. (2004). A one dimensional model study of the mechanism of halogen liberation and vertical transport in the polar troposphere. *Atmospheric Chemistry and Physics*, *4*(11/12), 2427–2440. https://doi.org/10.5194/acp-4-2427-2004

Li, M., Zhang, Q., Streets, D. G., He, K. B., Cheng, Y. F., Emmons, L. K., et al. (2014). Mapping Asian anthropogenic emissions of non-methane volatile organic compounds to multiple chemical mechanisms. *Atmospheric Chemistry and Physics*, *14*(11), 5617–5638. https://doi.org/10.5194/acp-14-5617-2014

Liang, Q., Stolarski, R. S., Kawa, S. R., Nielsen, J. E., Douglass, A. R., Rodriguez, J. M., et al. (2010). Finding the missing stratospheric Br_y: a global modeling study of $CHBr_3$ and CH_2Br_2. *Atmospheric Chemistry and Physics*, *10*(5), 2269–2286. https://doi.org/10.5194/acp-10-2269-2010

Liang, Q., E. Atlas, Blake, D., Dorf, M., Pfeilsticker, K., & Schauffler, S. (2014). Convective transport of very short lived bromocarbons to the stratosphere. *Atmospheric Chemistry and Physics*, *14*(11), 5781–5792. https://doi.org/10.5194/acp-14-5781-2014

Liao, J., Sihler, H., Huey, L. G., Neuman, J. A., Tanner, D. J., Friess, U., et al. (2011). A comparison of Arctic BrO measurements by chemical ionization mass spectrometry and long path-differential optical absorption spectroscopy. *Journal of Geophysical Research*, *116*(D00R02). https://doi.org/10.1029/2010jd014788

Liao, J., Huey, L. G., Tanner, D. J., Brough, N., Brooks, S., Dibb, J. E., et al. (2011). Observations of hydroxyl and peroxy radicals and the impact of BrO at Summit, Greenland in 2007 and 2008. *Atmospheric Chemistry and Physics*, *11*(16), 8577–8591. https://doi.org/10.5194/acp-11-8577-2011

Liao, J., Huey, L. G., Tanner, D. J., Flocke, F. M., Orlando, J. J., Neuman, J. A., et al. (2012). Observations of inorganic bromine (HOBr, BrO, and Br2) speciation at Barrow, Alaska, in spring 2009. *Journal of Geophysical Research*, *117*(D14). https://doi.org/10.1029/2011jd016641

Liao, J., Huey, L. G., Liu, Z., Tanner, D. J., Cantrell, C. A., Orlando, J. J., et al. (2014). High levels of molecular chlorine in the Arctic atmosphere. *Nature Geoscience*, *7*(2), 91–94. https://doi.org/10.1038/ngeo2046

Liu, H., Jacob, D. J., Bey, I., & Yantosca, R. M. (2001). Constraints from210Pb and7Be on wet deposition and transport in a global three-dimensional chemical tracer model driven by assimilated meteorological fields. *Journal of Geophysical Research*, *106*(D11), 12109–12128. https://doi.org/10.1029/2000jd900839

Liu, T., & Abbatt, J. P. D. (2020). An Experimental Assessment of the Importance of S(IV) Oxidation by Hypohalous Acids in the Marine Atmosphere. *Geophysical Research Letters*, *47*(4), D23202. https://doi.org/10.1029/2019GL086465

Liu, Y., Fan, Q., Chen, X., Zhao, J., Ling, Z., Hong, Y., et al. (2018). Modeling the impact of chlorine emissions from coal combustion and prescribed waste incineration on tropospheric ozone formation in China. *Atmospheric Chemistry and Physics*, *18*(4), 2709–2724. https://doi.org/10.5194/acp-18-2709-2018

Maffezzoli, N., Risebrobakken, B., Miles, M. W., Vallelonga, P., Berben, S. M. P., Scoto, F., et al. (2021). Sea ice in the northern North Atlantic through the Holocene: Evidence from ice cores and marine sediment records. *Quaternary Science Reviews*, *273*, 107249. https://doi.org/10.1016/j.quascirev.2021.107249

Mahoney, A. R., Barry, R. G., Smolyanitsky, V., & Fetterer, F. (2008). Observed sea ice extent in the Russian Arctic, 1933–2006. *Journal of Geophysical Research*, *113*(C11). https://doi.org/10.1029/2008jc004830

Marelle, L., Thomas, J. L., Ahmed, S., Tuite, K., Stutz, J., Dommergue, A., et al. (2021). Implementation and impacts of surface and blowing snow sources of Arctic bromine activation within WRF‐Chem 4.1.1. *Journal of Advances in Modeling Earth Systems*. https://doi.org/10.1029/2020ms002391

van Marle, M. J. E., Kloster, S., Magi, B. I., Marlon, J. R., Daniau, A.-L., Field, R. D., et al. (2017). Historic global biomass burning emissions for CMIP6 (BB4CMIP) based on merging satellite observations with proxies and fire models (1750–2015). *Geoscientific Model Development*, *10*(9), 3329–3357. https://doi.org/10.5194/gmd-10-3329-2017

Maselli, O. J., Chellman, N. J., Grieman, M., Layman, L., McConnell, J. R., Pasteris, D., et al. (2017). Sea ice and pollution-modulated changes in Greenland ice core methanesulfonate and bromine. *Climate of the Past*, *13*(1), 39–59. https://doi.org/10.5194/cp-13-39-2017

Matveev, V., Peleg, M., Rosen, D., Tov-Alper, D. S., Hebestreit, K., Stutz, J., et al. (2001). Bromine oxide-ozone interaction over the Dead Sea. *Journal of Geophysical Research*, *106*(D10), 10375–10387. https://doi.org/10.1029/2000jd900611

McConnell, Burke, & Dunbar. (2017). Synchronous volcanic eruptions and abrupt climate change∼ 17.7 ka plausibly linked by stratospheric ozone depletion. *Proceedings of the Estonian Academy of Sciences. Biology, Ecology = Eesti Teaduste Akadeemia Toimetised. Bioloogia, Okoloogia*. Retrieved from https://www.pnas.org/content/114/38/10035?tab=metrics&utm_source=TrendMD&utm_medium=cpc&utm_campaign=Proc_Natl_Acad_Sci_U_S_A_TrendMD_1

McConnell, J. C., Henderson, G. S., Barrie, L., Bottenheim, J., Niki, H., Langford, C. H., & Templeton, E. M. J. (1992). Photochemical bromine production implicated in Arctic boundary-layer ozone depletion. *Nature*, *355*(6356), 150–152. https://doi.org/10.1038/355150a0

McConnell, J. R., Maselli, O. J., Sigl, M., Vallelonga, P., Neumann, T., Anschütz, H., et al. (2014). Antarctic-wide array of high-resolution ice core records reveals pervasive lead pollution began in 1889 and persists today. *Scientific Reports*, *4*, 5848. https://doi.org/10.1038/srep05848

McConnell, J. R., Chellman, N. J., Wilson, A. I., Stohl, A., Arienzo, M. M., Eckhardt, S., et al. (2019). Pervasive Arctic lead pollution suggests substantial growth in medieval silver production modulated by plague, climate, and conflict. *Proceedings of the National Academy of Sciences of the United States of America*, *116*(30), 14910–14915. https://doi.org/10.1073/pnas.1904515116

McCulloch, A., Aucott, M. L., Graedel, T. E., Kleiman, G., Midgley, P. M., & Li, Y.-F. (1999). Industrial emissions of trichloroethene, tetrachloroethene, and dichloromethane: Reactive Chlorine Emissions Inventory. *Journal of Geophysical Research*, *104*(D7), 8417–8427. https://doi.org/10.1029/1999jd900011

McDuffie, E. E., Smith, S. J., O'Rourke, P., Tibrewal, K., Venkataraman, C., Marais, E. A., et al. (2020). A global anthropogenic emission inventory of atmospheric pollutants from sector- and fuel-specific sources (1970–2017): an application of the Community Emissions Data System (CEDS). *Earth System Science Data*, *12*(4), 3413–3442. https://doi.org/10.5194/essd-12-3413-2020

McTigue, N. E., Cornwell, D. A., Graf, K., & Brown, R. (2014). Occurrence and consequences of increased bromide in drinking water sources. *Journal - American Water Works Association*, *106*(11), E492–E508. https://doi.org/10.5942/jawwa.2014.106.0141

Meinshausen, M., Vogel, E., Nauels, A., Lorbacher, K., Meinshausen, N., Etheridge, D. M., et al. (2017). Historical greenhouse gas concentrations for climate modelling (CMIP6). *Geoscientific Model Development*, *10*(5), 2057–2116. https://doi.org/10.5194/gmd-10-2057-2017

Michalowski, B. A., Francisco, J. S., Li, S.-M., Barrie, L. A., Bottenheim, J. W., & Shepson, P. B. (2000). A computer model study of multiphase chemistry in the Arctic boundary layer during polar sunrise. *Journal of Geophysical Research*, *105*(D12), 15131–15145. https://doi.org/10.1029/2000jd900004

Millero, F. J., Feistel, R., Wright, D. G., & McDougall, T. J. (2008). The composition of Standard Seawater and the definition of the Reference-Composition Salinity Scale. *Deep Sea Research Part I: Oceanographic Research Papers*, *55*(1), 50–72. https://doi.org/10.1016/j.dsr.2007.10.001

Moch, J. M., Dovrou, E., Mickley, L. J., Keutsch, F. N., Liu, Z., Wang, Y., et al. (2020). Global Importance of Hydroxymethanesulfonate in Ambient Particulate Matter: Implications for Air Quality. *Journal of Geophysical Research, D: Atmospheres*, *125*(18), e2020JD032706. https://doi.org/10.1029/2020JD032706

Mozurkewich, M. (1995). Mechanisms for the release of halogens from sea-salt particles by free radical reactions. *Journal of Geophysical Research*, *100*(D7), 14199. https://doi.org/10.1029/94jd00358

Murray, L. T. (2016). Lightning NOxand Impacts on Air Quality. *Current Pollution Reports*, *2*(2), 115–133. https://doi.org/10.1007/s40726-016-0031-7

Nandan, V., Geldsetzer, T., Yackel, J., Mahmud, M., Scharien, R., Howell, S., et al. (2017). Effect of snow salinity on CryoSat-2 arctic first-year sea ice freeboard measurements. *Geophysical Research Letters*, *44*(20), 10,419-10,426. https://doi.org/10.1002/2017gl074506

Nriagu, J. O. (1990). The rise and fall of leaded gasoline. *The Science of the Total Environment*, *92*, 13–28. https://doi.org/10.1016/0048-9697(90)90318-O

Oltmans, S. J., Schnell, R. C., Sheridan, P. J., Peterson, R. E., Li, S.-M., Winchester, J. W., et al. (1989). Seasonal surface ozone and filterable bromine relationship in the high Arctic. *Atmospheric Environment*, *23*(11), 2431–2441. https://doi.org/10.1016/0004-6981(89)90254-0

Oltmans, Samuel J., Johnson, B. J., & Harris, J. M. (2012). Springtime boundary layer ozone depletion at Barrow, Alaska: Meteorological influence, year-to-year variation, and long-term change. *Journal of Geophysical Research*, *117*(D14). https://doi.org/10.1029/2011jd016889

Opel, T., Fritzsche, D., & Meyer, H. (2013). Eurasian Arctic climate over the past millennium as recorded in the Akademii Nauk ice core (Severnaya Zemlya). *Climate of the Past*, *9*(5), 2379–2389. https://doi.org/10.5194/cp-9-2379-2013

Ordóñez, C., Lamarque, J.-F., Tilmes, S., Kinnison, D. E., E. L. Atlas, Blake, D. R., et al. (2012). Bromine and iodine chemistry in a global chemistry-climate model: description and evaluation of very short-lived oceanic sources. *Atmospheric Chemistry and Physics*, *12*(3), 1423–1447. https://doi.org/10.5194/acp-12-1423-2012

Oum, K. W., Lakin, M. J., & Finlayson-Pitts, B. J. (1998). Bromine activation in the troposphere by the dark reaction of O3with seawater ice. *Geophysical Research Letters*, *25*(21), 3923–3926. https://doi.org/10.1029/1998gl900078

Parizek, B. R., & Alley, R. B. (2004). Implications of increased Greenland surface melt under global-warming scenarios: ice-sheet simulations. *Quaternary Science Reviews*, *23*(9), 1013–1027. https://doi.org/10.1016/j.quascirev.2003.12.024

Parrella, J. P., Jacob, D. J., Liang, Q., Zhang, Y., Mickley, L. J., Miller, B., et al. (2012). Tropospheric bromine chemistry: implications for present and pre-industrial ozone and mercury. *Atmospheric Chemistry and Physics*, *12*(15), 6723–6740. https://doi.org/10.5194/acp-12-6723-2012

Passing, H., & Bablok. (1983). A new biometrical procedure for testing the equality of measurements from two different analytical methods. Application of linear regression procedures for method comparison studies in clinical chemistry, Part I. *Journal of Clinical Chemistry and Clinical Biochemistry. Zeitschrift Fur Klinische Chemie Und Klinische Biochemie*, *21*(11), 709–720. https://doi.org/10.1515/cclm.1983.21.11.709

Pasteris, D., McConnell, J. R., Edwards, R., Isaksson, E., & Albert, M. R. (2014). Acidity decline in Antarctic ice cores during the Little Ice Age linked to changes in atmospheric nitrate and sea salt concentrations. *Journal of Geophysical Research, D: Atmospheres*, *119*(9), 5640–5652. https://doi.org/10.1002/2013JD020377

Pasteris, D. R., McConnell, J. R., & Edwards, R. (2012). High-resolution, continuous method for measurement of acidity in ice cores. *Environmental Science & Technology*, *46*(3), 1659–1666. https://doi.org/10.1021/es202668n

Peterson, P. K., Pöhler, D., Zielcke, J., General, S., Frieß, U., Platt, U., et al. (2018). Springtime Bromine Activation over Coastal and Inland Arctic Snowpacks. *ACS Earth and Space Chemistry*, *2*(10), 1075–1086. https://doi.org/10.1021/acsearthspacechem.8b00083

Peterson, P. K., Hartwig, M., May, N. W., Schwartz, E., Rigor, I., Ermold, W., et al. (2019). Snowpack measurements suggest role for multi-year sea ice regions in Arctic atmospheric bromine and chlorine chemistry. *Elem Sci Anth*, *7*(1), 14. https://doi.org/10.1525/elementa.352

Piot, M., & von Glasow, R. (2008). The potential importance of frost flowers, recycling on snow, and open leads for ozone depletion events. *Atmospheric Chemistry and Physics*, *8*(9), 2437–2467. https://doi.org/10.5194/acp-8-2437-2008

Piot, Matthias, & Glasow, R. von. (2009). Modelling the multiphase near-surface chemistry related to ozone depletions in polar spring. *Journal of Atmospheric Chemistry*, *64*(2), 77–105. https://doi.org/10.1007/s10874-010-9170-1

Platt, U., Allan, W., & Lowe, D. (2004). Hemispheric average Cl atom concentration from 13C/12C ratios in atmospheric methane. *Atmospheric Chemistry and Physics*. Retrieved from https://www.atmos-chem-phys.net/4/2393/2004/acp-4-2393-2004.html

Pratt, K. A., Custard, K. D., Shepson, P. B., Douglas, T. A., Pöhler, D., General, S., et al. (2013). Photochemical production of molecular bromine in Arctic surface snowpacks. *Nature Geoscience*, *6*(5), 351–356. https://doi.org/10.1038/ngeo1779

Preunkert, S., & Legrand, M. (2001). Sulfate trends in a Col du Dome (French Alps) ice core: A record of anthropogenic sulfate levels in the European midtroposphere over the twentieth century. *Journal of Geophysical Research*. https://doi.org/10.1029/2001JD000792

Pszenny, A. A. P., Fischer, E. V., Russo, R. S., Sive, B. C., & Varner, R. K. (2007). Estimates of Cl atom concentrations and hydrocarbon kinetic reactivity in surface air at Appledore Island, Maine (USA), during International Consortium for Atmospheric Research on Transport and Transformation/Chemistry of Halogens at the Isles of Shoals: Cl-NHMC CHEMISTRY DURING ICARTT/CHAiOS. *Journal of Geophysical Research*, *112*(D10), 1. https://doi.org/10.1029/2006JD007725

Quack, B., & Wallace, D. W. R. (2003). Air-sea flux of bromoform: Controls, rates, and implications. *Global Biogeochemical Cycles*, *17*(1). https://doi.org/10.1029/2002gb001890

Raff, J. D., Njegic, B., Chang, W. L., Gordon, M. S., Dabdub, D., Gerber, R. B., & Finlayson-Pitts, B. J. (2009). Chlorine activation indoors and outdoors via surface-mediated reactions of nitrogen oxides with hydrogen chloride. *Proceedings of the National Academy of Sciences of the United States of America*, *106*(33), 13647–13654. https://doi.org/10.1073/pnas.0904195106

Reeves, C. E. (2003). Atmospheric budget implications of the temporal and spatial trends in methyl bromide concentration. *Journal of Geophysical Research*, *108*(D11). https://doi.org/10.1029/2002jd002943

Riley, J. P., & Tongudai, M. (1967). The major cation/chlorinity ratios in sea water. *Chemical Geology*, *2*, 263–269. https://doi.org/10.1016/0009-2541(67)90026-5

Röthlisberger, R. (2003). Limited dechlorination of sea-salt aerosols during the last glacial period: Evidence from the European Project for Ice Coring in Antarctica (EPICA) Dome C ice core. *Journal of Geophysical Research*, *108*(D16), 3645. https://doi.org/10.1029/2003JD003604

Röthlisberger, R., Hutterli, M. A., Wolff, E. W., Mulvaney, R., Fischer, H., Bigler, M., et al. (2002). Nitrate in Greenland and Antarctic ice cores: a detailed description of post-depositional processes. *Annals of Glaciology*, *35*, 209–216. https://doi.org/10.3189/172756402781817220

Ruggieri, E. (2013). A Bayesian approach to detecting change points in climatic records. *International Journal of Climatology*, *33*(2), 520–528. https://doi.org/10.1002/joc.3447

Sander, R., Keene, W. C., & Pszenny, A. A. P. (2003). Inorganic bromine in the marine boundary layer: a critical review. *Atmospheric*. Retrieved from https://www.atmos-chem-phys.net/3/1301/

Savelyev, S. A., Gordon, M., Hanesiak, J., Papakyriakou, T., & Taylor, P. A. (2006). Blowing snow studies in the Canadian Arctic Shelf Exchange Study, 2003–04. *Hydrological Processes*, *20*(4), 817–827. https://doi.org/10.1002/hyp.6118

Sherwen, T., Schmidt, J. A., Evans, M. J., Carpenter, L. J., Großmann, K., Eastham, S. D., et al. (2016). Global impacts of tropospheric halogens (Cl, Br, I) on oxidants and composition in GEOS-Chem. *Atmospheric Chemistry and Physics*, *16*(18), 12239–12271. https://doi.org/10.5194/acp-16-12239-2016

Sherwen, T., Evans, M. J., Carpenter, L. J., Schmidt, J. A., & Mickley, L. J. (2017). Halogen chemistry reduces tropospheric O_3 radiative forcing. *Atmospheric Chemistry and Physics*, *17*(2), 1557–1569. https://doi.org/10.5194/acp-17-1557-2017

Sigl, M., Winstrup, M., McConnell, J. R., Welten, K. C., Plunkett, G., Ludlow, F., et al. (2015). Timing and climate forcing of volcanic eruptions for the past 2,500 years. *Nature*, *523*(7562), 543–549. https://doi.org/10.1038/nature14565

Sigl, Michael, McConnell, J. R., Layman, L., Maselli, O., McGwire, K., Pasteris, D., et al. (2013). A new bipolar ice core record of volcanism from WAIS Divide and NEEM and implications for climate forcing of the last 2000 years: A 2000YR BIPOLAR VOLCANO RECORD. *Journal of Geophysical Research*, *118*(3), 1151–1169. https://doi.org/10.1029/2012jd018603

Simpson, W. R., King, M. D., Beine, H. J., Honrath, R. E., & Zhou, X. (2002). Radiation-transfer modeling of snow-pack photochemical processes during ALERT 2000. *Atmospheric Environment*, *36*(15), 2663–2670. https://doi.org/10.1016/S1352-2310(02)00124-3

Simpson, W. R., Carlson, D., Hönninger, G., Douglas, T. A., Sturm, M., Perovich, D., & Platt, U. (2007). First-year sea-ice contact predicts bromine monoxide (BrO) levels at Barrow, Alaska better than potential frost flower contact. *Atmospheric Chemistry and Physics*, *7*(3), 621–627. https://doi.org/10.5194/acp-7-621-2007

Simpson, W. R., von Glasow, R., Riedel, K., Anderson, P., Ariya, P., Bottenheim, J., et al. (2007). Halogens and their role in polar boundary-layer ozone depletion. *Atmospheric Chemistry and Physics Discussions: ACPD*, *7*(2), 4285–4403. https://doi.org/10.5194/acpd-7-4285-2007

Sjostedt, S. J., & Abbatt, J. P. D. (2008). Release of gas-phase halogens from sodium halide substrates: heterogeneous oxidation of frozen solutions and desiccated salts by hydroxyl radicals. *Environmental Research Letters: ERL [Web Site]*, *3*(4), 045007. https://doi.org/10.1088/1748-9326/3/4/045007

Smith, S. J., van Aardenne, J., Klimont, Z., Andres, R. J., Volke, A., & Delgado Arias, S. (2011). Anthropogenic sulfur dioxide emissions: 1850–2005. *Atmospheric Chemistry and Physics*, *11*(3), 1101–1116. https://doi.org/10.5194/acp-11-1101-2011

Spicer, C. W., Plastridge, R. A., Foster, K. L., Finlayson-Pitts, B. J., Bottenheim, J. W., Grannas, A. M., & Shepson, P. B. (2002). Molecular halogens before and during ozone depletion events in the Arctic at polar sunrise: concentrations and sources. *Atmospheric Environment*, *36*(15), 2721–2731. https://doi.org/10.1016/S1352-2310(02)00125-5

Spolaor, A., Vallelonga, P., Plane, J. M. C., Kehrwald, N., Gabrieli, J., Varin, C., et al. (2013). Halogen species record Antarctic sea ice extent over glacial–interglacial periods. *Atmospheric Chemistry and Physics*, *13*(13), 6623–6635. https://doi.org/10.5194/acp-13-6623-2013

Spolaor, A., Gabrieli, J., Martma, T., Kohler, J., Björkman, M. B., Isaksson, E., et al. (2013). Sea ice dynamics influence halogen deposition to Svalbard. *The Cryosphere*, *7*(5), 1645–1658. https://doi.org/10.5194/tc-7-1645-2013

Spolaor, A., Vallelonga, P., Gabrieli, J., Martma, T., Björkman, M. P., Isaksson, E., et al. (2014). Seasonality of halogen deposition in polar snow and ice. *Atmospheric Chemistry and Physics*, *14*(18), 9613–9622. https://doi.org/10.5194/acp-14-9613-2014

Spolaor, A., Vallelonga, P., Turetta, C., Maffezzoli, N., Cozzi, G., Gabrieli, J., et al. (2016). Canadian Arctic sea ice reconstructed from bromine in the Greenland NEEM ice core. *Scientific Reports*, *6*, 33925. https://doi.org/10.1038/srep33925

Spolaor, A., Opel, T., McConnell, J. R., Maselli, O. J., Spreen, G., Varin, C., et al. (2016). Halogen-based reconstruction of Russian Arctic sea ice area from the Akademii Nauk ice

core (Severnaya Zemlya). *The Cryosphere*, *10*(1), 245–256. https://doi.org/10.5194/tc-10-245-2016

Steffen, A., Douglas, T., Amyot, M., & Ariya, P. (2008). A synthesis of atmospheric mercury depletion event chemistry in the atmosphere and snow. *Atmospheric*. Retrieved from https://www.atmos-chem-phys.net/8/1445/2008/acp-8-1445-2008.pdf

Stein, A. F., Draxler, R. R., Rolph, G. D., Stunder, B. J. B., Cohen, M. D., & Ngan, F. (2015). NOAA's HYSPLIT Atmospheric Transport and Dispersion Modeling System. *Bulletin of the American Meteorological Society*. https://doi.org/10.1175/bams-d-14-00110.1

Strode, S. A., Wang, J. S., Manyin, M., Duncan, B., Hossaini, R., Keller, C. A., et al. (2020). Strong sensitivity of the isotopic composition of methane to the plausible range of tropospheric chlorine [Data set]. https://doi.org/10.5194/acp-20-8405-2020

Sturges, W. T., & Barrie, L. A. (1988). Chlorine, Bromine AND Iodine in arctic aerosols. *Atmospheric Environment*, *22*(6), 1179–1194. https://doi.org/10.1016/0004-6981(88)90349-6

Stutz, J., Thomas, J. L., Hurlock, S. C., Schneider, M., von Glasow, R., Piot, M., et al. (2011). Longpath DOAS observations of surface BrO at Summit, Greenland. *Atmospheric Chemistry and Physics*, *11*(18), 9899–9910. https://doi.org/10.5194/acp-11-9899-2011

Swanson, W. F., Holmes, C. D., Simpson, W. R., Confer, K., Marelle, L., Thomas, J. L., et al. (2022). Comparison of model and ground observations finds snowpack and blowing snow aerosols both contribute to Arctic tropospheric reactive bromine. *Atmospheric Chemistry and Physics*, *22*(22), 14467–14488. https://doi.org/10.5194/acp-22-14467-2022

Thomas, J. L., Stutz, J., Lefer, B., Huey, L. G., Toyota, K., Dibb, J. E., & von Glasow, R. (2011). Modeling chemistry in and above snow at Summit, Greenland – Part 1: Model description and results. *Atmospheric Chemistry and Physics*, *11*(10), 4899–4914. https://doi.org/10.5194/acp-11-4899-2011

Thomas, J. L., Dibb, J. E., Huey, L. G., Liao, J., Tanner, D., Lefer, B., et al. (2012). Modeling chemistry in and above snow at Summit, Greenland – Part 2: Impact of snowpack chemistry on the oxidation capacity of the boundary layer. *Atmospheric Chemistry and Physics*, *12*(14), 6537–6554. https://doi.org/10.5194/acp-12-6537-2012

Thomas, J. L., Dibb, J. E., Stutz, J., von Glasow, R., Brooks, S., Huey, L. G., & Lefer, B. (2012). Overview of the 2007 and 2008 campaigns conducted as part of the Greenland Summit Halogen-HO_x Experiment (GSHOX). *Atmospheric Chemistry and Physics*, *12*(22), 10833–10839. https://doi.org/10.5194/acp-12-10833-2012

Thomas, V. M., Bedford, J. A., & Cicerone, R. J. (1997). Bromine emissions from leaded gasoline. *Geophysical Research Letters*, *24*(11), 1371–1374. https://doi.org/10.1029/97gl01243

Thornton, J. A., Kercher, J. P., Riedel, T. P., Wagner, N. L., Cozic, J., Holloway, J. S., et al. (2010). A large atomic chlorine source inferred from mid-continental reactive nitrogen chemistry. *Nature*, *464*(7286), 271–274. https://doi.org/10.1038/nature08905

Toyota, K., McConnell, J. C., Lupu, A., Neary, L., McLinden, C. A., Richter, A., et al. (2011). Analysis of reactive bromine production and ozone depletion in the Arctic boundary layer using 3-D simulations with GEM-AQ: inference from synoptic-scale patterns. *Atmospheric Chemistry and Physics*, *11*(8), 3949–3979. https://doi.org/10.5194/acp-11-3949-2011

Toyota, K., McConnell, J. C., Staebler, R. M., & Dastoor, A. P. (2014). Air--snowpack exchange of bromine, ozone and mercury in the springtime Arctic simulated by the 1-D model PHANTAS--Part 1: In-snow bromine activation and its impact on ozone. *Atmospheric Chemistry and Physics*, *14*(8), 4101–4133. Retrieved from https://acp.copernicus.org/articles/14/4101/2014/

Travis, K. R., Jacob, D. J., Fisher, J. A., Kim, P. S., Marais, E. A., Zhu, L., et al. (2016). Why do Models Overestimate Surface Ozone in the Southeastern United States? *Atmospheric Chemistry and Physics*, *16*(21), 13561–13577. https://doi.org/10.5194/acp-16-13561-2016

Uppala, S. M., KÅllberg, P. W., Simmons, A. J., Andrae, U., Bechtold, V. D. C., Fiorino, M., et al. (2005). The ERA-40 re-analysis. *Quarterly Journal of the Royal Meteorological Society*, *131*(612), 2961–3012. https://doi.org/10.1256/qj.04.176

US EPA. (2016, September 22). 2014 national emissions inventory (NEI) data. Retrieved February 1, 2021, from https://www.epa.gov/air-emissions-inventories/2014-national-emissions-inventory-nei-data

Vallelonga, P., Maffezzoli, N., Saiz-Lopez, A., Scoto, F., Kjær, H. A., & Spolaor, A. (2021). Sea-ice reconstructions from bromine and iodine in ice cores. *Quaternary Science Reviews*, *269*, 107133. https://doi.org/10.1016/j.quascirev.2021.107133

van Herpen, M. M. J. W., Li, Q., Saiz-Lopez, A., Liisberg, J. B., Röckmann, T., Cuevas, C. A., et al. (2023). Photocatalytic chlorine atom production on mineral dust-sea spray aerosols over the North Atlantic. Proceedings of the National Academy of Sciences of the United States of America, 120(31), e2303974120. https://doi.org/10.1073/pnas.2303974120

Wang, Q., Jacob, D. J., Fisher, J. A., Mao, J., Leibensperger, E. M., Carouge, C. C., et al. (2011). Sources of carbonaceous aerosols and deposited black carbon in the Arctic in winter-spring: implications for radiative forcing. *Atmospheric Chemistry and Physics*, *11*(23), 12453–12473. https://doi.org/10.5194/acp-11-12453-2011

Wang, Q., Jacob, D. J., Spackman, J. R., Perring, A. E., Schwarz, J. P., Moteki, N., et al. (2014). Global budget and radiative forcing of black carbon aerosol: Constraints from pole-to-pole (HIPPO) observations across the Pacific: GLOBAL BC BUDGET AND RADIATIVE FORCING. *Journal of Geophysical Research*, *119*(1), 195–206. https://doi.org/10.1002/2013jd020824

Wang, S., & Pratt, K. A. (2017). Molecular halogens above the arctic snowpack: Emissions, diurnal variations, and recycling mechanisms. *Journal of Geophysical Research*, *122*(21), 11,991-12,007. https://doi.org/10.1002/2017jd027175

Wang, S., McNamara, S. M., Moore, C. W., Obrist, D., Steffen, A., Shepson, P. B., et al. (2019). Direct detection of atmospheric atomic bromine leading to mercury and ozone depletion. *Proceedings of the National Academy of Sciences of the United States of America*, *116*(29), 14479–14484. https://doi.org/10.1073/pnas.1900613116

Wang, X., Jacob, D. J., Eastham, S. D., Sulprizio, M. P., Zhu, L., Chen, Q., et al. (2019). The role of chlorine in global tropospheric chemistry. *Atmospheric Chemistry and Physics*, *19*(6), 3981–4003. https://doi.org/10.5194/acp-19-3981-2019

Wang, X., Jacob, D. J., Downs, W., Zhai, S., Zhu, L., Shah, V., et al. (2021, June 2). *Global tropospheric halogen (Cl, Br, I) chemistry and its impact on oxidants*. https://doi.org/10.5194/acp-2021-441

Wang, Y., Jacob, D. J., & Logan, J. A. (1998). Global simulation of tropospheric O3-NOx-hydrocarbon chemistry: 1. Model formulation. *Journal of Geophysical Research*, *103*(D9), 10713–10725. https://doi.org/10.1029/98jd00158

Warren, S. G. (1982). Optical properties of snow. *Reviews of Geophysics* , *20*(1), 67. https://doi.org/10.1029/RG020i001p00067

Watson, R. T. (1977). Rate constants for reactions of ClOx of atmospheric interest. *Journal of Physical and Chemical Reference Data*, *6*(3), 871–918. https://doi.org/10.1063/1.555558

Wesely, M. L. (1989). Parameterization of surface resistances to gaseous dry deposition in regional-scale numerical models. *Atmospheric Environment*, *23*(6), 1293–1304. https://doi.org/10.1016/0004-6981(89)90153-4

Whiticar, M., & Schaefer, H. (2007). Constraining past global tropospheric methane budgets with carbon and hydrogen isotope ratios in ice. *Philosophical Transactions. Series A, Mathematical, Physical, and Engineering Sciences*, *365*(1856), 1793–1828. https://doi.org/10.1098/rsta.2007.2048

Winton, V. H. L., Ming, A., Caillon, N., Hauge, L., Jones, A. E., Savarino, J., et al. (2020). Deposition, recycling, and archival of nitrate stable isotopes between the air–snow interface: comparison between Dronning Maud Land and Dome C, Antarctica. *Atmospheric Chemistry and Physics*, *20*(9), 5861–5885. https://doi.org/10.5194/acp-20-5861-2020

Wren, S. N., Kahan, T. F., Jumaa, K. B., & Donaldson, D. J. (2010). Spectroscopic studies of the heterogeneous reaction between O 3 (g) and halides at the surface of frozen salt solutions. *Journal of Geophysical Research*, *115*(D16), 660. https://doi.org/10.1029/2010JD013929

Xie, H.-B., Ma, F., Yu, Q., He, N., & Chen, J. (2017). Computational Study of the Reactions of Chlorine Radicals with Atmospheric Organic Compounds Featuring NHx-π-Bond (x = 1, 2) Structures. *The Journal of Physical Chemistry. A*, *121*(8), 1657–1665. https://doi.org/10.1021/acs.jpca.6b11418

Yang, X., Cox, R. A., Warwick, N. J., Pyle, J. A., Carver, G. D., O'Connor, F. M., & Savage, N. H. (2005). Tropospheric bromine chemistry and its impacts on ozone: A model study. *Journal of Geophysical Research*, *110*(D23), 3719. https://doi.org/10.1029/2005JD006244

Yang, X., Pyle, J. A., & Cox, R. A. (2008). Sea salt aerosol production and bromine release: Role of snow on sea ice. *Geophysical Research Letters*, *35*(16). https://doi.org/10.1029/2008gl034536

Young, C. J., Washenfelder, R. A., Edwards, P. M., Parrish, D. D., Gilman, J. B., Kuster, W. C., et al. (2014). Chlorine as a primary radical: evaluation of methods to understand its role in initiation of oxidative cycles. *Atmospheric Chemistry and Physics*, *14*(7), 3427–3440. https://doi.org/10.5194/acp-14-3427-2014

Zhai, S., Wang, X., McConnell, J. R., Geng, L., Cole-Dai, J., Sigl, M., et al. (2021). Anthropogenic impacts on tropospheric reactive chlorine since the preindustrial. *Geophysical Research Letters*. https://doi.org/10.1029/2021gl093808

Zhai, S., Swanson, W., McConnell, J. R., Chellman, N., Opel, T., Sigl, M., et al. (2023). Implications of snowpack reactive bromine production for Arctic ice core bromine preservation. *Journal of Geophysical Research*, *128*(20). https://doi.org/10.1029/2023jd039257

Zhang, L., Gong, S., Padro, J., & Barrie, L. (2001). A size-segregated particle dry deposition scheme for an atmospheric aerosol module. *Atmospheric Environment*, *35*(3), 549–560. https://doi.org/10.1016/S1352-2310(00)00326-5

Zhu, L., Jacob, D. J., Eastham, S. D., Sulprizio, M. P., Wang, X., Sherwen, T., et al. (2019). Effect of sea salt aerosol on tropospheric bromine chemistry. *Atmospheric Chemistry and Physics*, *19*(9), 6497–6507. https://doi.org/10.5194/acp-19-6497-2019

APPENDIX A

Appendix A provides Supporting Information for Chapter 2.

Introduction

This supporting information includes a detailed description of the GEOS-Chem model and the setup of the historical simulations (Text A1, Table A2), volcanic years marked in Figure 1(Text A2), additional information and analysis of ice cores (Figure A1,S3, Table A1), HYSPLIT model simulated backward trajectory probability map (Figure A2), and additional information from GEOS-Chem historical simulations on zonal distribution of Cl_y (Figure A4), cycling of tropospheric Cl_y analysis (Figure A5), surface distribution and trends of NO_x emissions, N_2O_5 mixing ratios, and anthropogenic HCl emissions (Figure A6-8). In addition, the details of correlation analysis between snow acidity and Cl_{exc} for individual ice cores are shown in Table A3, and the sources and sinks of TRJ tropospheric Cl• from the historical simulations is shown in Table A4. Snow accumulation rates for the Greenland ice cores are shown in Figure A9 and Table A5, and additional discussions on model uncertainties besides anthropogenic emissions are in Text A3.

Text A1. Detailed model description

The model version used in this study is version 11-02d (available on https://github.com/geoschem/geos-chem/tree/v11-02d-prelim, last accessed on 05 April 2021) Description of the model's tropospheric halogen (Cl, Br, and I) chemistry can be found in references (Sherwen et al., 2016; Wang et al., 2019; Zhu et al., 2019). The model includes both open ocean and blowing snow sources of sea-salt aerosol as described in references (Huang & Jaeglé, 2017; Jaeglé et al., 2011). Sea-salt Cl^- is converted to HCl via acid-displacement by HNO_3 and H_2SO_4 (Jacob et al., 1985) and is calculated using the ISORROPIA II thermodynamic equilibrium model (Fountoukis & Nenes, 2007) for the accumulation-mode aerosol and a modified equilibrium model to account for the mass transfer limitation for the coarse-mode aerosol (Wang et al., 2019). Cloud pH is calculated based on Moch et al. (2020). Heterogeneous reactions in clouds are limited by cloud entrainment rates as described in Holmes et al. (2019). We use the updated rate coefficients from Liu & Abbatt (2020) for reactions of HOBr/HOCl and HSO_3^-/SO_3^{2-} in the model, which is important for converting more reactive forms of halogens (HOBr, HCl) to less reactive species (HBr, HCl) (Chen et al., 2017).

Sinks of halogen species include dry and wet deposition for both the gases and aerosol. The wet deposition scheme in GEOS-Chem is described by H. Liu et al. (2001) for water-soluble aerosols and by Amos et al. (2012) for gases. Scavenging of aerosol by snow and cold/mixed precipitation is described by references (Q. Wang et al., 2011, 2014). Dry deposition is based on the resistance-in-series scheme of Wesely (1989) as implemented by Y. Wang et al. (1998). Aerosol deposition scheme is from Zhang et al. (2001). Aerosol deposition to snow/ice is described by Fisher et al. (2011). Sea-salt deposition scheme is from Jaeglé et al. (2011).

The model uses UCX (Eastham et al., 2014) scheme to calculate stratospheric chemistry. Long-lived ozone-depleting substances (ODSs), such as CFCs, HCFCs, and halons are set with fixed surface mixing ratios in the respective years, advected and lost as part of the chemistry mechanism, and their concentrations are set to zero in PI simulation. To exclude the contribution from anthropogenic emissions for historical simulations (described below), we scale stratospheric Br_y concentrations from very short-lived substances ($CHBr_3$, CH_2Br_2, etc.) by 56% following previous studies (Liang et al., 2010; Sherwen et al., 2017).

We use CEDS (Hoesly et al., 2018) and BB4CMIP6 (van Marle et al., 2017) of individual years (1750, 1975, 2007) for anthropogenic and biomass-burning emissions, respectively. For PD simulation, the global anthropogenic emission inventory (CEDS) is superseded by the following regional inventories: NEI11v1 from EPA 2014 for the US (Travis et al., 2016), MIX inventory for East Asia (Li et al., 2014), and DICE-Africa inventory for Africa (Marais & Wiedinmyer, 2016). Based on emission factors for different land types from van Marle et al. (2017), we include the biomass-burning emitted HCl into BB4CMIP6. The only available global inventory of anthropogenic HCl is from McCulloch et al. (1999), but it is shown to overestimate HCl observations over the US (X. Wang et al., 2019), and is biased high compared to current regional emission inventories from the US (US EPA, 2016) and China (Fu et al., 2018; Y. Liu et al., 2018). HCl and SO_2 are co-emitted from combustion sources (mainly coal combustion and waste incineration), and the implementation of the flue-gas desulphurization (FGD) technologies that were designed to remove SO_2 exhaust has been shown to be highly effective in removing other acidic gases such as HCl (Haskins et al., 2020; McCulloch et al., 1999). Therefore, we implement an anthropogenic HCl emission inventory based on CEDS SO_2 emission (Hoesly et al., 2018) and assume a HCl:SO_2 emission ratio of 0.033 as observed in coal-fired power plant plumes (Lee et al., 2018). We use this ratio to scale HCl emissions to SO_2 emissions from the

CEDS working sectors that contain most combustion sources. This implementation will reflect not only the increasing HCl emissions since the Industrial Revolution, but also the decline of HCl emissions resulting from recent emission control strategies. Figure A8 shows the global distribution of anthropogenic HCl emissions from the model. There are uncertainties associated with this approach since CEDS sectors do not separate combustion and non-combustion emissions and we apply the same scaling factor globally. However, the scaling factor is based on observations from coal combustion, which represents the majority (40–80%) of anthropogenic SO_2 emissions (Smith et al., 2011). HCl:SO_2 emission ratio is also subject to changes induced by the application and update of clean coal technologies, as flue gas desulphurization may not be equally effective at removing SO_2 and HCl (i.e., the HCl:SO_2 emissions ratio may be different before and after the implementation of air pollution control technologies). McCulloch et al. (1999) estimates a global HCl emission of 4.6±4.3Tg Cl from fossil fuel combustion in 1990, while the HCl emissions based on the fixed HCl:SO_2 emission ratio is 2.3Tg Cl in PA (1975), 50% less than the mean value in McCulloch et al. (1999). It is possible that our approach represents a lower limit of HCl emissions in PA, which could be the cause of the underestimation of PA Cl_y in the model.

Text A2. Volcanic years in Figure 1

In Figure 1, Green stars mark large and moderate volcanic eruption years based on Cole-Dai et al. (2013) and Sigl et al. (2013), and only eruptions with volcanic sulfate deposition flux >10 kg km^{-2} are shown: Pinatubo(Indonesia) in 1991, Katmai (Alaska) in 1912, Krakatoa (Indonesia) in 1883, Makian (Indonesia) in 1862, Cosiguina (Nicaragua) in 1835, Babuyan (Philippines) in 1831, Galunggung (Indonesia) in 1822, Tambora (Indonesia) in 1815, unknown eruption in 1809, Laki (Iceland) in 1782, Hekla (Iceland) in 1766, and unknown eruption in 1761. Note that volcanic signals in polar ice cores may last 2–3 years, usually with maximum concentration of volcanic sulfate flux appearing 1 year after the eruption.

Text A3. Model uncertainties analysis

We acknowledge that the uncertainties causing the discrepancy between model and ice-core trends may stem from other factors than anthropogenic emissions. We designed the study to

exclude impacts of changes in meteorology (which also are a source of uncertainty) to only focus on the anthropogenic contribution on the observed Cl_{exc} trends.

The changes in snow accumulation rates may impact ice core concentrations. The water equivalent snow accumulation rates from the five Greenland ice cores (excluding Summit07) are shown in Figure A9. We calculated the Sen's slope of the snow accumulation rates since the preindustrial for the five Greenland ice core locations (Table A5). Significant trends exist only in the ACT_11d core, and for the post-1940 period at NEEM, but other sites did not show significant trends. Thus, we can rule out the impacts of snow accumulation rate changes on the observed consistent trends between the different Greenland ice cores.

Another source of potential model bias is the lack of Cl_2 production from snow photochemistry on snowpack and ice surfaces (Halfacre et al., 2019; Liao et al., 2014; Custard et al., 2017). However, the mechanism of snow Cl_2 production remains highly uncertain and is thus difficult to parameterize into models. We also expect this source to be minor under the high snow accumulation rates in the Greenland region (Röthlisberger, 2003).

We examined the representativeness of year 2007 meteorology fields for our historical simulations. Variations in meteorological fields may impact transport patterns and sea salt emission. For transport patterns, we compared the 5-day back trajectory probability from year 2007 (Fig.A10) with the averaged back trajectory probability for 1959–2010 (Fig.S2), and found that the source regions are quite similar. Thus we are convinced that year 2007 is not special enough to alter the transport pattern in Greenland ice core source regions. For sea salt emissions, which are dependent on wind speed, sea surface temperatures, and sea ice extent as described in Jaeglé et al. (2011), we calculated the annual mean sea salt emissions in 30–90°N from 2006 to 2014 (Fig. A11) in the model. For this time period, year 2007 does not stand out in sea salt production either. Therefore, we think 2007 should be a representative year to use for our study.

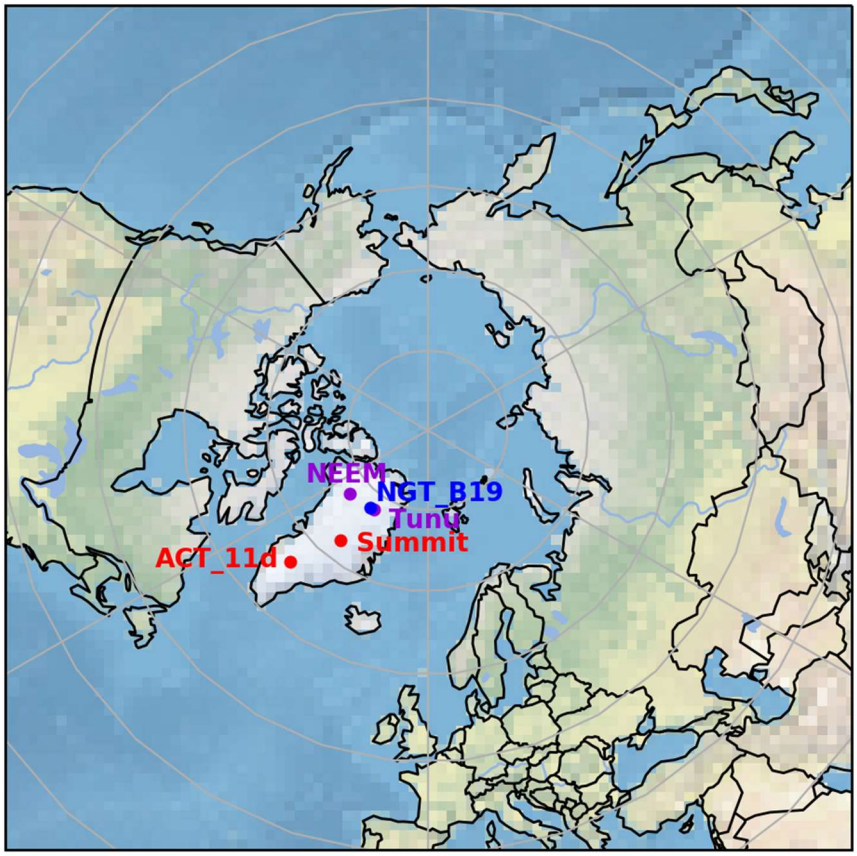

Figure A1. Locations of the six Greenland ice-core sites used in this study. Different colors distinguish higher (purple and blue), and lower latitude (red) ice-core sites.

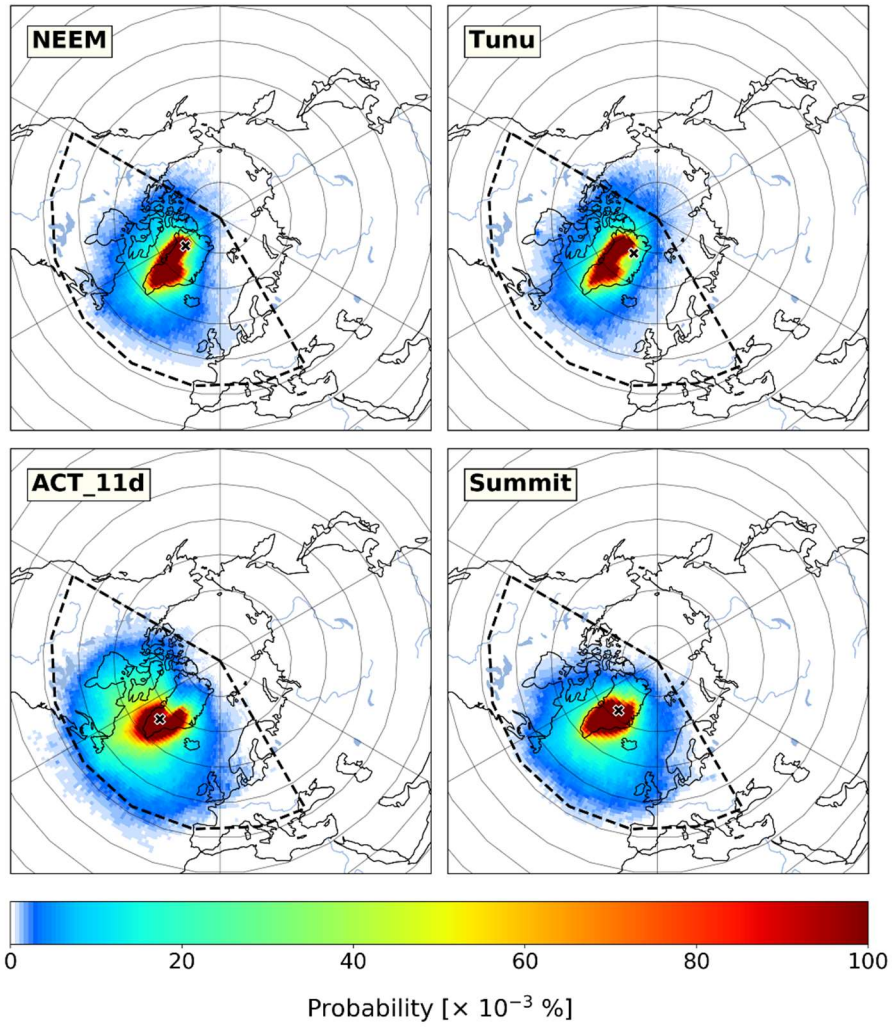

Figure A2. 5-day back trajectory probability of NEEM, Tunu, ACT_11d, and Summit calculated by the HYSPLIT model for the time period 1959-2010. Ice-core sites on each panel are marked as black crosses, and dashed black lines indicate the back trajectory region used for chlorine budget analysis.

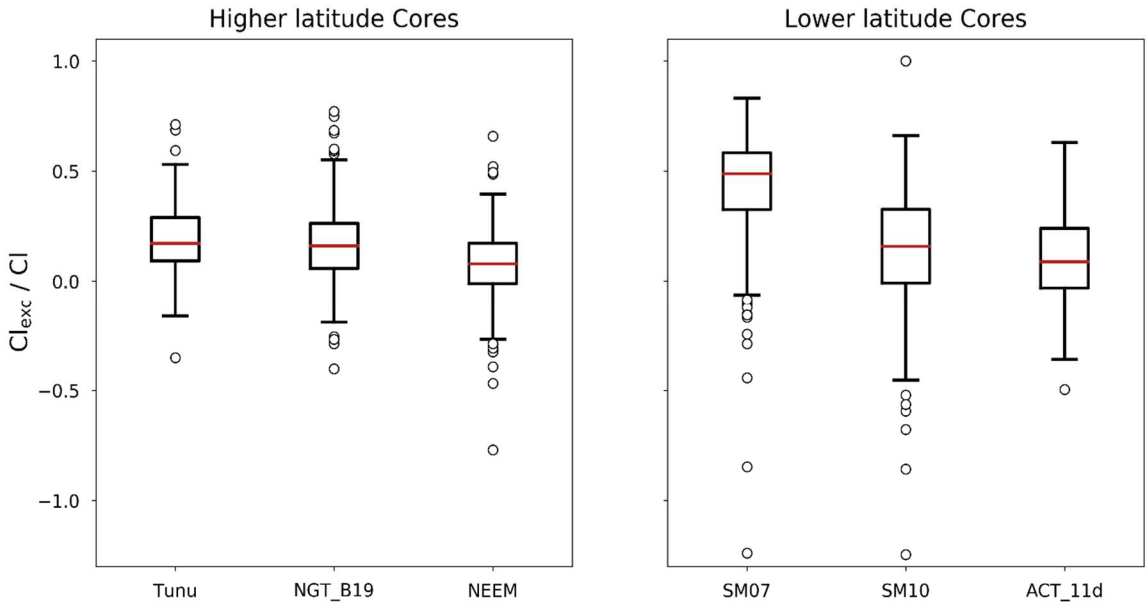

Figure A3. Boxplot of Cl_{exc}/Cl ratio for the six Greenland ice cores. Red lines represent the median values, and circles denote outliers. Statistics refer to the full reported time period for each core.

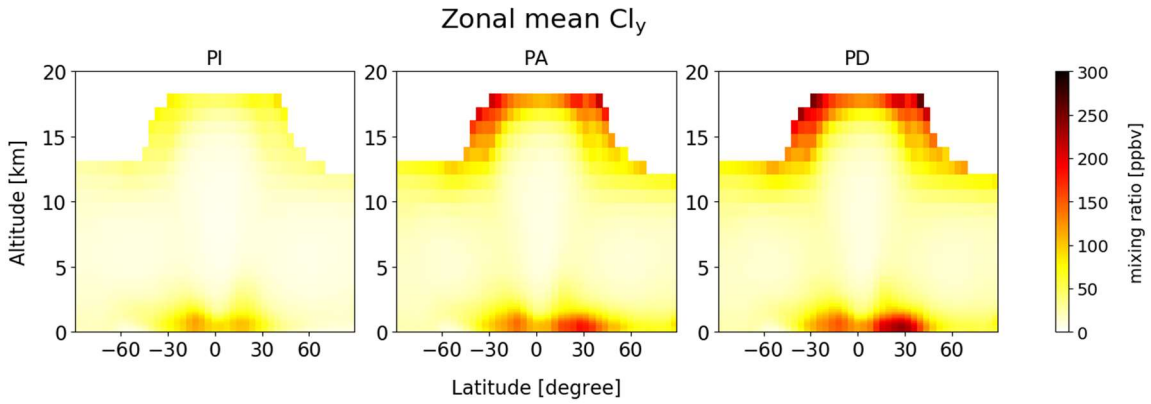

Figure A4. Simulated zonal mean mixing ratio of Cl_y as a function of latitude and altitude for PI (1750), PA (1975), and PD (2007).

Cl_PI

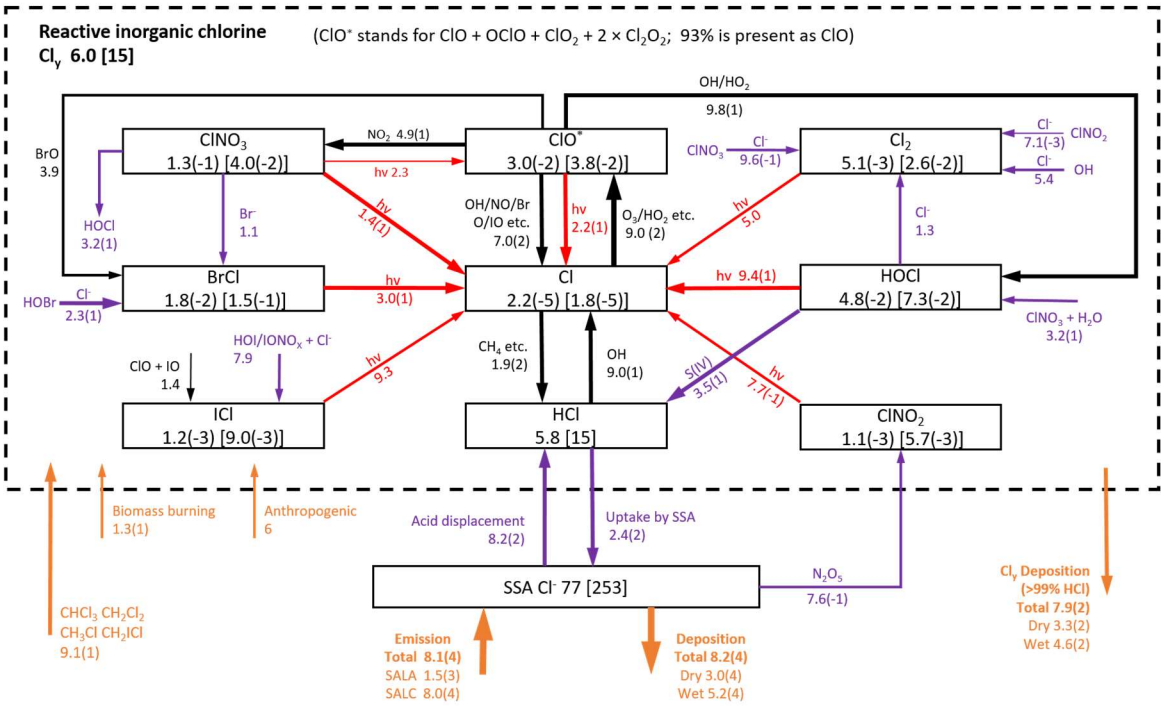
Reactive inorganic chlorine
Cl$_y$ 6.0 [15]
(ClO* stands for ClO + OClO + ClO$_2$ + 2 × Cl$_2$O$_2$; 93% is present as ClO)
OH/HO$_2$
9.8(1)
ClNO$_3$
1.3(-1) [4.0(-2)]
NO$_2$ 4.9(1)
hv 2.3
ClO*
3.0(-2) [3.8(-2)]
ClNO$_3$ Cl$^-$ 9.6(-1)
Cl$_2$
5.1(-3) [2.6(-2)]
Cl$^-$ 7.1(-3) ClNO$_2$
Cl$^-$ 5.4 OH
BrO 3.9
HOCl 3.2(1)
Br$^-$ 1.1
hv 1.4(1)
OH/NO/Br O/IO etc. 7.0(2)
hv 2.2(1)
O$_3$/HO$_2$ etc. 9.0 (2)
hv 5.0
Cl$^-$ 1.3
BrCl
1.8(-2) [1.5(-1)]
HOBr Cl$^-$ 2.3(1)
hv 3.0(1)
Cl
2.2(-5) [1.8(-5)]
hv 9.4(1)
HOCl
4.8(-2) [7.3(-2)]
ClNO$_3$ + H$_2$O 3.2(1)
ClO + IO 1.4
HOI/IONO$_x$ + Cl$^-$ 7.9
hv 9.3
CH$_4$ etc. 1.9(2)
OH 9.0(1)
S(IV) 3.5(1)
hv 7.7(-1)
ICl
1.2(-3) [9.0(-3)]
HCl
5.8 [15]
ClNO$_2$
1.1(-3) [5.7(-3)]
Biomass burning 1.3(1)
Anthropogenic 6
Acid displacement 8.2(2)
Uptake by SSA 2.4(2)
SSA Cl$^-$ 77 [253]
N$_2$O$_5$ 7.6(-1)
Cl$_y$ Deposition (>99% HCl) Total 7.9(2) Dry 3.3(2) Wet 4.6(2)
CHCl$_3$ CH$_2$Cl$_2$ CH$_3$Cl CH$_2$ICl 9.1(1)
Emission Total 8.1(4) SALA 1.5(3) SALC 8.0(4)
Deposition Total 8.2(4) Dry 3.0(4) Wet 5.2(4)

Cl_PA

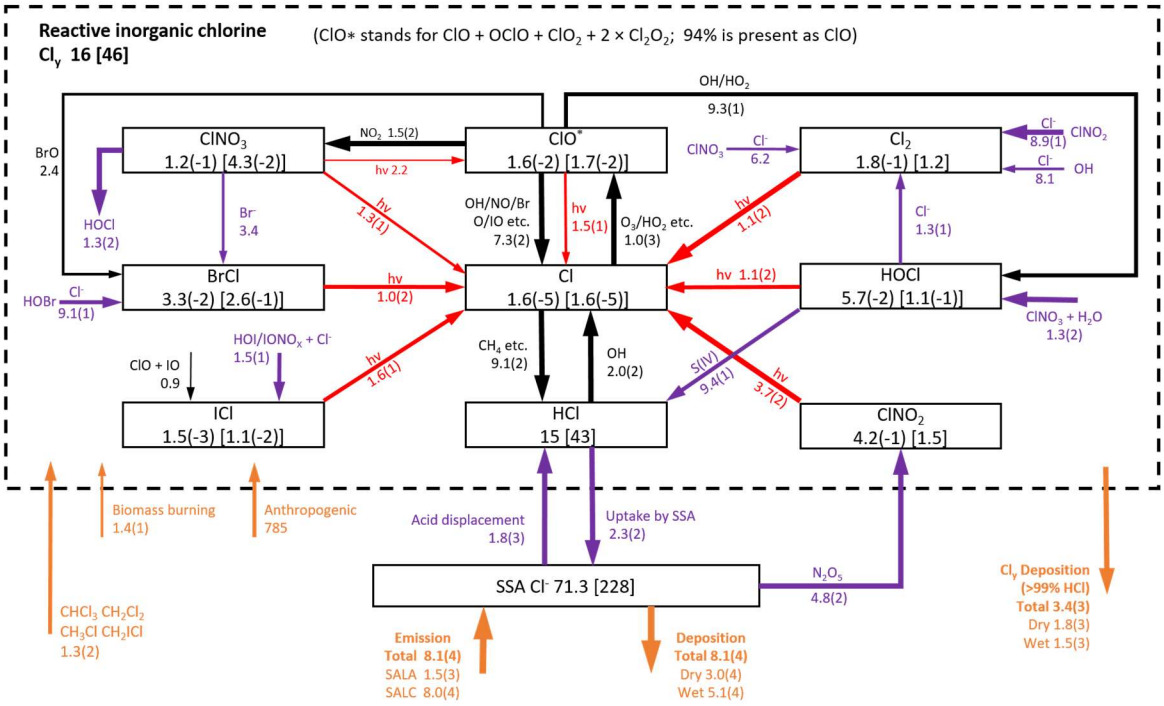
Reactive inorganic chlorine
Cl$_y$ 16 [46]
(ClO* stands for ClO + OClO + ClO$_2$ + 2 × Cl$_2$O$_2$; 94% is present as ClO)
OH/HO$_2$
9.3(1)
ClNO$_3$
1.2(-1) [4.3(-2)]
NO$_2$ 1.5(2)
hv 2.2
ClO*
1.6(-2) [1.7(-2)]
ClNO$_3$ Cl$^-$ 6.2
Cl$_2$
1.8(-1) [1.2]
Cl$^-$ 8.9(1) ClNO$_2$
Cl$^-$ 8.1 OH
BrO 2.4
HOCl 1.3(2)
Br$^-$ 3.4
hv 1.3(1)
OH/NO/Br O/IO etc. 7.3(2)
hv 1.5(1)
O$_3$/HO$_2$ etc. 1.0(3)
hv 1.1(2)
Cl$^-$ 1.3(1)
BrCl
3.3(-2) [2.6(-1)]
HOBr Cl$^-$ 9.1(1)
hv 1.0(2)
Cl
1.6(-5) [1.6(-5)]
hv 1.1(2)
HOCl
5.7(-2) [1.1(-1)]
ClNO$_3$ + H$_2$O 1.3(2)
ClO + IO 0.9
HOI/IONO$_x$ + Cl$^-$ 1.5(1)
hv 1.6(1)
CH$_4$ etc. 9.1(2)
OH 2.0(2)
S(IV) 9.4(1)
hv 3.7(2)
ICl
1.5(-3) [1.1(-2)]
HCl
15 [43]
ClNO$_2$
4.2(-1) [1.5]
Biomass burning 1.4(1)
Anthropogenic 785
Acid displacement 1.8(3)
Uptake by SSA 2.3(2)
SSA Cl$^-$ 71.3 [228]
N$_2$O$_5$ 4.8(2)
Cl$_y$ Deposition (>99% HCl) Total 3.4(3) Dry 1.8(3) Wet 1.5(3)
CHCl$_3$ CH$_2$Cl$_2$ CH$_3$Cl CH$_2$ICl 1.3(2)
Emission Total 8.1(4) SALA 1.5(3) SALC 8.0(4)
Deposition Total 8.1(4) Dry 3.0(4) Wet 5.1(4)

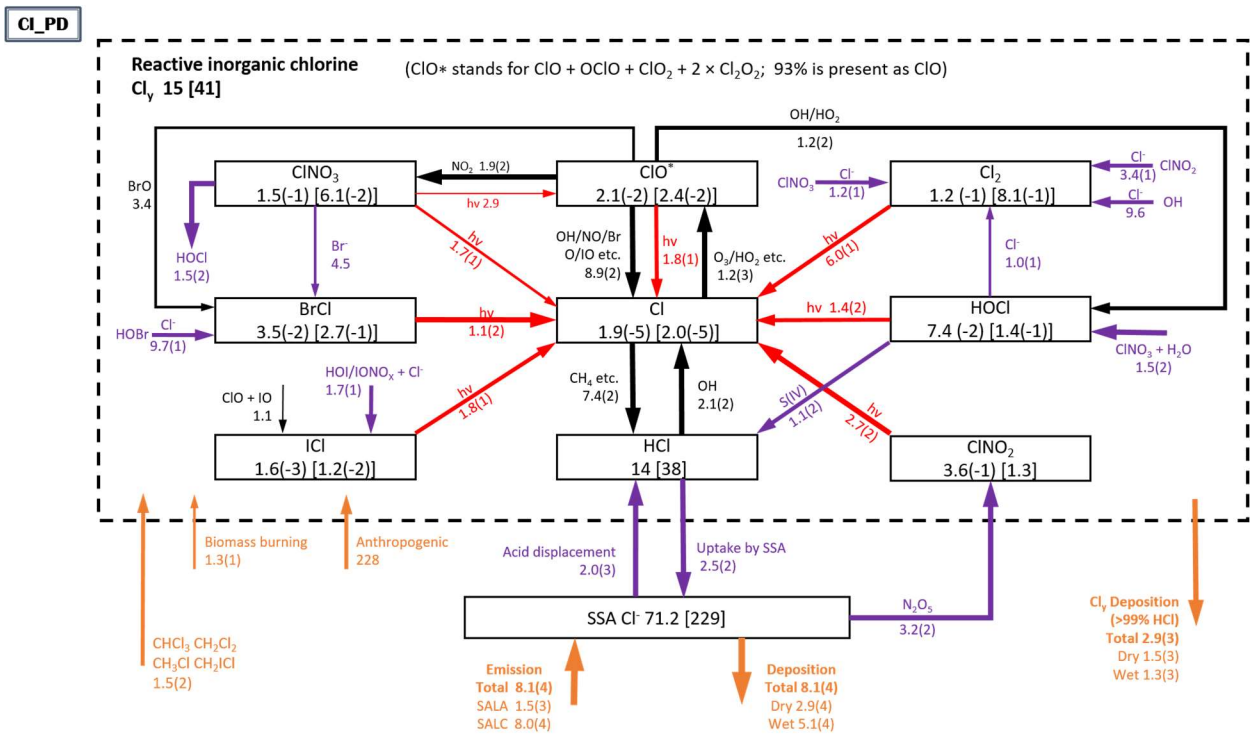

Figure A5. TRJ (longitude 120ºW–30ºE, latitude 42ºN–90ºN) regional budget and chemical cycling of tropospheric chlorine species in GEOS-Chem for PI, PA, and PD. Average regional annual mean masses (Gg Cl) and mixing ratios (ppt, in square brackets) are shown in the squares with key chlorine species. Arrows show the regional annual mean reaction rates (Gg Cl a^{-1}), and the thickness of arrows are proportional to the orders of magnitude of the reaction rates. Read 6.1(−2) as 6.1×10^{-2}. Gas phase, heterogeneous, and photolysis chemistry are shown in black, purple, and red arrows, respectively, and orange arrows indicate the sources and sinks. The dotted box group together the Cl_y family, and arrows in and out of the box represent general sources and sinks of Cl_y. $IONO_x$ = IONO + $IONO_2$.

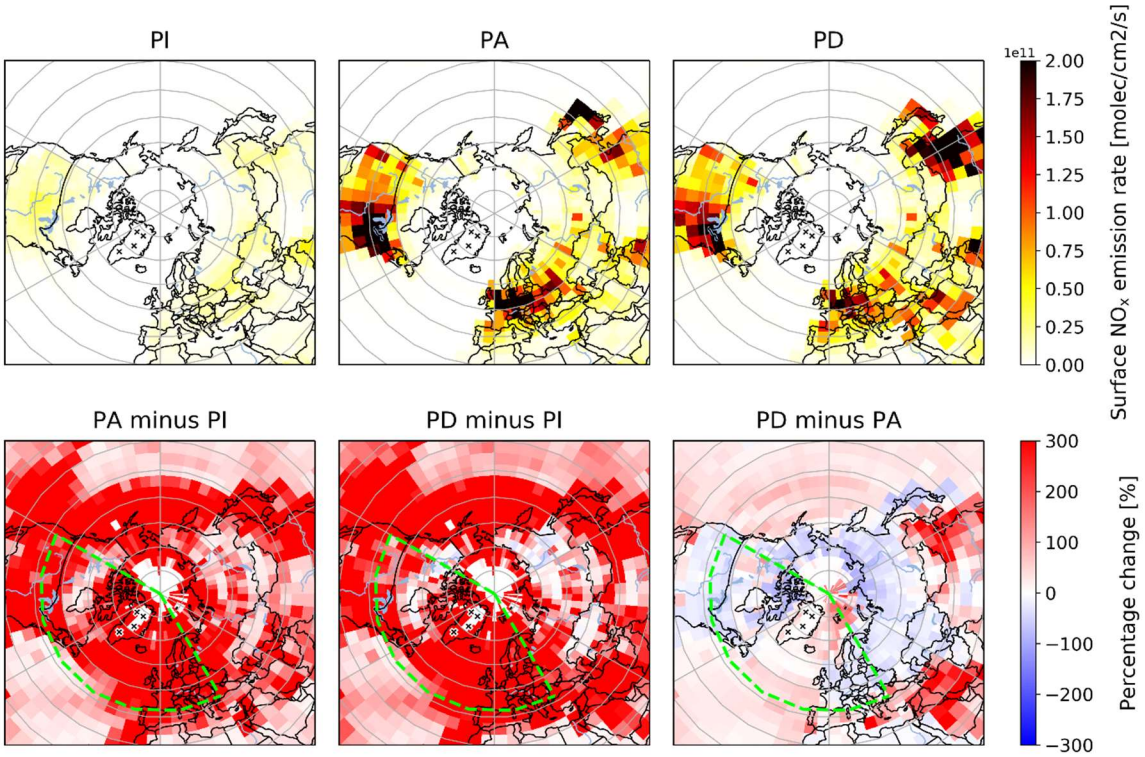

Figure A6. Simulated annual mean distribution of NO_x emissions in the 30–90ºN region during historical time periods (upper panel), and percentage changes between them (lower panel). Dashed green lines indicate the TRJ region.

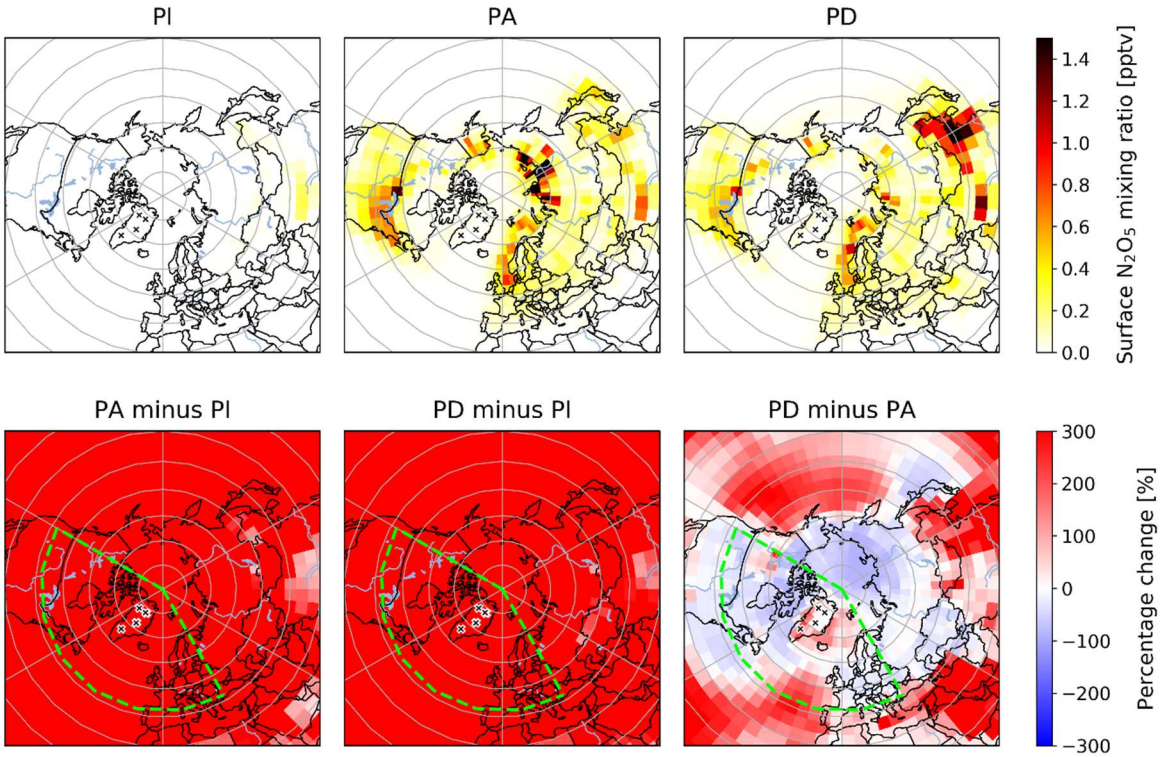

Figure A7. Simulated annual mean surface mixing ratio of N_2O_5 in the 30-90ºN region during historical time periods (upper panel) and percentage changes between them (lower panel). Dashed green lines indicate the TRJ region.

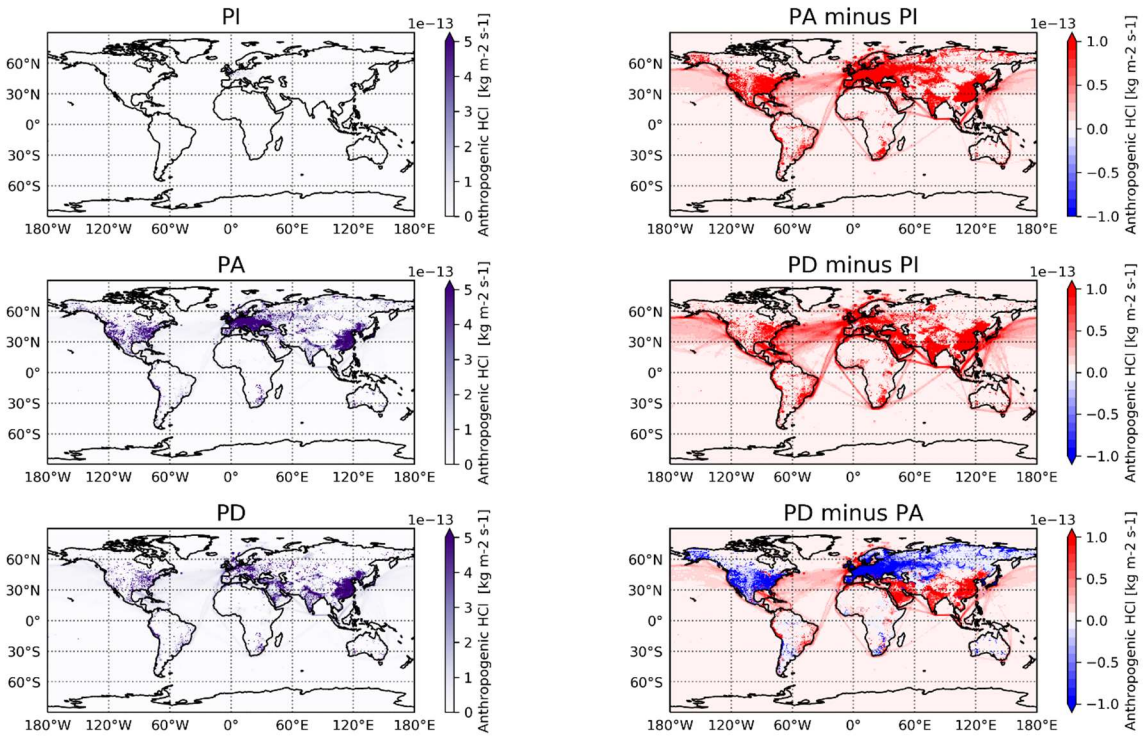

Figure A8. Simulated global distribution of anthropogenic HCl emissions (kg m^{-2} s^{-1}) applied in this study. Left three panels show the distribution in PI, PA, and PD, right three panels show the absolute change between the three time periods.

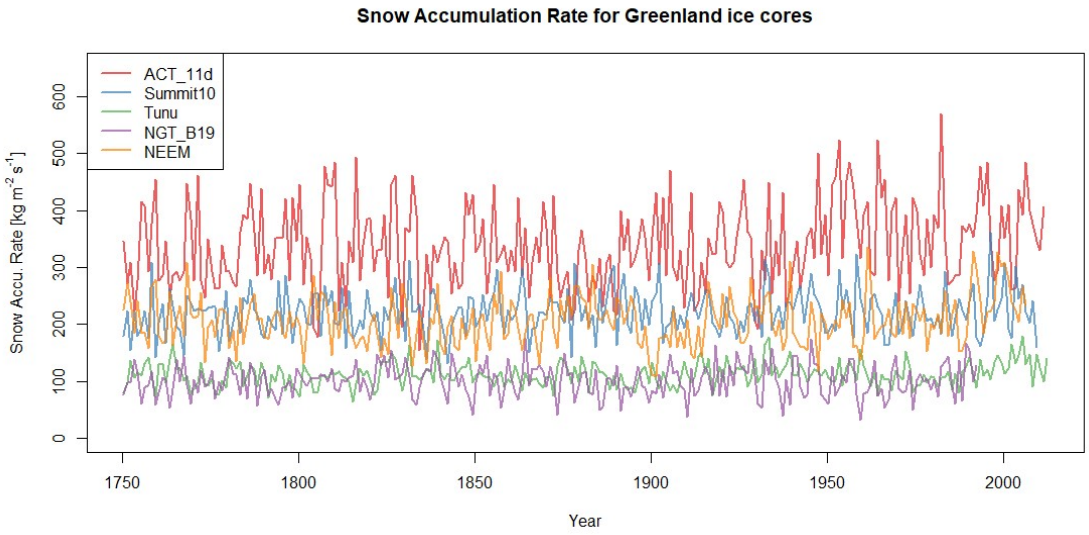

Figure A9. Time series of water-equivalent snow accumulation rate for 5 Greenland ice cores.

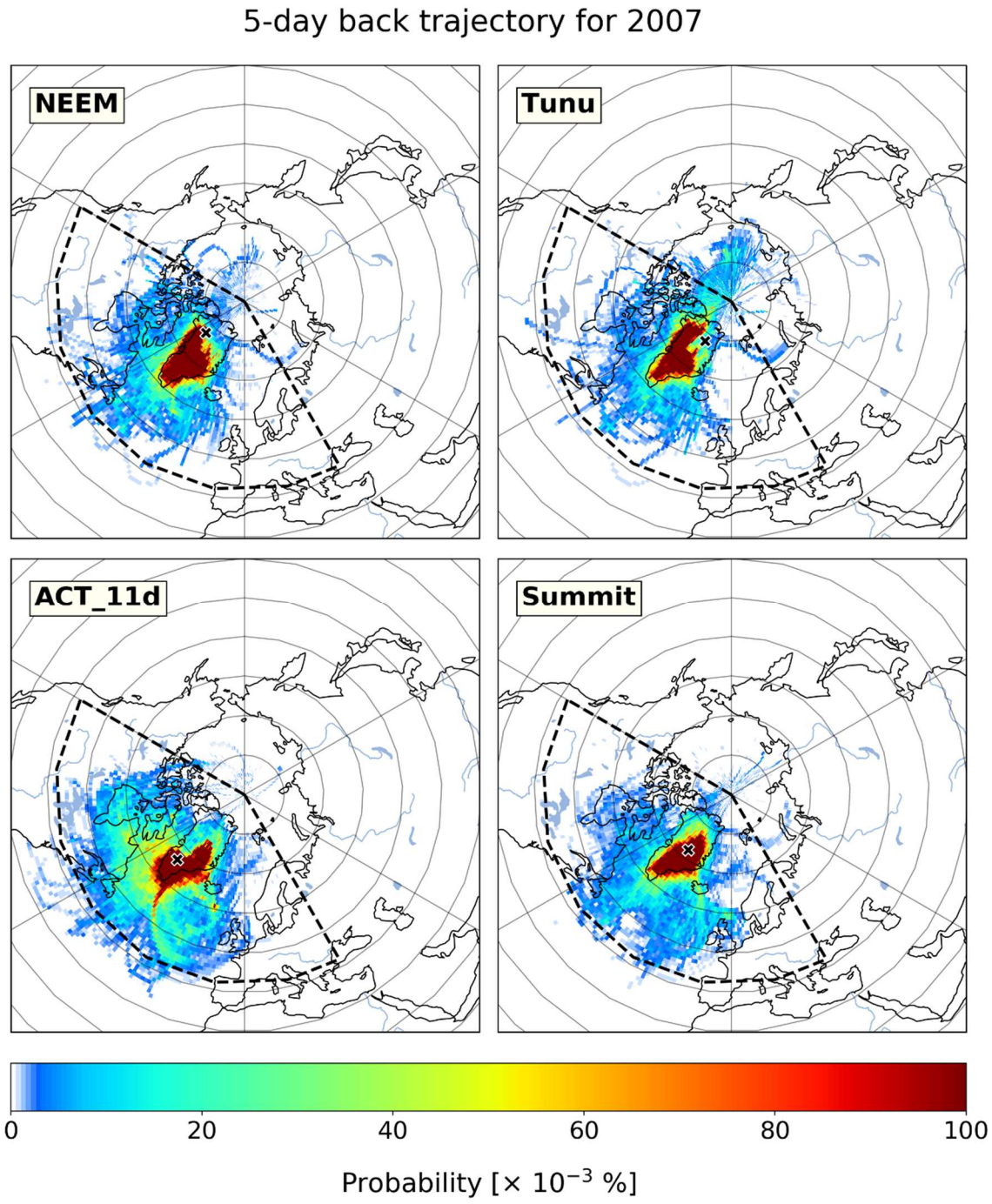

Figure A10. 5-day back trajectory probability of NEEM, Tunu, ACT_11d, and Summit calculated by the HYSPLIT model for year 2007. Ice-core sites on each panel are marked as black crosses, and dashed black lines indicate the back trajectory region used for chlorine budget analysis.

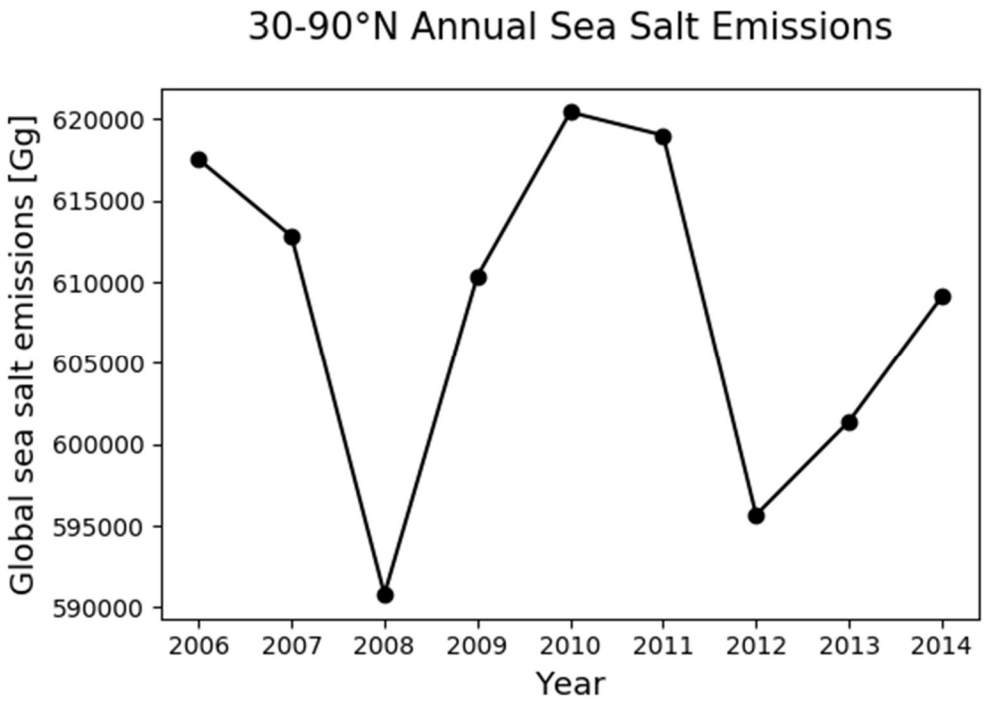

Figure A11. Annual mean sea salt emissions in 30–90°N from 2006 to 2014. Results are generated from offline HEMCO simulations, using meteorological fields for different years from MERRA-2.

Table A1. Location and other information for the six ice cores included in this study

Ice cores	Formal Name	Latitude	Longitude	Elevation (m)	Drilling Year	Length (m)	Recent Snow Accum. (kg m^{-2} yr^{-1})	Time Period	Previously unpublished except
Tunu	Tunu_2013	78.0 ºN	33.9 ºW	2105	2013	213.4	108	275-2012	Acidity and Sodium (1750-2010) (Maselli et al., 2017)
	Tunu_2013r[a]	78.0 ºN	33.9 ºW	2105	2013	213.4	108	275-2012	
NGT_B19	NGT_B19	78.0 ºN	36.4 ºW	2270	1993	150.4	100	746-1993	-
NEEM	NEEM_2011_S1	77.5 ºN	51.1 ºW	2454	2011	410.8	211	88-1999	-
Summit07	Summit_2007	72.6 ºN	38.6 ºW	3216	2007	80.0	226	1772-2006	Acidity (Geng et al., 2014)
Summit10	Summit_2010	72.3 ºN	38.3 ºW	3258	2010	87.3	226	1743-2010	Acidity and Sodium (Maselli et al., 2017)
	Summit_2010r[a]	72.3 ºN	38.3 ºW	3258	2010	87.3	226	1743-2009	
ACT_11d	ACT_11d	66.5 ºN	46.3 ºW	2148	2011	299.4	334	1161-2010	-

Note: All data are previously unpublished except as noted in the last column. See McConnell et al. (2019) for ice core descriptions of Tunu, NGT_B19, NEEM, Summit10, and ACT_11d, and Cole-Dai et al. (2013) and Geng et al. (2014) for Summit07. [a]Tunu_2013r and Summit_2010r are independent elemental measurements from parallel samples taken from Tunu_2013 and Summit_2010 ice cores, respectively. Acidity was only measured for Tunu_2013 and Summit_2010. Average values of the two independent measurements for Na, Cl, and the calculated Cl_{exc} are presented for Tunu and Summit10 in **Figure 1** in the main text, while **Figure 2** only shows Na, Cl, and Cl_{exc} based on the first measurement (Summit_2010 and Tunu_2013) to be consistent with acidity.

Table A2. Model setup for historical simulations of PI, PA and PD

	PI (1750)	PA (1975)	PD (2007)
Year of Met Fields	2007	2007	2007
Anthropogenic and biofuel emissions	CEDS[a] 1750	CEDS 1975	CEDS 2007; Regional emissions
Biomass burning	BB4CMIP6[b] 1750	BB4CIMP6 1975	BB4CMIP6 2007
CH_4 concentrations	CMIP6[c] 1750	CMIP6 1975	NOAA GMD[d] 2007
Long lived organohalogens: CH_3Cl, CH_2Cl_2, $CHCl_3$ and CH_3Br	CMIP6[c] 1750	CMIP6 1975	CMIP6 2007
Long lived anthropogenic ODSs[e]: CFCs, Halons, etc.	Set to 0	GMI[e] 1975	GMI 2007
VSL[f] species: $CHBr_3$ and CH_2Br_2	Liang_bromocarbon[f]	Liang_bromocarbon	Liang_bromocarbon
Iodocarbons: CH_3I, CH_2I_2, CH_2ICl, CH_2IBr	ORDONEZ_IODOCARB[g]	ORDONEZ_IODOCARB	ORDONEZ_IODOCARB
Stratospheric Br_y	56% of 2007 values[h]	56% of 2007 values	2007

[a]Global anthropogenic emission from the Community Emissions Data System (CEDS) inventory (Hoesly et al., 2018). For present day simulation, the CEDS inventory is superseded by improved inventories in regions where we have better information: the US (NEI11v1) from EPA (2016), as implemented by Travis et al. (2016); Canada (CAC) implemented by van Donkelaar et al. (2008) with updates; East Asia (MIX inventory (Li et al., 2014)); Africa for 2006 and 2013 (DICE-Africa inventory (Marais & Wiedinmyer, 2016)). [b]Historic global biomass burning emissions for CMIP6 (BB4CMIP) (van Marle et al., 2017). [c]Historical greenhouse gas concentrations for the Climate Model Intercomparison Project – Phase 6 (CMIP6) (Meinshausen et al., 2017). [d]Atmospheric methane dry air mole fractions from the NOAA ESRL Carbon Cycle Cooperative Global Air Sampling Network (Dlugokencky, 2016). Data available for 1979–2020. [e]Ozone depletion substances (ODSs) is set with fixed surface concentrations in the model (Eastham et al., 2014), based on NASA's Global Modeling Initiative (GMI) code. [f]Very short lived (VSL) halogen emissions are taken from Liang et al. (2010), and $CHBr_3$ at latitude>30 ºN is scaled according to Parrella et al. (2012). [g]Emission of iodocarbons are following Ordóñez et al. (2012). [h]Stratospheric Br_y concentrations are from the Liang et al. (2010), scaling for preindustrial and 1975 are following previous studies (Liang et al., 2010; Sherwen et al., 2017).

Table A3. Correlation coefficient between Na and Cl, Acidity and Cl_{exc} for the six ice-core records

no outliers	Na vs. Cl			Acidity vs. Cl_{exc}		
r(n)	Full data	Pre-1940	Post-1940	Full data	Pre-1940	Post-1940
Tunu	0.94 (251)	0.96 (180)	0.93 (57)	0.46 (231)	0.24 (169)	0.33 (67)
NGT_B19	0.86 (222)	0.93 (166)	0.73 (56)	0.40 (206)	0.26 (145)	0.33 (54)
NEEM	0.87 (225)	0.89 (174)	0.87 (55)	0.00 (196)	0.18 (164)	0.38 (49)
Summit07	0.49 (225)	0.45 (160)	0.62 (64)	0.57 (226)	0.43 (158)	0.67 (63)
Summit10	0.68 (253)	0.81 (185)	0.73 (70)	0.36 (243)	−0.02 (175)	0.72 (66)
ACT_11d	0.80 (248)	0.89 (176)	0.85 (70)	0.61 (243)	0.32 (168)	0.70 (69)

raw data	Na vs. Cl			Acidity vs. Cl_{exc}		
r(n)	Full data	Pre-1940	Post-1940	Full data	Pre-1940	Post-1940
Tunu	0.98 (264)	0.99 (190)	0.94 (58)	0.40 (264)	0.14 (190)	0.34 (73)
NGT_B19	0.89 (248)	0.91 (190)	0.78 (58)	0.30 (248)	0.28 (190)	0.34 (58)
NEEM	0.94 (248)	0.94 (190)	0.91 (58)	0.20 (248)	0.22 (190)	0.38 (58)
Summit07	0.44 (235)	0.32 (168)	0.78 (67)	0.43 (235)	0.23 (168)	0.64 (67)
Summit10	0.55 (264)	0.87 (190)	0.37 (74)	0.31 (259)	0.02 (190)	0.51 (69)
ACT_11d	0.83 (262)	0.90 (190)	0.84 (72)	0.70 (262)	0.51 (190)	0.75 (72)

Note: *r*(n) represents correlation coefficients *r* with numbers (n) of pairs used in the calculation. The upper table shows values after removing outliers outside of 1.5×IQR, and the lower table shows the calculation using the raw data. All *r* values are significant, with *p*-values smaller than 0.05.

Table A4. Sources and sinks of TRJ tropospheric Cl• from PI to PD simulations

Rates (Gg Cl a^{-1})	PI	PA	PD
Cl^* photolysis	158	833	679
Organochlorines	91	128	147
Total source	**249**	**961**	**826**
Net Cl• → HCl	100	715	527
Net Cl• → ClO^*	180	270	338
Total sink	**279**	**985**	**865**
Burden (kg Cl)	**21.8**	**16.0**	**19.2**

Note: Net Cl• → HCl is the net sink of Cl• to form HCl, which includes Cl• reaction with alkanes (methane, ethane, etc.), alkenes (isoprene, propene, etc.), alcohols (methanol, ethanol, etc.), formaldehyde, peroxides (hydrogen peroxide and hydroperoxyl radical), organic chlorine species (chloromethane, dichloromethane, chloroform), and acids (formic acid, acetic acid, etc.). Net Cl• → ClO^* is the net sink of Cl• to form ClO^*, including Cl• reaction with ozone, hydroxyl radical, chlorine dioxide, methylperoxy radical, and ethylperoxy radical.

Table A5 Sen's Slopes for 5 Greenland ice core snow accumulation rates for the full record and post-1940

Full Record	Sen's Slope (95% C.I.)	*p*-value	Trends
ACT_11d	0.165 (0.033, 0.287)	0.008	yes
Summit10	0.045 (−0.014, 0.109)	0.145	no
Tunu	0.037 (0, 0.071)	0.032	no
NGT_B19	0.007 (−0.043, 0.067)	0.745	no
NEEM	0.042 (−0.030, 0.116)	0.261	no

Post-1940	Sen's Slope (95% C.I.)	*p*-value	Trends
ACT_11d	0 (−0.940, 0.818)	0.930	no
Summit10	−0.139 (−0.566, 0.355)	0.577	no
Tunu	0.237 (0, 0.472)	0.041	no
NGT_B19	0.274 (−0.417, 0.844)	0.514	no
NEEM	1.036 (0.500, 1.556)	0	yes

Note: We consider there are no trends when one of the following conditions are violated: 1. *p*-values > 0.05; 2. 0 is within the 95% Confidence Interval (95% C.I.).

APPENDIX B

Appendix B provides Supporting Information for Chapter 3.

Text B1. Extended explanation on potential factors influencing bromine preservation in snowpack

If the photochemistry-dominated deep snow production is the major loss process of bromine from the snowpack, the extent of snow bromine preservation is at least partly determined by how quickly a snow layer is buried beneath the snow photic zone and isolated from solar radiation, similar to the photolysis-driven post-depositional loss of nitrate in snowpack (Röthlisberger et al., 20147; Winton et al., 2020; Akers et al., 2022). We assume that the depth of the snow photic zone is 30 cm, following Thomas et al. (2011) based on measurements for snowpack at Summit, Greenland (Galbavy et al., 2007). Table B3 summarizes the snowfall rate, the number of days needed to accumulate 10 cm of snow (assuming constant snowfall rate), and the duration of polar night at the six ice core locations.

AN has the highest snowfall rate and takes 28 days to accumulate 10 cm of snow. This means that about 44 cm snow is accumulated during the dark time of year (124 days), and at least 14 cm of this snow is buried underneath the snow photic zone (~3 times of e-folding depth, 30cm) at polar sunrise and this layer experiences minimal photochemical loss. In contrast, Greenland ice cores do not have snow layers that are completely isolated from the sunlight due to slower snow accumulation rate and lower latitude (fewer dark days).

To take seasonal variations in snowfall rate (Figure B8) into consideration, Table B4 calculated the depth of snow accumulated during polar night period for each ice core, based on monthly mean snow accumulation rate from MERRA2 reanalysis in year 2007 and 2008. Only AN in 2008 has accumulated over 30 cm of snow during darkness, and Greenland ice cores accumulate a maximum of 16 cm (NEEM_2011_S1 in 2007) during darkness. Therefore, even if none of these ice core sites have snow layers completely isolated from the sunlight (e.g. year 2007), AN would still be the best preserved ice core among the six ice core sites.

A second factor that may regulate snowpack bromine release is the relative contribution of dry and wet deposition, which we hypothesize to have an effect on the location of impurities in snow grains. Snow impurities, including bromide, can reside in different locations based on snow formation and evolution processes. These locations include bulk and surface of ice crystals, grain boundaries, liquid brines, and in aerosol particles trapped in snow (Bartels-Rausch et al., 2014; Domine et al., 2013). How chemical reactivity of impurities differs with different locations in snow grains remain highly uncertain (Domine et al., 2013). Dry deposited bromine will at least initially be located at the snow grain surface and thus is more exposed for surface reactions. Wet deposited bromine, on the other hand, may be less reactive, as it may be trapped in the bulk ice crystals through rimming, in airborne particles as ice condensation nuclei, or from scavenging process during precipitation (Beine et al., 2011; Domine et al., 2004). The fact that ice core bromine concentrations in these Arctic cores never reach zero suggests that there is some fraction of snow bromine that is isolated from photochemical reactions and is thus preserved, although essentially all (below detection limits) bromine is lost at some very low snow accumulation ice core sites on the East Antarctic Plateau where dry deposition probably dominates (McConnell et al., 2017). If wet deposition contains a significant proportion of bromine that is not photochemically reactive, it may be isolated from photochemical loss and thus preserved. Under this assumption, more wet deposition implies higher bromine preservation. Fig.S9 shows that the model predicts that AN and ACT_11d have the highest fraction of bromine that is wet deposited. This may also explain the apparent preservation of bromine trends from the mid-latitude ice core in French Alps, Col du Dome (Legrand et al., 2021), which has a high fraction of wet deposited bromine (80% based on our model simulations).

Lastly, recent studies (Burd et al., 2017; Jeong et al., 2022; Kim et al., 2018) have shown that surface melting can effectively shut down snowpack bromine reactions in summertime. In warm years like 2007, this shut down mechanism occurs for AN and ACT_11d in July, leading to better preservation at these two sites (Fig. 4 and Table 3). As the frequency and duration of surface melting increases in the Greenland ice sheet under a warming climate (Colosio et al., 2021; Parizek & Alley, 2004), it is likely that snowpack bromine emission will be shut down during most of the sunlit period in Greenland locations. However, it is uncertain how excessive

melt of surface snow and possible thaw-refreezing cycles will impact ion re-distribution and snow morphology, and thus the chemical reactivity of snow impurities in the future.

Text B2. Extended explanation of change point analysis.

Figure B2 shows the Br_{enr} values from the six Arctic ice cores since the pre-industrial along with Bayesian Change Point model results. Only AN has a high probability for significant trends in Br_{enr}, increasing from 1930 to 1975 at a rate of 0.079 ± 0.009 per year, decreasing afterwards at a rate of −0.230 ± 0.101. NGT_B19 has some low-probability change points, with the largest one (around 1960) driven by an outlier value, and there is no significant difference in trends before and after the outlier. A rate of change of 0.004 ± 0.005 is found for NGT_B19 over the entire record, indicating there is no significant long-term trend either. For the other four Greenland ice cores, no change point is identified by any of the 500 sampled solutions during Bayesian Change Point analysis, and the rate of changes over the whole ice core time period are similar to variations, with the calculated trends over the entire record being 0.118 ± 0.103 for ACT_11d, 0.000 ± 0.010 for NEEM_2011_S1, −0.002 ± 0.004 for Tunu, and 0.003 ± 0.005 for Summit.

Figure B3 shows that the statistical analysis detects change points in both AN and Tunu with probabilities greater than 10%. AN Br_{exc} increased from 1930 to 1975, with a rate of change of 0.114±0.033 $ng \cdot g^{-1} \cdot yr^{-1}$, and decreased after 1975 with a rate of −0.156±0.033 $ng \cdot g^{-1} \cdot yr^{-1}$. Tunu Br_{exc} has a relatively stable trend before the change point at 1958, with a rate of change of −0.001±0.000 $ng \cdot g^{-1} \cdot yr^{-1}$ between 1750 and 1958. After 1958 Br_{exc} quickly increased until 1962 (0.062±0.031 $ng \cdot g^{-1} \cdot yr^{-1}$), then slightly decreased (−0.002±0.002 $ng \cdot g^{-1} \cdot yr^{-1}$) since then. Overall Br_{exc} at Tunu shows a rate of change of 0.000±0.000 $ng \cdot g^{-1} \cdot yr^{-1}$ throughout the entire record. No significant change points nor trends (0.000±0.000 $ng \cdot g^{-1} \cdot yr^{-1}$) over the entire record are detected for Br_{exc} at NGT_B19. Change points detected in NEEM_2011_S1 and ACT_11d are driven by outliers and Br_{exc} at these two sites show no long-term trends (0.001±0.000 $ng \cdot g^{-1} \cdot yr^{-1}$ for both sites). Summit sees a group of potential change points between 1855 and 1900, but none of them show a probability larger than 10%. There is a minor decreasing trend from 1750 to 1850

(−0.001±0.000 $ng \cdot g^{-1} \cdot yr^{-1}$), and a minor increasing trend from 1900 to the end of the core (0.001±0.000 $ng \cdot g^{-1} \cdot yr^{-1}$).

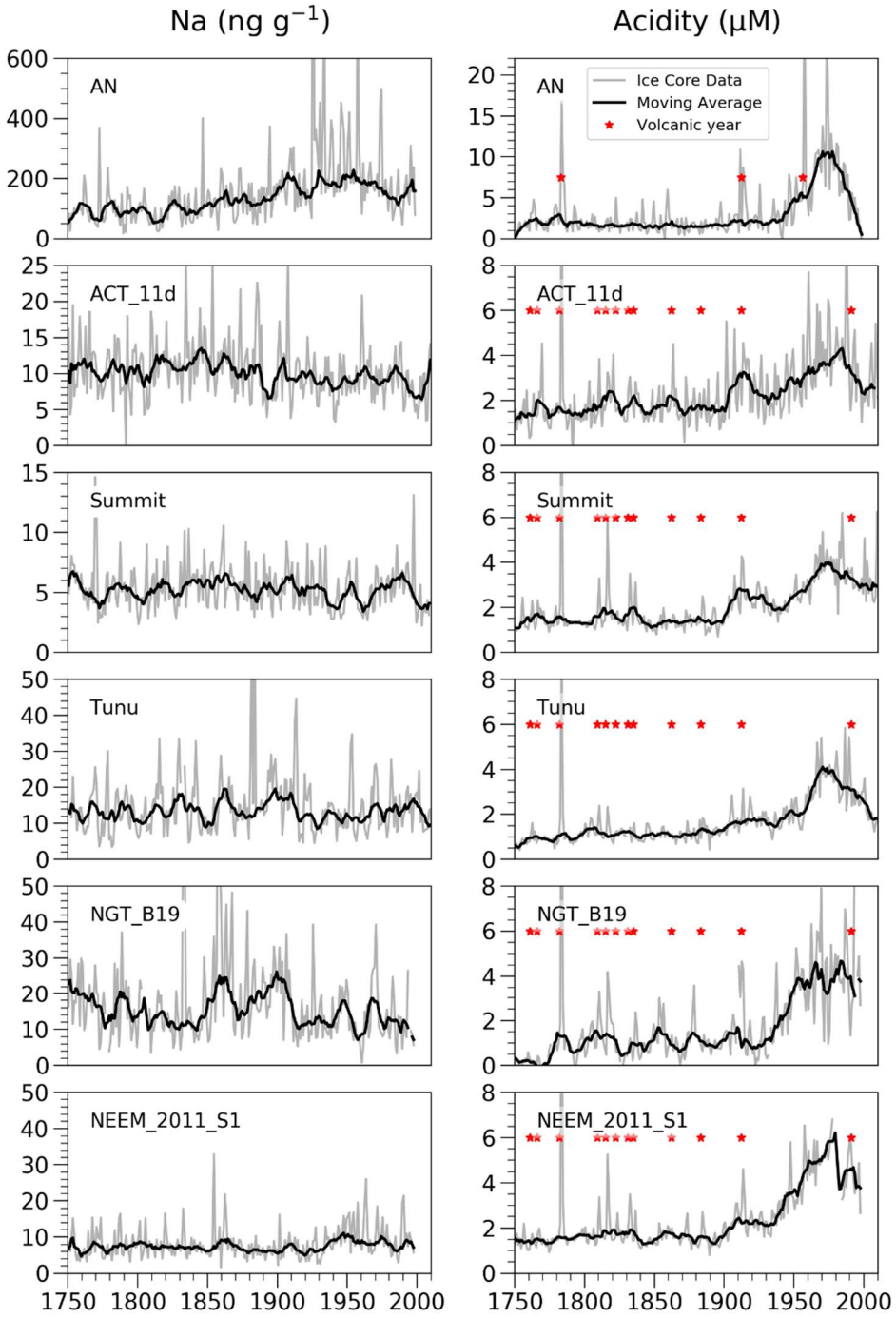

Figure B1. Ice core sodium (left) and acidity concentrations (right) in Akademii Nauk, ACT_11d, Summit, Tunu, NGT_B19, and NEEM_2011_S1 ice cores. Gray lines are the measured annual ice core concentrations, and black lines are the 9-year running average of the concentrations or calculations, with outliers outside of 1.5×IQR (interquartile range) removed. Red stars mark the large and moderate volcanic years identified in previous studies. Specifically,

Opel et al. (2013) identified volcanic eruptions at Laki in 1783, Katmai in 1912, and Bezymianny in 1956 for AN, and those for Greenland ice cores are based on Cole-Dai et al. (2013) and Sigl et al. (2013) as described in Zhai et al., 2021 Text B2.

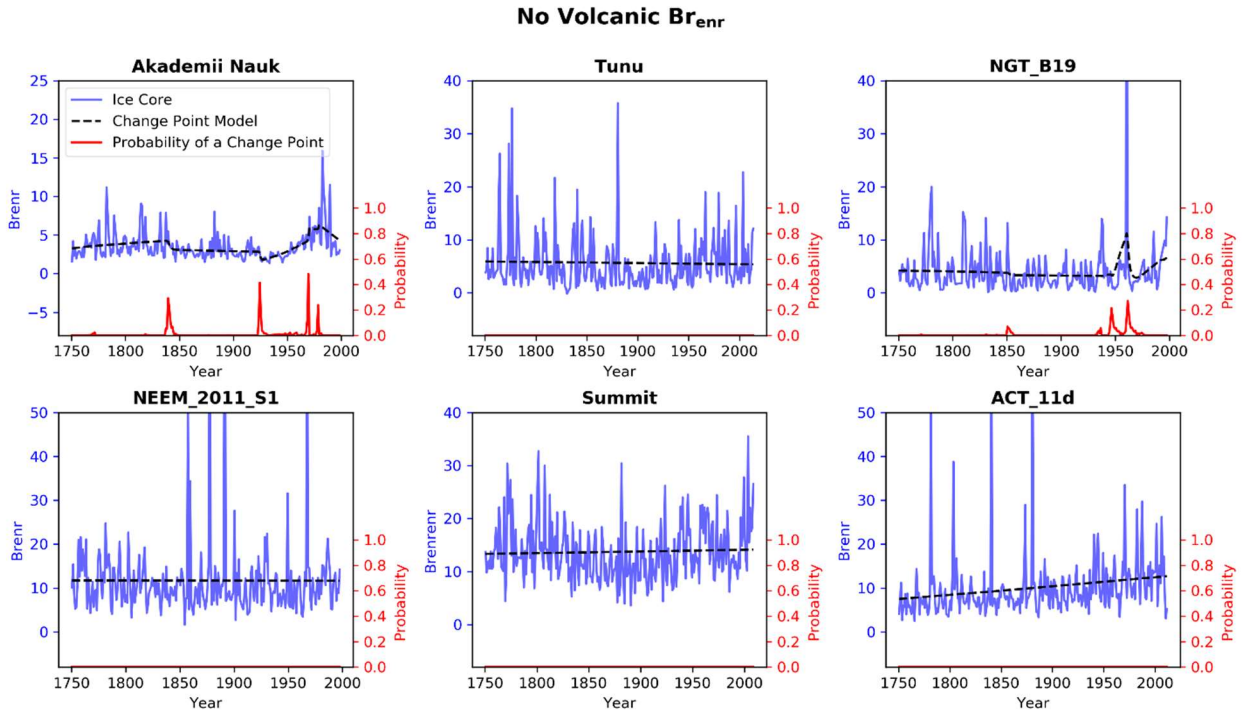

Figure B2. Br_{enr} records and trend analysis since year 1750 from six Arctic ice cores. Blue lines are ice core Br_{enr} values calculated based on ice core measurements of sea-salt sodium and bromine, with previously identified volcanic years removed (Opel et al., 2013; Cole-Dai et al., 2013; Sigl et al., 2013). Dashed black lines are the model predicted trends by the Bayesian Change Point algorithm. The heights of red spikes at the bottom of each panel indicate the probability of a potential change point. Tall, narrow spikes suggest relative certainty in the timing of a change point, where shorter and wider spikes suggest more uncertainty. No spikes are visible if no change points are identified by any of the 500 sampled solutions.

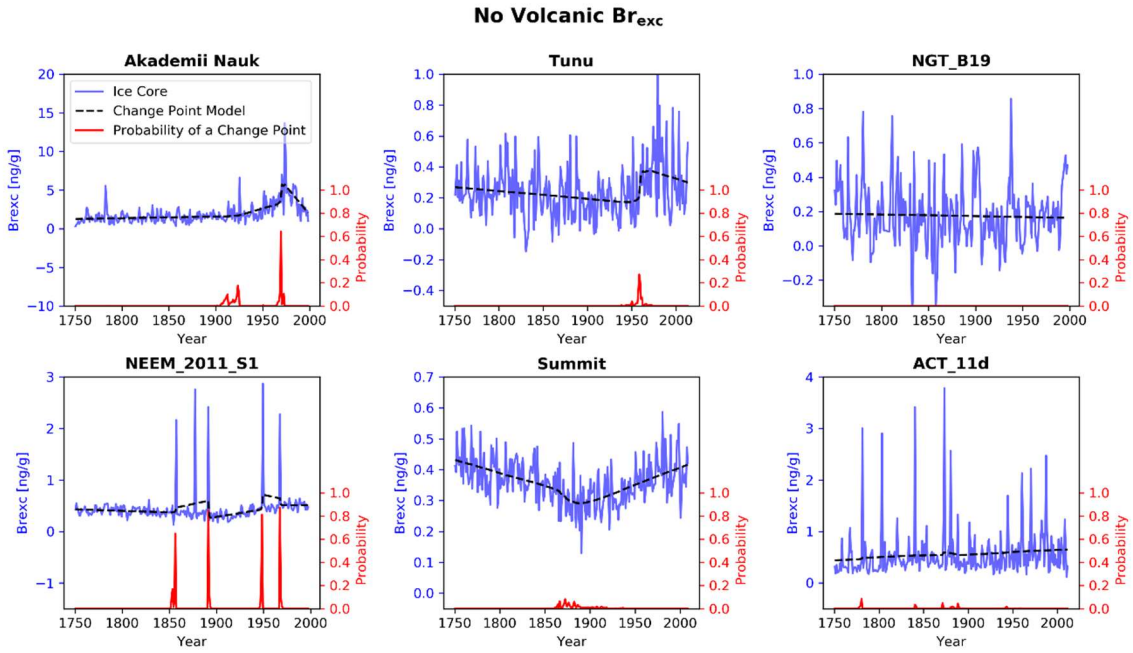

Figure B3. Similar to SI Figure B2 but for Br_{exc}.

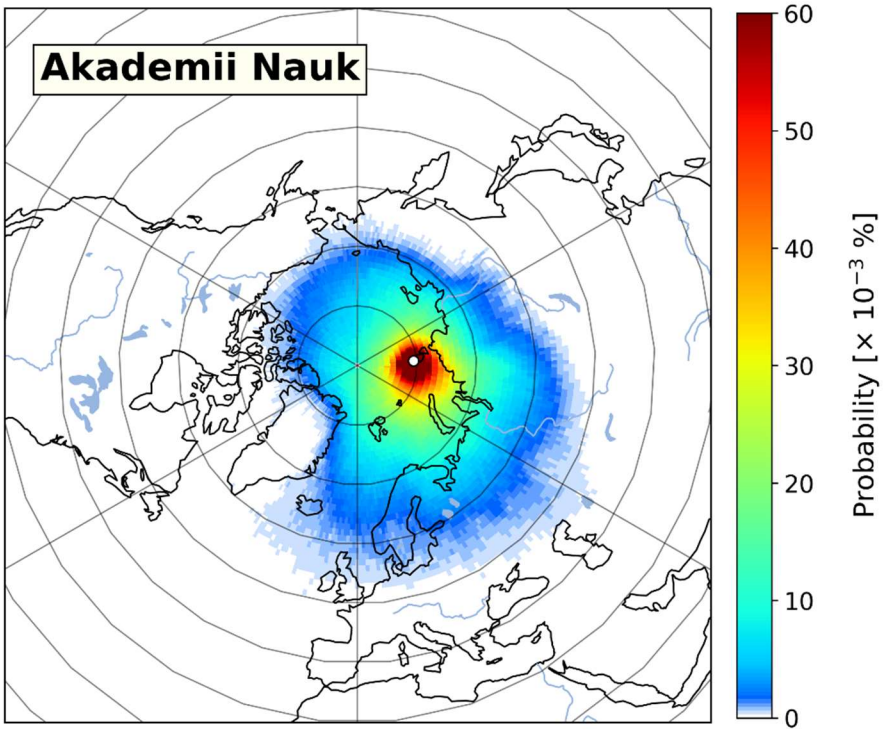

Figure B4 5-day back trajectory probability at Akademii Nauk calculated by the HYSPLIT model for the time period 1959-2010. The Akademii Nauk ice core site is marked as an open circle. Details of the HYSPLIT model parameters and settings are described in Zhai et al. (2021).

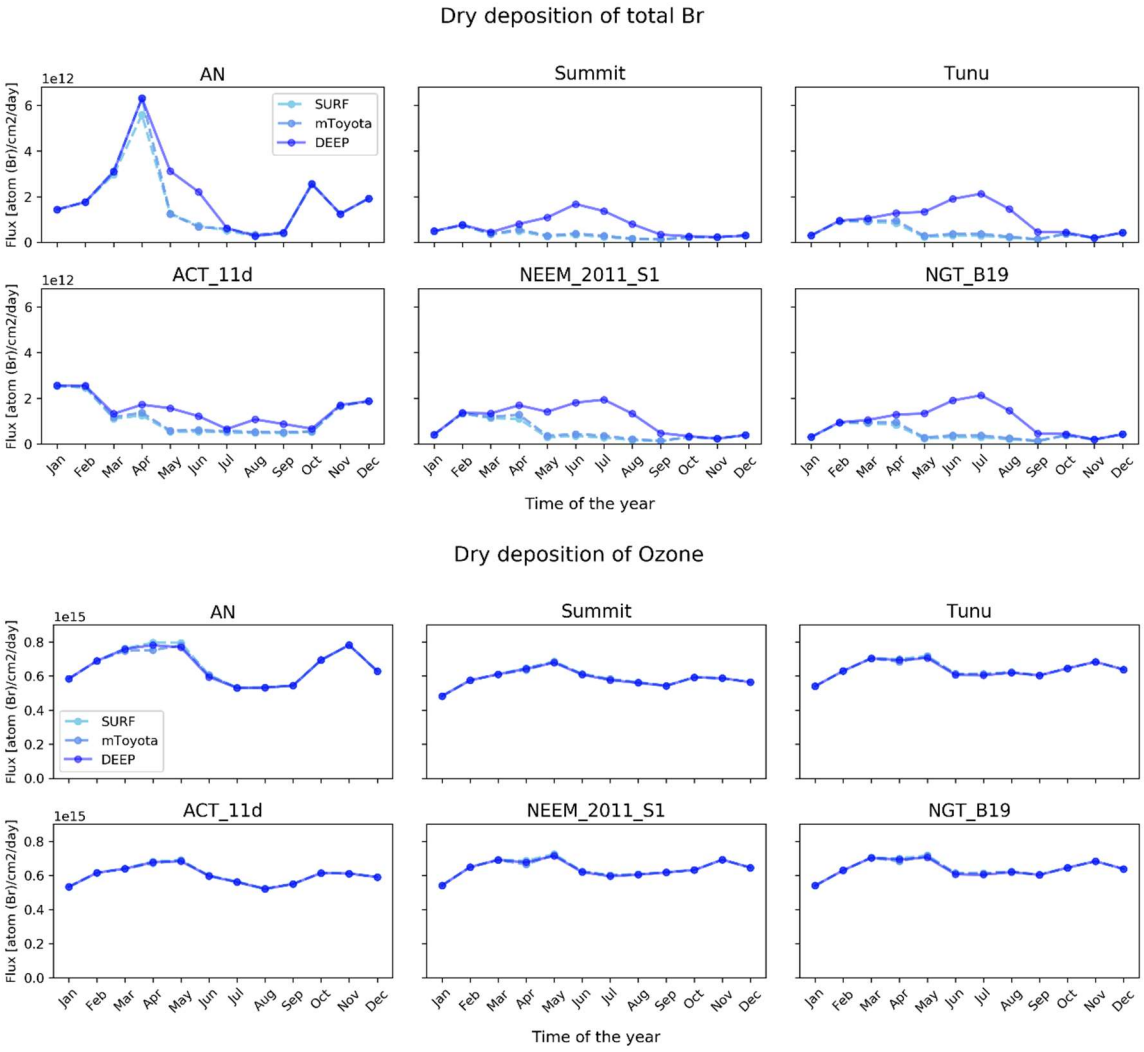

Figure B5. Modeled monthly mean dry deposition fluxes of total bromine (Br_y + sea salt Br^-) (top panels) and ozone (bottom panels) in the three simulations for the six ice core locations in year 2007.

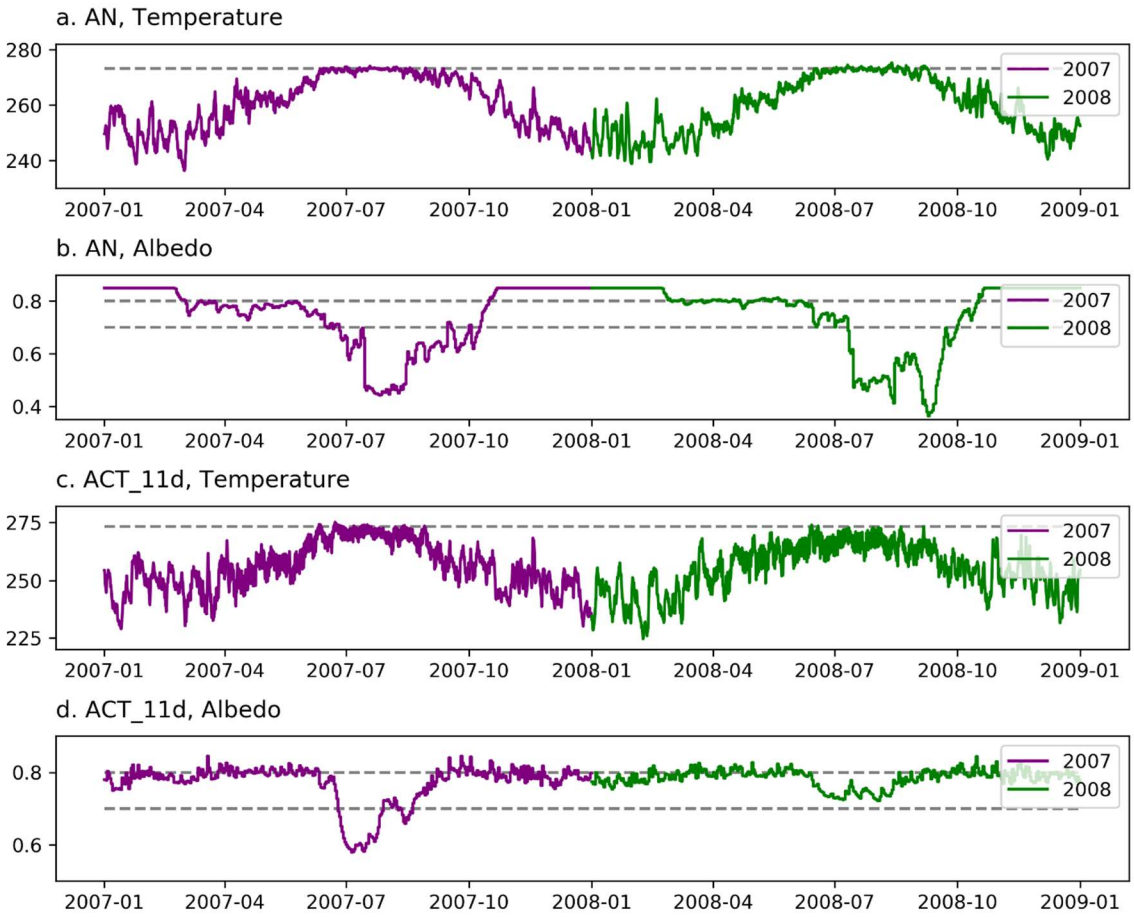

Figure B6. MERRA2 daily 2-meter air temperature (a, c) and surface albedo (b, d) at AN (a, b) and ACT_11d (c, d) for year 2007 and year 2008. Dashed gray lines mark either the temperature threshold of 273.15K, or the albedo values of 0.8 and 0.7. Snow bromine emission mechanisms are shut down when temperature goes above 273.15K or surface albedo is below 0.7 in this study.

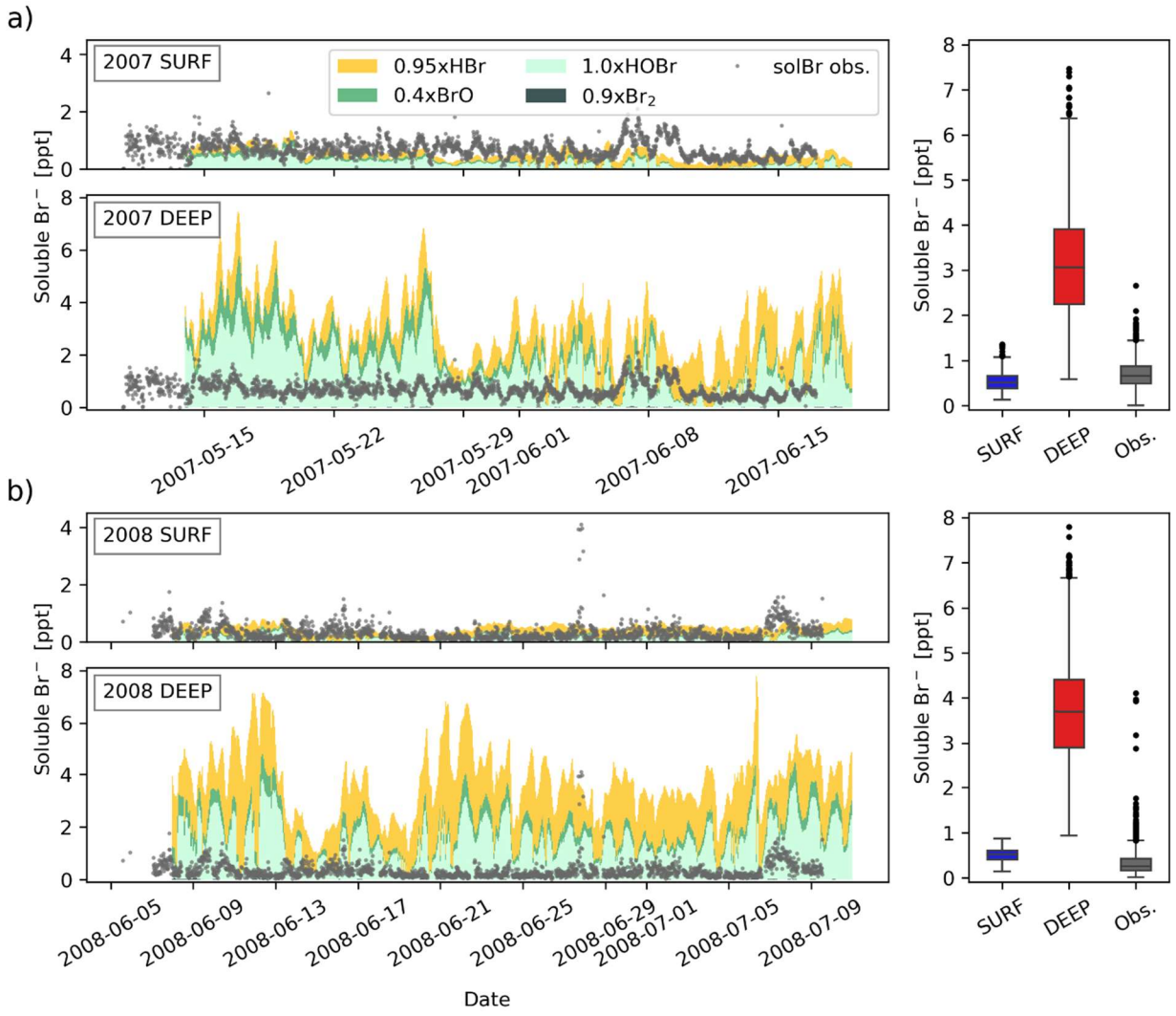

Figure B7 Comparison between the modeled hourly surface soluble bromide concentrations at Summit during a) May–June in 2007 and b) June–July in 2008 from SURF and DEEP simulations, and the Mist Chamber observed soluble bromide concentrations from Dibb et al. (2010). Soluble bromide is defined as in Liao et al. (2012), where $[Br^-] = 0.9[Br_2] + 1.0[HOBr] + 0.4[BrO] + 0.95[HBr]$. $0.9\times Br_2$ is minimal compared to other constituents and is barely visible in the plot. SURF modeled mean soluble bromide is 0.5 ppt for both 2007 and 2008 seasons, similar to those reported in Dibb et al. (2010).

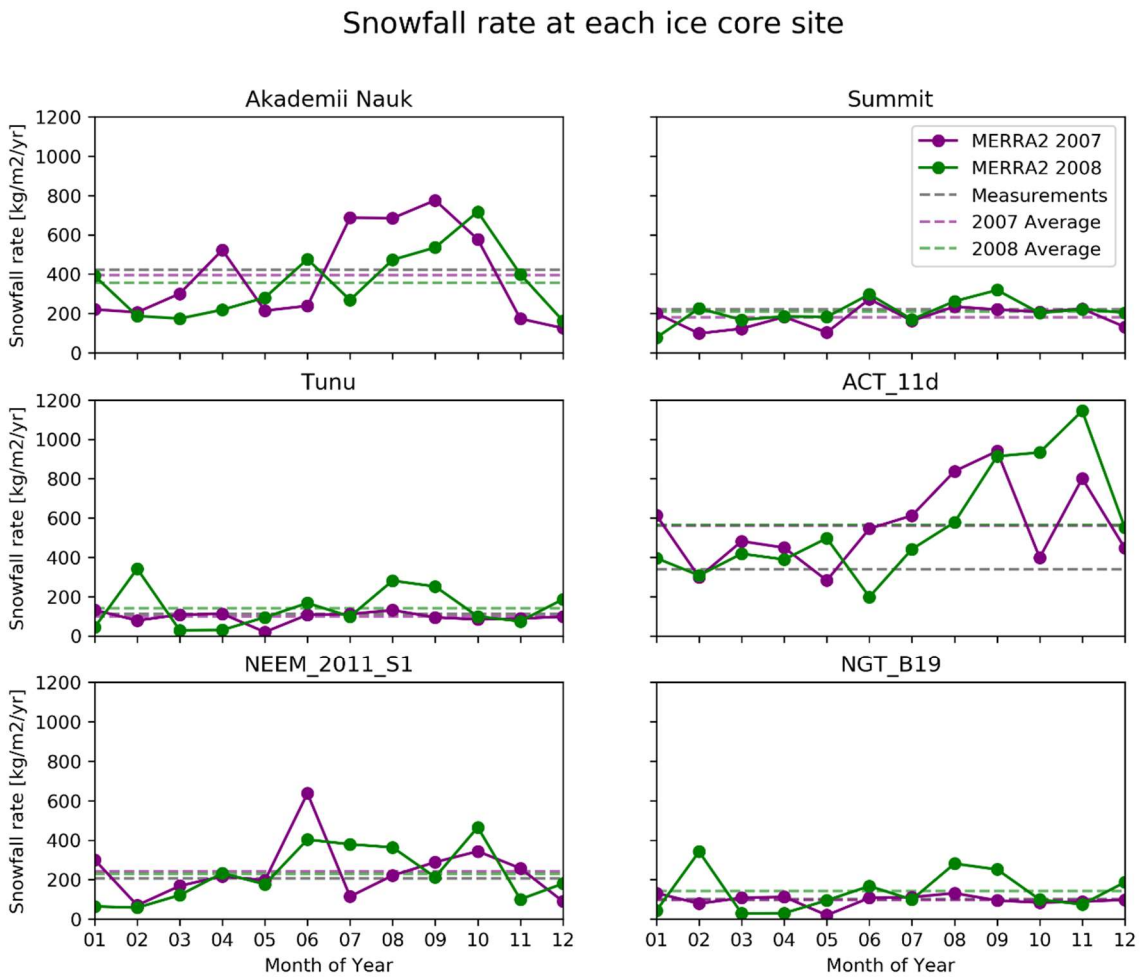

Figure B8. MERRA2 monthly snowfall rate at each ice core location for year 2007 (solid purple lines) and 2008 (solid green lines). Dashed gray lines mark the annual average snowfall rate calculated based on ice core records, and dashed purple and green lines are annual average snowfall rate from MERRA2 for year 2007 and 2008, respectively.

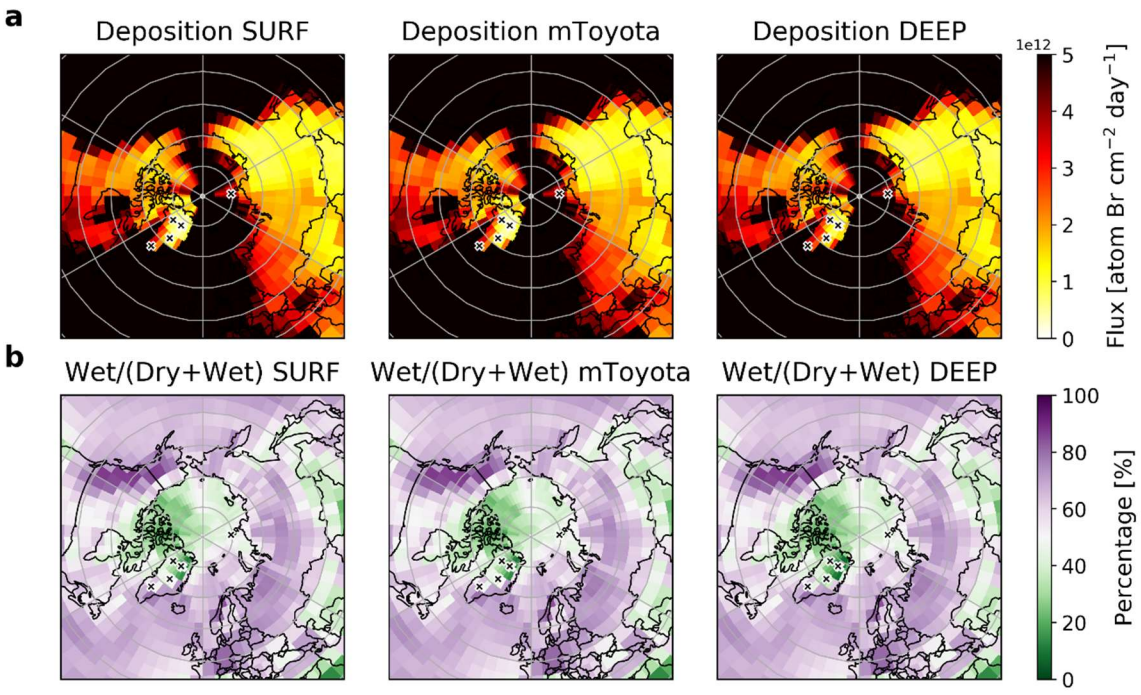

Figure B9. Simulated Arctic spatial distribution of annual mean a) total bromine deposition, and b) percentage of bromine wet deposition in total bromine deposition from the 3 simulations, SURF, mToyota, and DEEP. Red stars mark the ice core locations.

Table B1. Snowpack-air exchange fluxes of total bromine (total deposition, emission, net upward flux, and post-depositional loss) at the six ice core locations calculated from the mToyota simulation.

Ice core	Total deposition [atom Br cm^{-2} day^{-1}]	Emission (Br_2+BrCl) [atom Br cm^{-2} day^{-1}]	Net upward flux [atom Br cm^{-2} day^{-1}]	Post-depositional loss (Emission / Deposition)
AN	3.4×10^{12}	7.1×10^{11}	-2.7×10^{12}	21%
Summit	4.6×10^{11}	1.1×10^{11}	-3.4×10^{11}	25%
Tunu	5.1×10^{11}	1.2×10^{11}	-3.9×10^{11}	24%
ACT_11d	2.3×10^{12}	3.1×10^{11}	-2.0×10^{12}	13%
NEEM_2011_S1	7.7×10^{11}	1.4×10^{11}	-6.3×10^{11}	18%
NGT_B19	5.1×10^{11}	1.2×10^{11}	-3.9×10^{11}	24%

Table B2. Comparison of ice-core and SURF model-calculated annual mean concentrations of snow bromide

Ice core	Ice-core snow bromide (ng g^{-1})	Modeled snow bromide (ng g^{-1})
AN	2.7±1.3	4.04
Summit	0.4±0.1	1.16
Tunu	0.3±0.2	2.37
ACT_11d	0.6±0.5	1.93
NEEM	0.5±0.3	1.43
NGT_B19	0.3±0.2	2.37

Table B3. Comparison of the annual mean snowfall rate and duration of polar night at the six ice cores in this study. 30 cm is the snow photic zone depth.

	Akademii Nauk	Summit	Tunu	ACT_11d	NEEM_2011_S1	NGT_B19
Annual mean snowfall rate [kg m^{-2} yr^{-1}]	421	222	112	339	206	101
Time to accumulate 30cm snow [days]	84	159	312	105	171	348
Polar night	Oct.20 – Feb.21	Nov.15 – Jan.26	Oct.27 – Feb.14	≥2 hours daylight	Oct.29 – Feb.12	Oct.27 – Feb.14
Days in dark [#]	124	72	110	0	106	110

Table B4. Snow depth accumulated during polar night at the six ice cores in this study based on MERRA2 monthly averaged snowfall rate in 2007 and 2008.

		Akademi i Nauk	Summit	Tunu	ACT_11d	NEEM_2011_S1	NGT_B19
Snow depth accumulated in dark days (cm)	2007	20	10	9	0	16	9
	2008	31	9	11		9	11

APPENDIX C

Appendix C provides Supporting Information for Chapter 4.

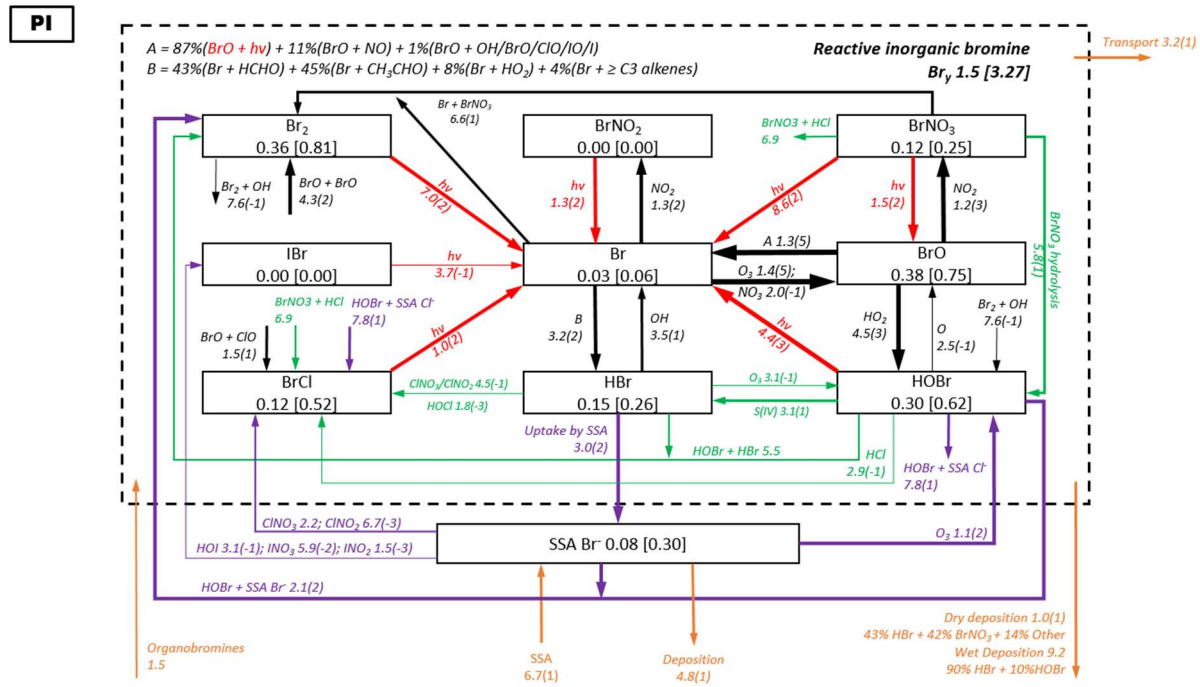

Figure C1. AN back trajectory regional budget and chemical cycling of tropospheric bromine species in GEOS-Chem for PI. Average regional annual mean masses (Gg Br) and mixing ratios (ppt, in square brackets) are shown in the squares with key bromine species. Arrows show the regional annual mean reaction rates (Gg Br a^{-1}), and the thickness of arrows are proportional to the orders of magnitude of the reaction rates. Read 8.6(2) as 8.6×10^{2}. Gas phase, aerosol multi-phase, cloud, and photolysis chemistry are shown in black, purple, green, and red arrows, respectively, and orange arrows indicate the sources and sinks. The dotted box group together the Br_y family, and arrows in and out of the box represent general sources and sinks of Br_y.

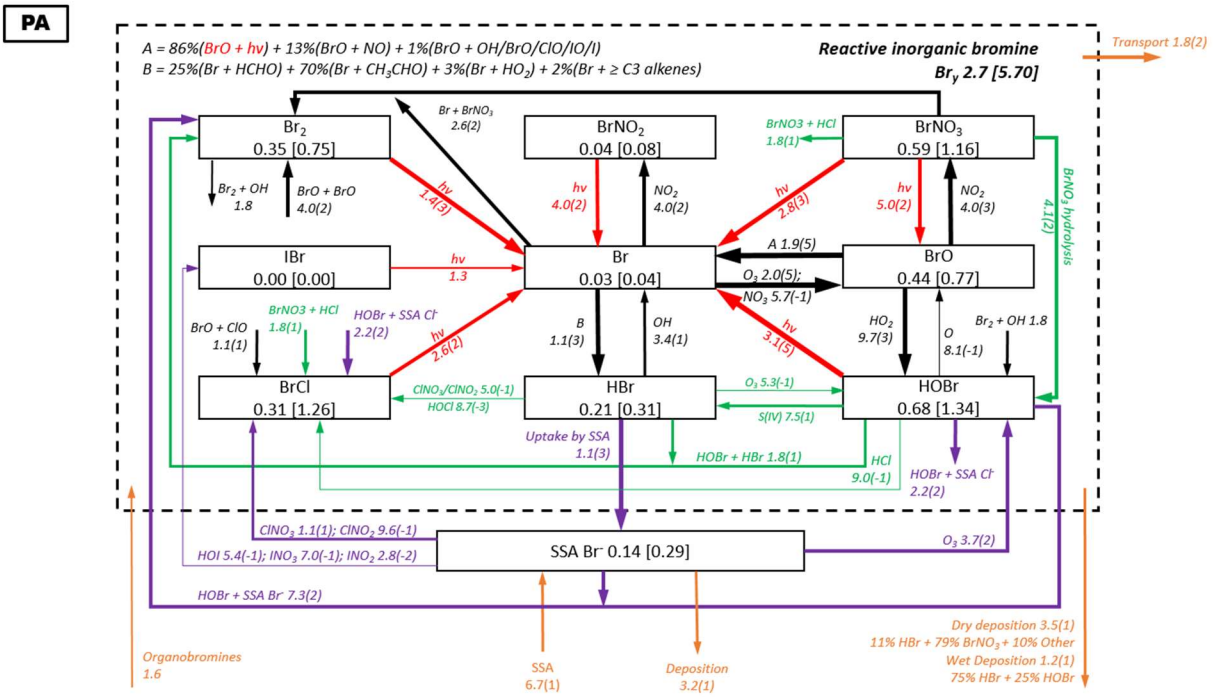

Figure C2. Similar to Figure C1 but for PA.

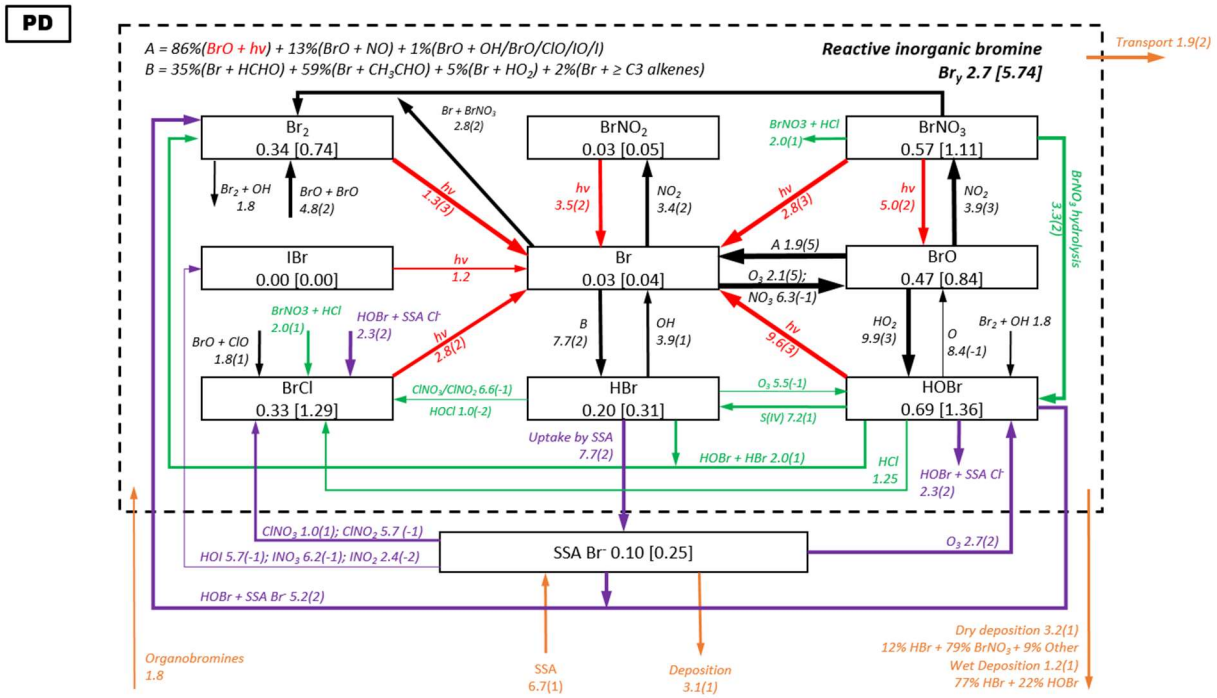

Figure C3. Similar to Figure C1 but for PD.

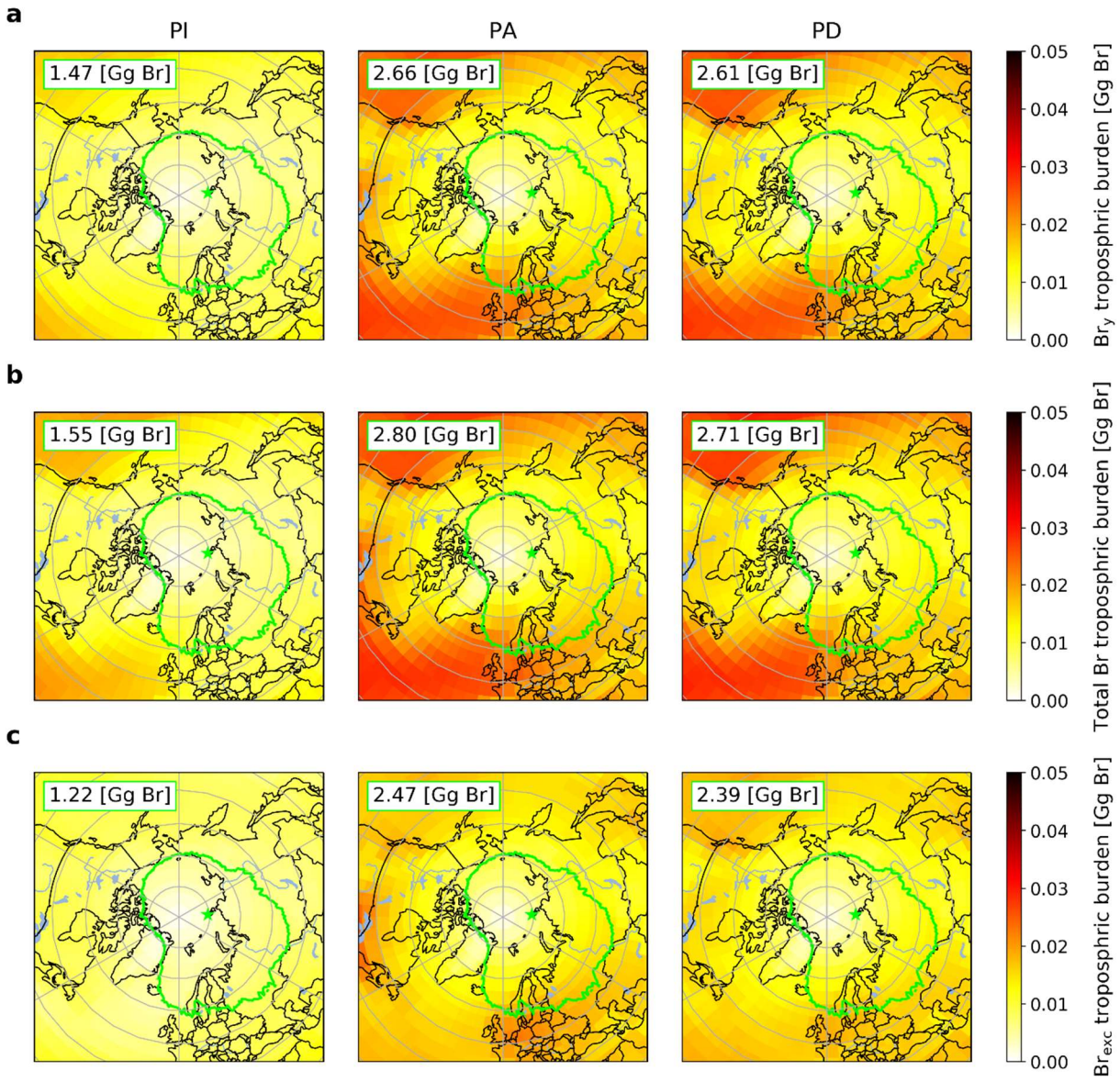

Figure C4. Regional distributions of annual mean tropospheric burden of a) Br_y b) total Br and c) Br_{exc} in the pre-industrial (PI = 1850), peak-acidity (PA = 1975), and present day (PD = 1999) simulated by GEOS-Chem. Gray grid lines show 10° latitude and 60° longitude distance, green star marks the AN ice-core location, and green lines show the 5-day back trajectory region (TRJ) for AN simulated by the HYSPLIT model (Fig.S5). Numbers on the top-left corners in are the annual mean tropospheric a) Br_y b) total Br and c) Brexc burdens in the AN TRJ for the three time periods.

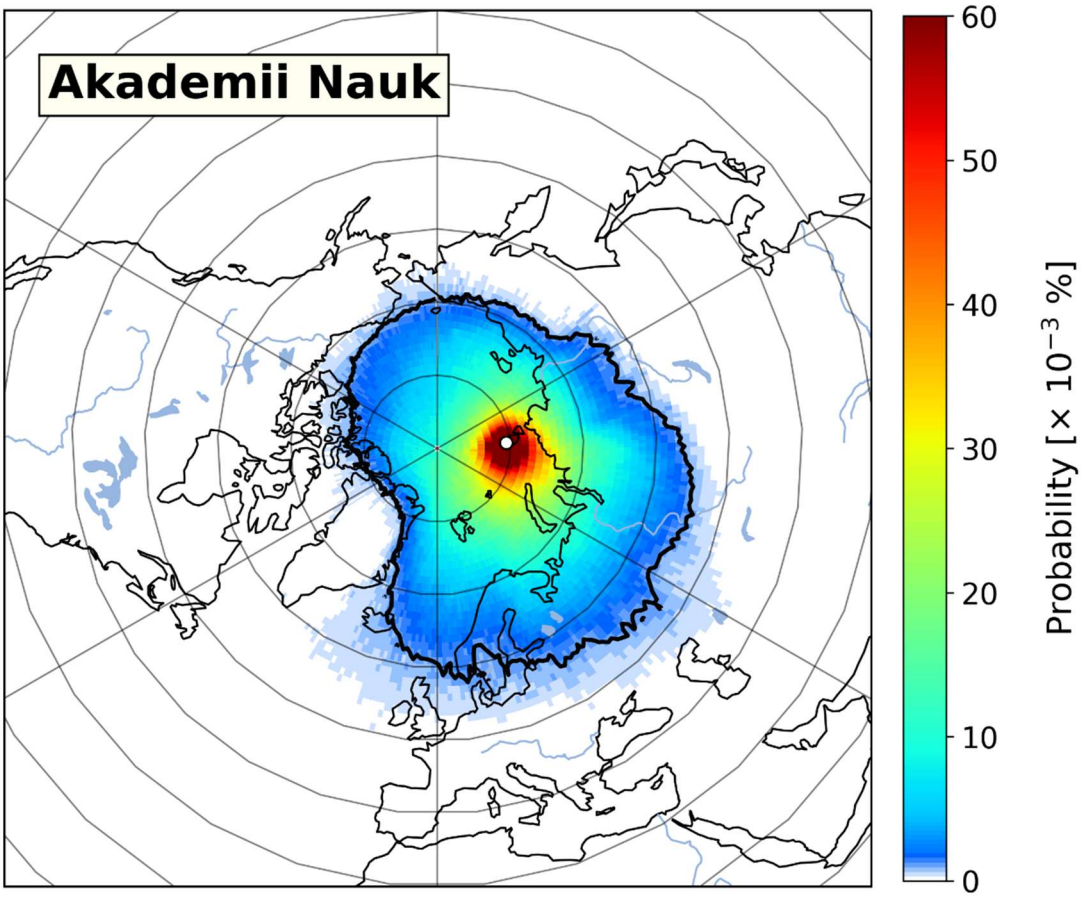

Figure C5. 5-day back trajectory probability of Akademii Nauk calculated by the HYSPLIT model for the time period 1959-2010. The Akademii Nauk site is marked as a white circle, and the black contour indicate the back trajectory region (probability > 1.2×10^{-3} %) used for bromine budget analysis.

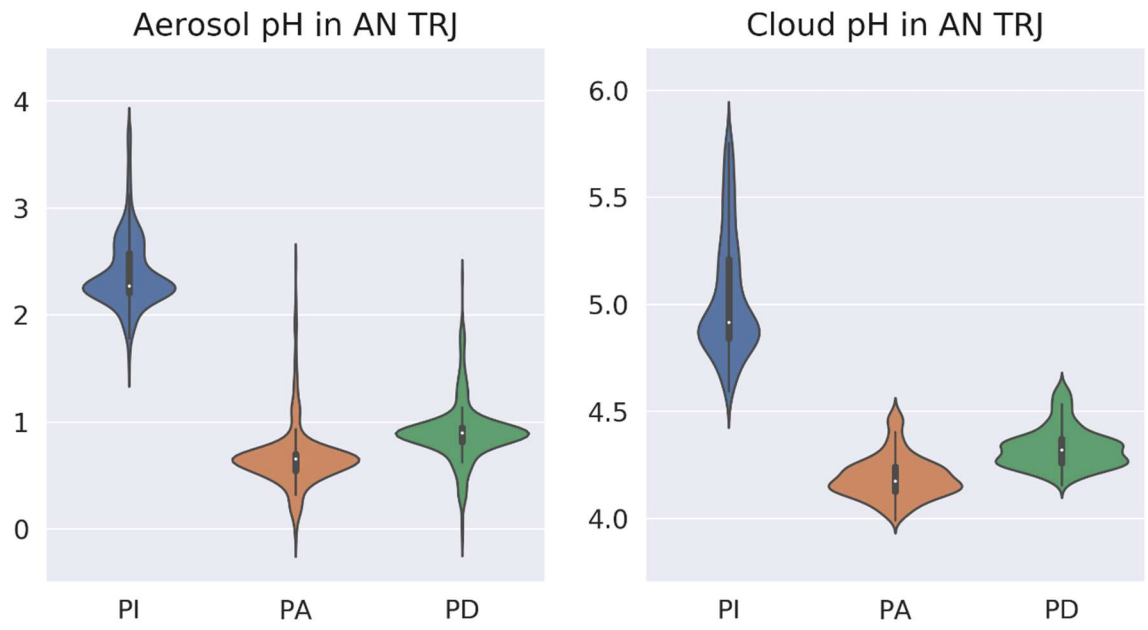

Figure C6. Violin plots of modeled annual mean left panel) aerosol pH and right panel) cloud pH in the AN back trajectory region for PI, PA, PD. The mean of aerosol pH in the AN back trajectory region for PI, PA, PD are 2.39, 0.66, 0.90, respectively. And the mean of cloud pH in the AN back trajectory region for PI, PA, PD are 4.98, 4.19, 4.33, respectively

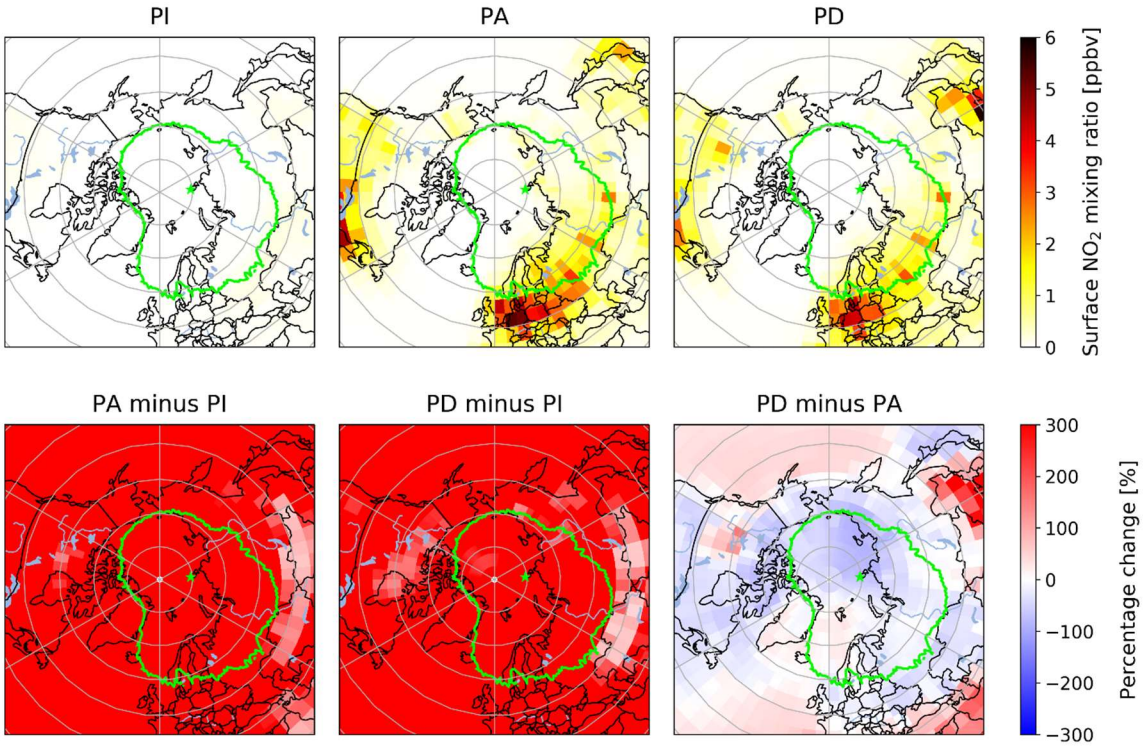

Figure C7. (Upper panels) Modeled NO2 surface mixing ratios in PI, PA, and PD and (Lower panels) their percentage changes in between the three time periods. Green star and circles show the location of AN ice core and its 5-day back trajectory region.

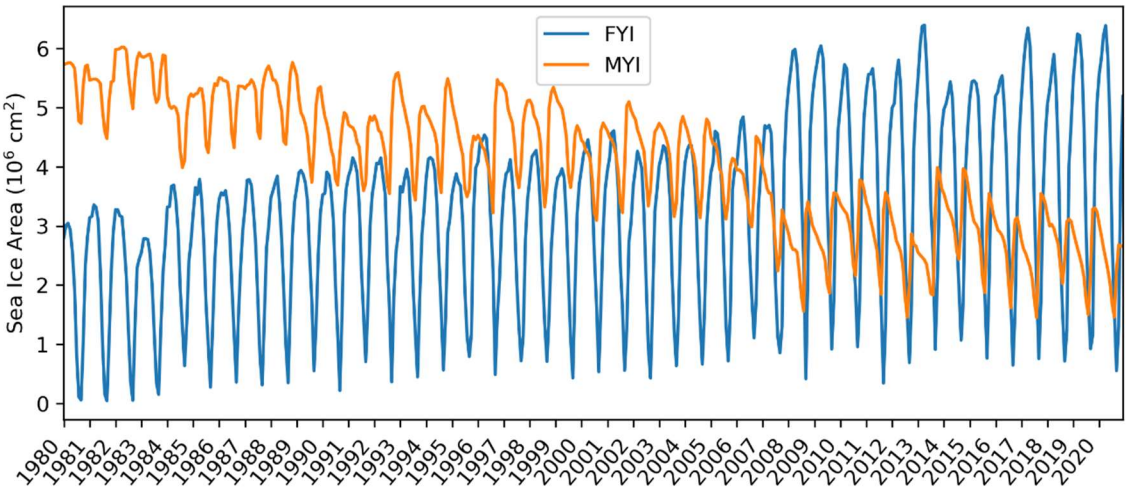

Figure C8. FYI and MYI trends in AN TRJ since 1980 based on Confer et al., 2023. FYI and MYI data are based on EASE-Grid Sea Ice Age for years after year 1984. Prior to year 1984 sea ice age is not available from observations, so MYI is based on the minimum sea ice extent in MERRA-2 at the end of summer.

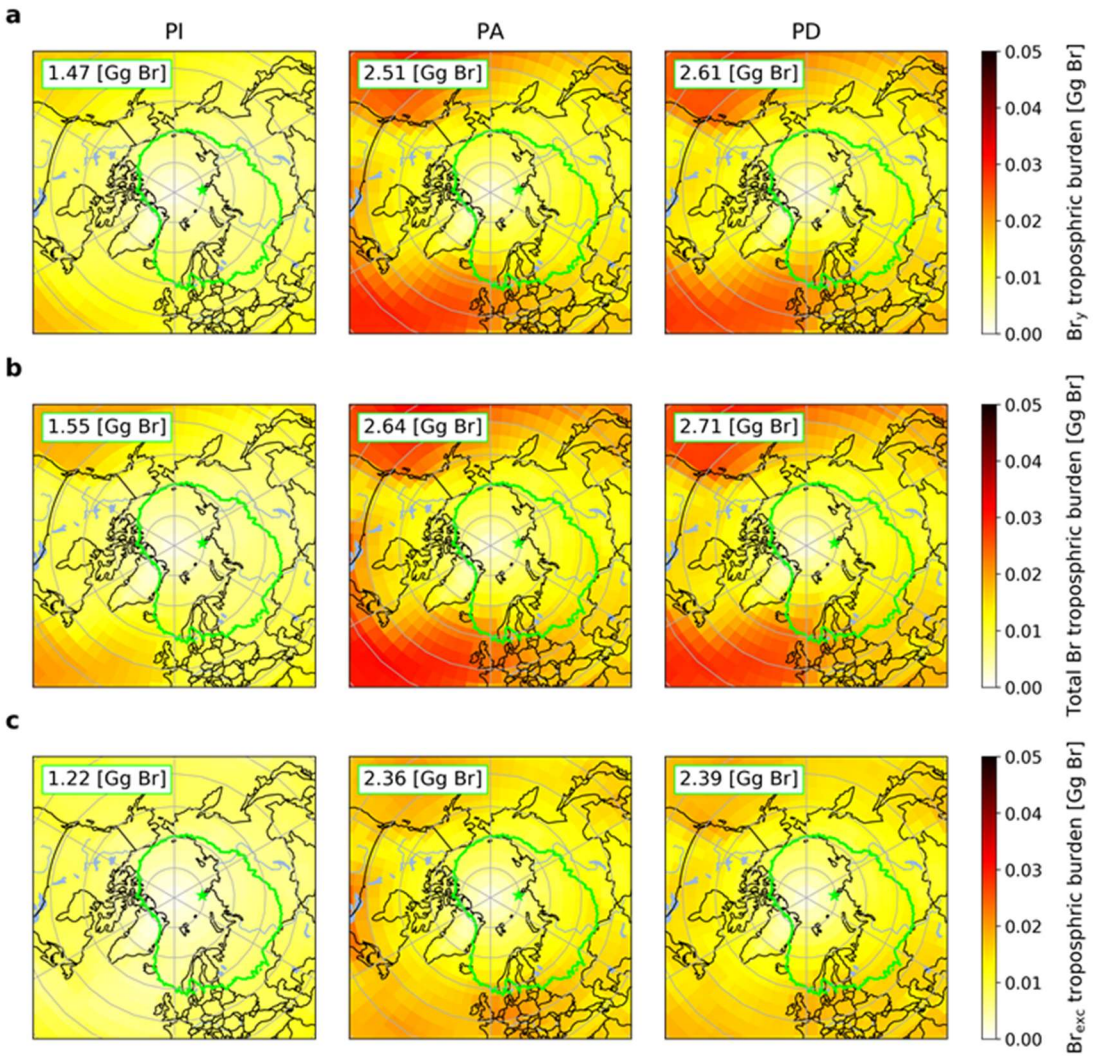

Figure C9. Similar to Figure C4 but for PA with 1980 (instead of 2007) meteorology.

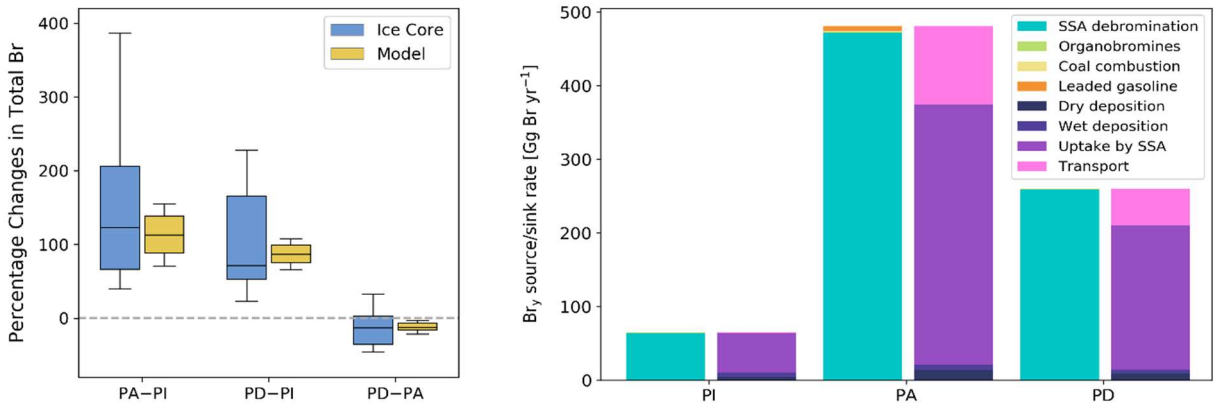

Figure C10. (left panel) Comparison of percentage changes in annual mean tropospheric total Br burdens between PI, PA, and PD from the CDD ice-core records and model simulations, and (right panel) modeled annual mean sources and sinks of tropospheric Bry in the CDD back trajectory region for PI, PA, PD. For each time period, left bar shows the sources and right bar shows the sinks. 'Transport' represents Bry that transported outside of the CDD back trajectory region.

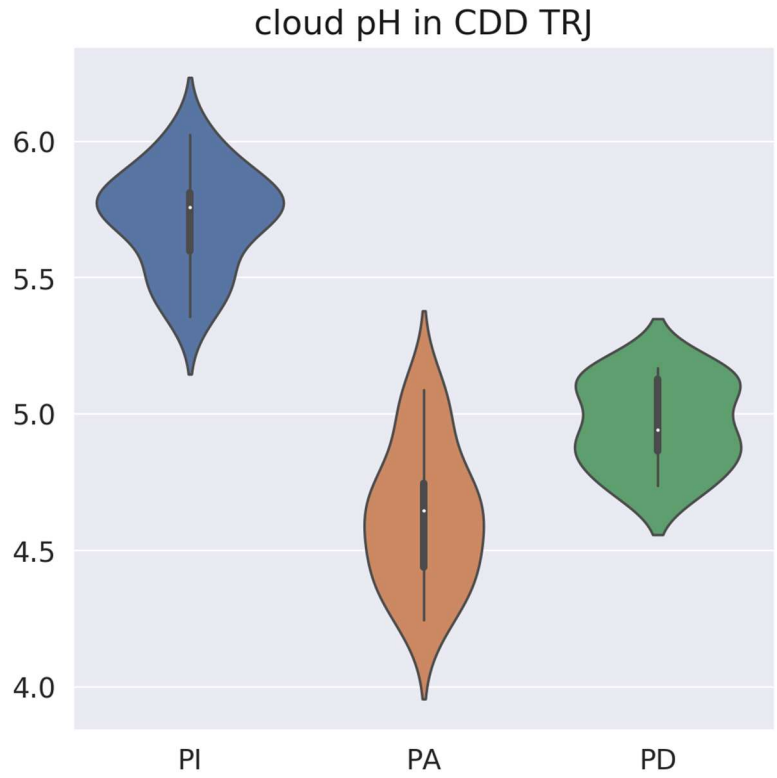

Figure C11. Violin plots of modeled annual mean cloud pH in the CDD back trajectory region for PI, PA, PD. The mean of cloud pH in the CDD back trajectory region for PI, PA, PD are 5.7, 4.6, 5.0, respectively.

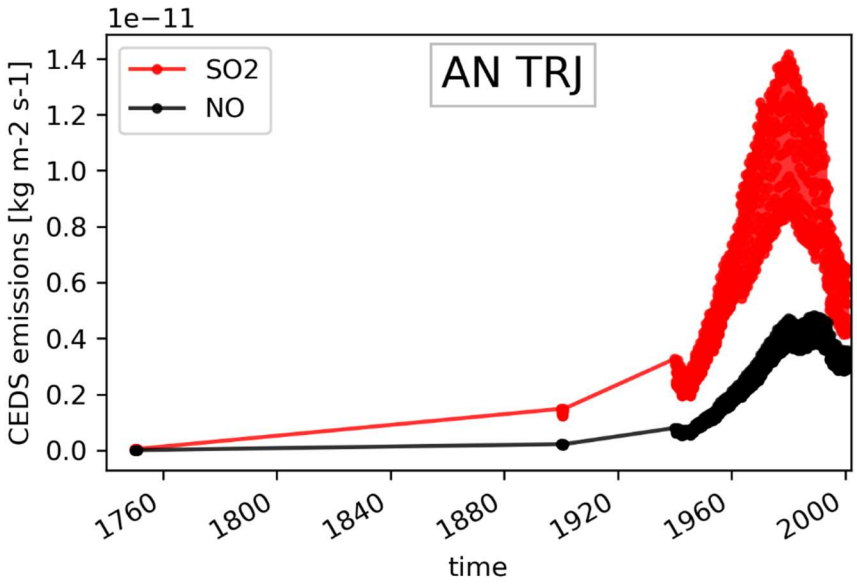

Figure C12. SO_2 and NO emissions in hourly resolution from the Community Emissions Data System (CEDS) (Hoesly et al., 2018) in the AN back trajectory region. Note that only 1750, 1900, and post-1940 data are shown.

Table C1. Average ice-core concentrations of nssNa, total Br, Brexc, and acidity at AN over different time periods.

Ice-core concentrations	nssNa (ng g^{-1})	Total Br (ng g^{-1})	Br_{exc} (ng g^{-1})	Acidity (μM)	Br_{exc}/Br
1750–1850	98.18±59.12	2.02±0.88	1.41±0.71	2.16±1.93	69%±11%
1750–1940	140.06±135.04	2.40±1.45	1.53±0.81	2.17±1.83	65%±12%
1970–1980	219.27±136.48	7.06±4.05	5.71±3.34	11.81±5.39	80%±6%
1988–1998	153.87±76.6	3.32±1.14	2.36±0.89	3.34±2.26	70%±11%

Note: Calculated from raw ice-core data, including years with volcanic activities.

Table C2. Annual mean tropospheric bromine burden and speciation in the AN back trajectory region for PI, PA, and PD from model simulations

Burden (Gg Br)	Br_2	Br	BrO	HOBr	HBr	$BrNO_2$
PI	0.358	0.032	0.381	0.303	0.150	0.002
PA	0.350	0.028	0.444	0.681	0.213	0.041
PD	0.345	0.029	0.465	0.676	0.201	0.027

(Continued)

Burden (Gg Br)	$BrNO_3$	IBr	BrCl	BrSALA	BrSALC	Br_{exc}
PI	0.120	0.000	0.122	0.040	0.044	1.221
PA	0.590	0.000	0.315	0.111	0.026	2.472
PD	0.551	0.000	0.316	0.078	0.026	2.389

VITA

Shuting Zhai comes from Houma City in Shanxi Province in China. She went to Yangzhou University for undergraduate studies and obtained a Bachelor Degree in Environmental Science. Motivated by her interests in air pollution and its measurements, she then attended Peking University, where she got a Master of Science Degree. Her Master's focused on the design and application of an online measuring system for ambient non-methane hydrocarbons, advised by Professor Limin Zeng. Driven by the curiosity in atmospheric modeling and climate change, she started her Ph.D. studies in the Department of Atmospheric Sciences at University of Washington, Seattle in 2017, advised by Professor Becky Alexander, and obtained her Ph.D. in Atmospheric Sciences in 2023.